ABSTRACT

Title of Thesis: HYDROLOGIC RESPONSE OF A SUBURBAN WATERSHED TO CLIMATE MODELS

Zhongrun Xiang, Masters of Science, 2017

Thesis Directed By: Associate Professor, Dr. Kaye Brubaker, Department of Civil and Environmental Engineering, and
Associate Professor, Dr. Hubert Montas, Fischell Department of Bioengineering

Non-Point Source (NPS) pollution is an important issue in the Chesapeake Bay areas of the northeastern U.S. The TMDLs established by the Environmental Protection Agency requires a reduction in sediments, nitrogen and phosphorus by preset amounts, by 2025. One approach to meeting these requirements is to implement Best Management Practices (BMPs) for NPS pollution control. BMPs are most effective when implemented on areas named Critical Source Areas (CSAs) that contribute excessively to the pollutant load relative to their spatial extent. Studies have shown that climate change may have significant influence on the hydrology and water quality variables, and can therefore influence CSA identification in the future. In this study, six climate models were used for the evaluation of the hydrologic response of a suburban watershed in Maryland. The Soil

and Water Assessment Tool (SWAT) was used for the model development, driven by the future climate from six models in four scenarios RCP2.6, RCP4.5, RCP6.0 and RCP8.5. Surface runoff, total suspended solids, total nitrogen and total phosphorus at the watershed outlet and on-land were assessed for two time horizons, mid-century and end-century. The simulations showed a significant increase of yields in all variables both in-stream and on-land among all models/scenarios/periods. CSAs identified using a relative threshold (eg. Top 20% of HRUs) did not vary markedly as climate was changed. However, CSAs identified using a fixed threshold increased substantially in area under future climate. Overall, results demonstrate the potential impacts of climate change on watershed hydrology across six models, and suggest that CSA identification based on relative threshold is most robust against future variability.

HYDROLOGIC RESPONSE OF A SUBURBAN WATERSHED TO CLIMATE MODELS

by

Zhongrun Xiang

Thesis submitted to the Faculty of the Graduate School of the
University of Maryland, College Park, in partial fulfillment
of the requirements for the degree of
Master of Science
2017

Advisory Committee:
Dr. Kaye Brubaker, Chair
Dr. Hubert Montas
Dr. Allen Davis

Acknowledgements

Thanks to my family, and all professors and friends I have had the pleasure to get to know at the University of Maryland.

Table of Contents

List of Tables

List of Figures

Chapter 1: Introduction

1.1 Background

The Chesapeake Bay is the largest estuary in United States. It is 320 km long, with an area of approximately 166,000 km^2 (Boesch et al., 2016). The Chesapeake Bay watershed covers six states and the District of Columbia, where over 18 million people live (Boesch et al., 2016). It is famous for its high production of fish and mollusks, which has great economic value. However, environmental issues, including habitat modification, overexploitation and pollution have been observed for decades.

In 1987, Virginia, Maryland, Pennsylvania, the District of Columbia, the Chesapeake Bay Commission and the U.S. Environmental Protection Agency (EPA) agreed to control and reduce the pollutant loading to the bay, from both point and nonpoint sources, by the Chesapeake Bay Agreement. In the agreement, the goal of a 40 percent reduction of nitrogen and phosphorus was set to be achieved by the year 2000 (CBP, 1992). However, this goal was not met, and one reason is that the agreement was mainly voluntary (Boesch et al., 2016). In 2010, the U.S. EPA issued the Chesapeake Bay Total Maximum Daily Load (TMDL), which is a reduction strategy for the restoration of Bay area (USEPA, 2010). The phase II Watershed Implementation Plan for the Chesapeake Bay TMDL, by the year 2025, requires a total reduction of nitrogen by 22% or 11.59 million pounds, phosphorus by 14.9% or 0.49 million pounds, and sediments must be reduced by 1.9% or 26 million pounds, relative to the values from 2010 (MDDoE, 2012).

The Chesapeake Bay watershed has a land-to-water area ratio of 14:1, which is the largest of all costal water bodies in the world (CBP, 2012). This suggests that on-land issues may impact the environment in the Bay more than in other watersheds, and that on-land controls, such as the Best Management Practices (BMPs) would be very important in achieving the target reductions.

Climate change is another challenge. It is reported that air and stream-water temperatures in the Chesapeake catchment increased at a rate of 0.023°C and 0.028°C per year in the past 50 years, while the estuarine surface water temperature increased from 0.05°C to 0.1°C per year in the past 30 years (Boesch et al., 2016). Globally, high emission of greenhouse gases are expected to cause higher temperatures in the future, and would affect oxygen solubility and biological metabolic rates in the ecosystem (Boesch et al., 2016). More importantly, increased rainfall was observed in the northeastern U.S. in the past 50 years, along with an increase in extreme precipitation events (Boesch et al., 2016). A continuation of this trend would increase the nutrient yields to the Bay and may exacerbate eutrophication and seasonal hypoxia as a result. Accordingly, in order to meet water quality objectives for the Bay, it is very important to assess its hydrologic response to climate change.

1.2 Nonpoint Source Pollution (NPS) and Critical Source Areas (CSAs)

Nonpoint source pollution is mainly generated by surface runoff, precipitation and atmospheric deposition (Niraula et al., 2013). When rainfall or snowmelt moves on and through the ground, it may carry away pollutants into lakes, rivers, wetlands, or ground water. In distinction to the pollution from industrial and treatment plants, NPS pollution comes from diffuse sources. Some examples of NPS pollution include fertilizers and

pesticides from agricultural and residential areas, oil and other toxic chemicals from urban runoff, sediments from eroding streambanks, bacteria or nutrients from livestock and pet wastes, and atmospheric deposition (Hagedorn et al., 1999; Niraula et al., 2013).

NPS pollution may result in significant environmental and ecological problems. High concentrations of nitrogen and phosphorus may cause toxic algal blooms and oxygen deficiency, and the water may not be suitable for drinking and commercial use (Niraula et al., 2013). It may also cause fish kills, and loss of biodiversity in the aquatic ecosystem (Ma et al., 2011; Niraula et al., 2013). In the U.S., several areas, including the Great Lakes and Chesapeake Bay, have been identified as phosphorus sensitive water bodies, where eutrophication has remained a problem for decades (Daniel et al., 1998). Sediments are another type of NPS pollutant which come from both natural and anthropogenic sources (Poleto et al., 2009). Large amount of sediments can be produced by soil erosion in natural areas and by construction activities in urban area (Poleto et al., 2009). High levels of suspended sediments in water cause negative biological responses in fish and shellfish (Wilber et al., 2001), and these sediments can be vectors for varieties of toxic organic and inorganic constituents (Poleto et al., 2009).

The control of NPS pollution is most effective and cost-efficient when critical controls are applied to areas that contribute the highest yields within a watershed (Pionke et al., 2000). These areas are commonly named Critical Sources Areas (CSAs) and frequently occupy only a small fraction of the area of a watershed. To meet a TMDL, or other management goals, the implementation of BMPs on CSAs is expected to provide maximum benefits for a given level of resource investment. Therefore, it is important to identify CSAs before setting up a BMP implementation plan.

1.3 Watershed Hydrology

The watershed is the geographic area that contributes to the flow into a stream (Bonan, 2015). This flow is what carries NPS pollutants to the stream and therefore, understanding the hydrologic and nutrient cycles is important to the identification of CSAs. This section summarizes some key components of the hydrologic cycle, the erosion process, and the nitrogen and phosphorus cycles along with some commonly used equations.

1.3.1 Hydrologic Cycle

A watershed can be as large as the Mississippi river basin, or can be a small creek basin of a few square kilometers. Despite size differences, the principles of the hydrologic cycle in such watersheds are the same. Figure 1-1 shows the typical hydrologic cycle in a watershed. Precipitation is the main input of water in the watershed and it may be partitioned into evapotranspiration, plant uptake, infiltration, surface storage, groundwater and direct runoff.

Runoff generation is a key component of the hydrologic cycle as it represents the fastest pathway by which rainfall can reach the outlet of a watershed. At the beginning of a rainfall event, the infiltration rate is typically very high because the soil is not saturated. As the soil absorbs water, its infiltration capacity decreases and may eventually drop below the rainfall rate, especially during long rainfall events. When rainfall rate exceeds the infiltration rate, surface ponding starts to occur, and when the ponded amount exceeds the surface storage, the surface runoff commences (Neitsch, 2011).

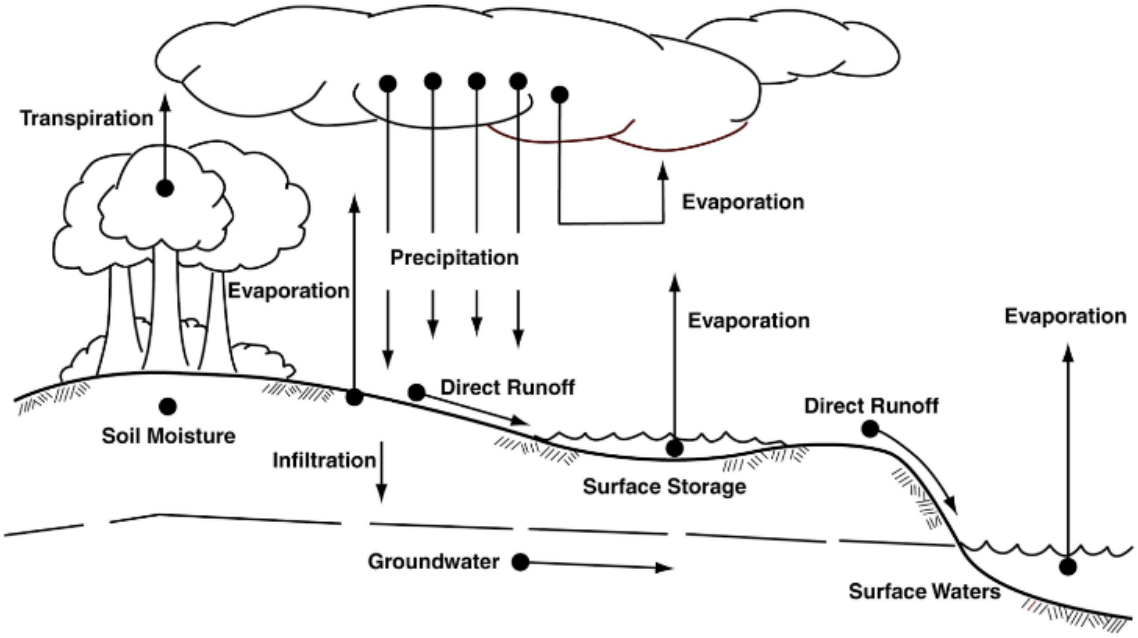

Figure 1-1. The Hydrologic Cycle in a Watershed (Horner, 1994)

There are several approaches to calculate runoff, including the Rational method, Green-Ampt method (GA), Horton's equation, and the SCS-CN methods. The GA and SCS-CN techniques are among the most used in hydrologic modeling and are presented here in some detail. They are best used over relatively homogeneous sub-areas of a watershed, with the results from all sub-areas combined to obtain the runoff from the whole watershed.

The Green-Ampt (GA) method assuming a uniform initial saturation profile, and calculates runoff as a function of soil suction head, porosity, hydraulic conductivity and time. The rate at which these processes occur is governed by several soil factors such as the hydraulic conductivity, effective porosity and wetting front capillary pressure head, which are necessary for the calculation (Rawls et al., 1983). When using this method, interception and soil storage should be estimated from the topography. The GA model is presented in equations (1) and (2) (Neitsch et al., 2011), where the K is Hydraulic

conductivity, φ_f is wetting front capillary pressure head, n is available porosity, t is the time, f and F are the infiltration rate and cumulative depth of infiltration. With this model, surface runoff rate is calculated as R minus f, where R is the current rainfall rate at time t.

$$f = \mathrm{K}\left(1 + \frac{n\varphi_f}{F}\right) \quad (1)$$

$$F - n\varphi_f \ln\left(1 + \frac{F}{n\varphi_f}\right) = \mathrm{Kt} \quad (2)$$

The SCS-CN is another common methods used for predicting runoff. It was developed by the USDA Soil Conservation Service (SCS) in the 1950s, and has the advantage of being much simpler than many other methods (Bosznay, 1989; Neitsch et al., 2011). As a first difference with the GA method, the rainfall intensity and duration are not considered in the SCS-CN, and only the rainfall volume is considered. A second difference is that rainfall abstraction processes, and especially infiltration, is not represented in detail but by a Curve Number (CN), which is calculated from tabulated values based on the hydrologic soil group, land use, and hydrologic condition of the area for which runoff is calculated (Bosznay, 1989). In this model, runoff is generated when rainfall volume is higher than the initial abstraction. A limitation of this approach is that some of the factors that affect runoff generation are not included in the CN, for example, slope and soil moisture would be additional parameters that affect this process. Equations (3), (4) and (5), below, are those normally used for the calculation of runoff in the Curve Number method, where Q is runoff depth, P is precipitation depth, S is the potential maximum soil moisture retention, I_a is the initial abstraction, and CN is the curve number value.

$$Q = \frac{(P-I_a)^2}{P-I_a+S} \quad \text{when} \quad P > I_a \cdots\cdots (3)$$

$$\mathrm{S} = \frac{1000}{\mathrm{CN}} - 10 \cdots\cdots (4)$$

$$I_a = 0.2S \cdots\cdots (5)$$

The GA and SCS-CN methods are sometimes combined when computing runoff over a mixed land-use watershed. In the hydrologic model SWAT (Soil Water Assessment Tool), for example, both methods are used for the calculation. In that model, hydraulic conductivity is taken as a function of curve number for moisture condition II (CN2). SWAT calculates the infiltration amount by the Green-Ampt model using this derived hydraulic conductivity, and the rest of rainfall becomes surface runoff (Neitsch et al., 2011).

1.3.2 Erosion and Sedimentation

Erosion is the detachments and transport of soil particles by the erosive forces of raindrops and surface runoff (Neitsch et al., 2011). The soil surface layer frequently contains high amounts of organic matter and nutrients, which are important for plant growth (Neitsch et al., 2011) and therefore erosion may degrade the soil to a point where crop production is reduced. In addition, the soil particles detached by the process may be transported by runoff into water bodies where, as suspended sediments, they can increase turbidity and hinder aquatic life.

Soil erosion can be calculated using kinetic energy based equations (Brebbia et al., 2008) or simpler methods such as the Modified Universal Soil Loss Equation (MUSLE) (Neitsch et al., 2011). The MUSLE is shown in Equation 6. In this equation, daily soil

sediment yield (tons) is a function of surface runoff Q (mm/ha), peak flow q (m^3/s), soil erodibility factor K (ton·m²·hr/(m³·metric·ton·cm)), a cover factor (C), a practice factor (P), a slope factor (LS) and a coarse fragment factor (CFRG). The equation predicts, as an example, that, for a given amount of runoff and rainfall, high plant cover, low land slope and cohesive soil, result in less erosion than would occur on bare and erodible soil on a steep slope.

$$sed = 11.8 \cdot \left(Q_{surf} \cdot q_{peak} \cdot area_{hru}\right)^{0.56} \cdot K_{usle} \cdot C_{usle} \cdot P_{usle} \cdot LS_{usle} \cdot CFRG \quad \text{..... (6)}$$

1.3.3 Nitrogen Cycle

Nitrogen is an important and essential element for plant growth, and almost 95% of total N in soil is in the soil organic matter (Neitsch et al., 2011). Nitrogen is normally applied to soil by fertilizer, manure, fixation processes, and atmospheric deposition (Neitsch et al., 2011). Within the soil, nitrogen undergoes a variety of processes, including mineralization, plant uptake, denitrification, nitrification, and volatilization (Neitsch et al., 2011). The processes form a complex cycle where the compound may be found as nitrate, nitrite and ammonium, in mineral and organic forms. The rates at which transformations from one form to another take place depend on soil moisture, temperature, carbon source, and nitrogen concentrations, among others (Neitsch et al., 2011). In a quantitative model, some of these processes would be expressed by empirical formulas with simplified rate coefficient.

Figure 1-2 shows the nitrogen cycle in a typical hydrologic and water quality model (SWAT) where five nitrogen pools (white circles) are considered. In the model,

both organic and mineral N can enter surface runoff in many ways. Additionally, the nitrate form of nitrogen is very susceptible to leaching due to its negative charge. It may enter surface flow and shallow aquifers, and be further transported into the main channel or deeper groundwater (Neitsch et al., 2011). Organic N attached to soil particles may be transported to the main channel by surface runoff, in which case its yield is a function of sediment yield (Neitsch et al., 2011). In addition, nitrate and ammonium from wet deposition may enter surface runoff directly during rainfall (Neitsch et al., 2011). All of these nitrogen species, together, constitute the total nitrogen in the watershed.

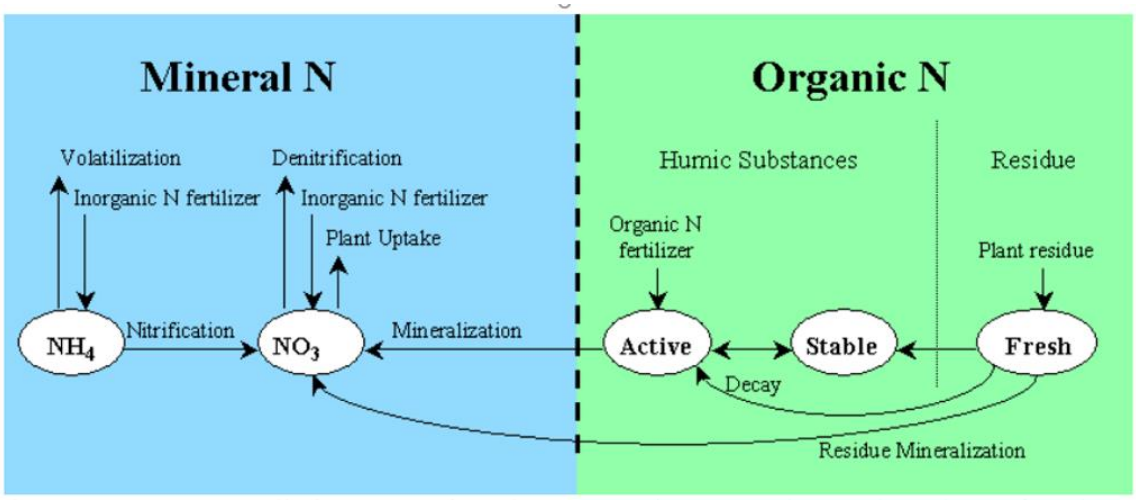

Figure 1-2. The Soil Nitrogen Processes in SWAT Model

1.3.4 Phosphorus Cycle

Phosphorus is another important plant nutrient and potential pollutant. Due to long term application of phosphorus as fertilizer, a high level of phosphorus has become a significant issue in many areas of the US, including the Great Lakes and Chesapeake Bay (Daniel et al., 2008). Figure 1-3 depicts the phosphorus cycle as conceptualized in a water quality model (here: SWAT). Phosphorus may be added to the soil by fertilizer,

manure and residue application, and its removal is normally by plant uptake and erosion (Neitsch et al., 2011). Phosphorus is not highly mobile, unlike nitrate-nitrogen, so the phosphorus would more easily combine with other particles, and be removed from soil surface by surface runoff (Neitsch et al., 2011). For the soluble phosphorus, only the soluble phosphorus in the top soil layer commonly interacts with the surface runoff (Neitsch et al., 2011).

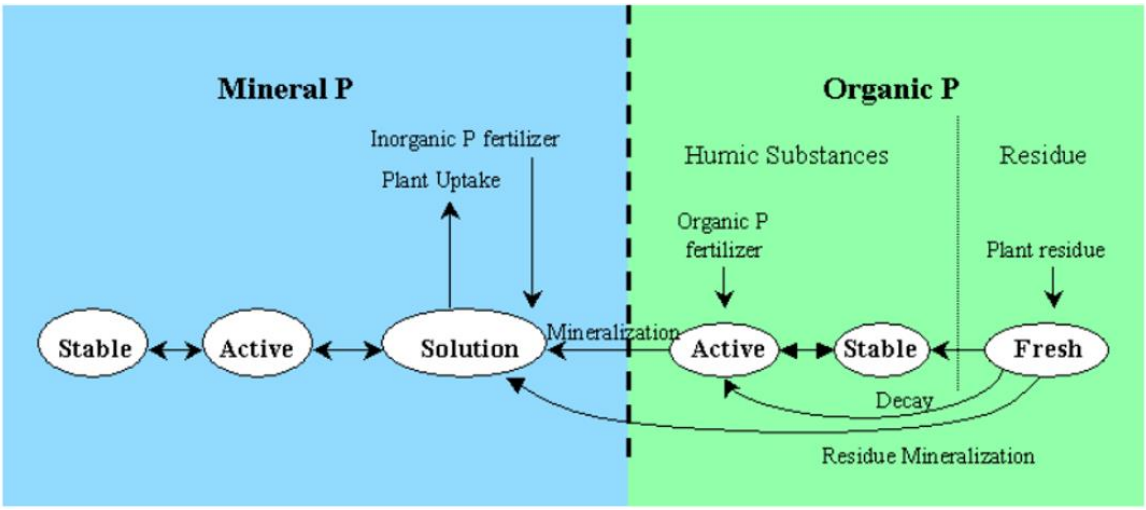

Figure 1-3. The Soil Phosphorus Processes in SWAT Model

1.3.5 Summary

The hydrologic cycle, erosion, the nitrogen cycle and the phosphorus cycle interact with land management and topography to create CSAs in a watershed. The spatial variability of land uses and soils, among others, generates a commensurate spatial variability in runoff, sediment and nutrient yields that affect the distribution and extent of CSAs. Excessive fertilizer application on bare, relatively impervious and erodible soil located on a steep slope, for example, would be a worst-case combination for runoff, sediment and nutrient export that, in a mixed land-use watershed, would most likely be

flagged as a CSA. Other combinations may also produce CSAs and identifying them, within a watershed, requires the quantification of constituent generation processes and taking into account the spatial variability of conditions in the watershed.

1.4 Water Quality Assessment and Models

1.4.1 The Development of Hydrological Modeling

In the United States, the idea of water quality assessment by modeling can be traced back to an analysis performed in the 1920s on pollution and natural purification of the Ohio River (Streeter, 1926), while modern modeling, using computers, started in the 1960s (Ambrose et al., 2009). Regulations were important drivers for water quality modeling, in particular, the Clean Water Act amendments of the 1956 Federal Water Pollution Control Act, voted in 1972, 1977, 1981, and 1987, which addressed environmental risks at the watershed scale (Ambrose et al., 2009). These spurred the development of watershed models such as the Hydrologic Model (HYMO) in the 1970s, and its many descendants, including the Hydrologic Simulation Program- Fortran (HSPF), the Simulator for Water Resources in Rural Basins (SWRRB) in 1980s, the Soil and Water Assessment Tool (SWAT) in the 1990s and the Storm Water Management Model (SWMM) (Huber & Roesner, 2012; Williams & Hann, 1972; Ambrose et al., 2009; Arnold et al., 2012). Government agencies, including the US Environmental Protection Agency (EPA), US Army Corps of Engineers' Hydrologic Engineering Center (HEC), National Oceanic and Atmospheric Administration (NOAA) and the US Department of Agriculture (USDA) contributed to these developments, along with researchers in academic institutions (Ambrose et al., 2009). Today, the application of

water quality models is recognized as an important tool that can provide insights into decision-making processes and Total Maximum Daily Load (TMDL) processes.

Hydrologic models can be categorized based on their spatial and temporal bases and on the type of environments for which they were developed. From a spatial perspective, a model could be one-, two- or three-dimensional, with the choice often a tradeoff between computational efficiency and accuracy. Contemporary models are mostly two-dimensional so that they can consider spatial variability of watershed properties. The MIKE 11 model started off as one-dimensional (Ahmad & Simonovic, 1999) and evolved into the MIKE 3 model that provide 3-D simulation of surface flow, sediment and water quality processes (Liungman & Moreno-Arancibia, 2010). From a temporal perspective, models can be event-based or continuous. Event-based models operate over a single runoff event during a period of hours or days, and require accurate initial conditions. Continuous models operate over years or decades, typically performing predictions on a daily basis, or coarser, and are commonly started by a warming period in which initial condition can be either known or assumed. The most common application environments for a model are urban and agricultural. SWMM, for example, is more widely used in highly urbanized area, while HSPF is more focused on nutrient and pesticide transport (Ambrose et a., 2009; Sun et al., 2014). SWAT emphasizes the agricultural environment, but is also good at managing complex watersheds with mixed land use (Ambrose et al., 2009).

As model use evolved to consider more comprehensive environments, both spatially and temporally, data preparation became increasingly important. As a result, data preparation assistant tools, like the EPA BASINS (Better Assessment Science

Integrating point & Non-point Sources), were developed to provide Geographical Information System (GIS) integration and ease the process. These tools also help in post-processing simulation results to aid in watershed management and TMDL development, and can provide a choice of surface water models, and ecological response models to use (Ambrose et al., 2009).

1.4.2 Introduction to SWAT

SWAT is a comprehensive basin model supported by the US Department of Agriculture (Arnold et al., 2012). The development history of SWAT is shown in Figure 1-4. SWAT was a direct outgrowth of the SWRRB model, in which additional models, including QUAL2E and CFARM, were included (Arnold et al., 2012; Abbaspour, 2015). SWAT considers a large amount of adjustable parameters, which can complicate model parameterization and calibration, but enhances its ability to represent complex landscapes (Arnold et al., 2012).

SWAT is a process based, continuous model, that operates on a daily step (Arnold et al., 2012; Ambrose et al., 2009). Model components include weather, soil, plant growth, land management and pesticides, among others, where most parameters can be adjusted (Arnold et al., 2012; Abbaspour, 2015). In SWAT, a watershed is divided into sub-watersheds, and then areas within each sub-watershed with the same land use, soil characteristics, slope and management are identified as Hydrologic Response Units (HRUs), which is the smallest computational unit used in the model (Arnold et al., 2012). The Soil Conservation Service Curve Number method (SCS-CN) or the Green-Ampt (GA) method can be used for calculating runoff volume (Ambrose et al., 2009). The

Modified Universal Soil Loss Equation (MUSLE) is used for calculating sediment yield (Arnold et al., 2012). For nutrients, all processes of the nitrogen and phosphorus cycles are simulated (Ambrose et al., 2009). Although SWAT is a 2D model, some third dimension variables, such as soil depth and groundwater depth, are included as well in the computations (Ambrose et al., 2009).

The operation of SWAT is similar to that of other hydrologic models, such as HSPF for example, where model parameters need to be calibrated before modeling. The first step in this process is to select the most sensitive parameters, or key parameters, by expert judgment or sensitivity analysis (Arnold et al., 2012).The second step is the actual calibration process, where the selected model parameters are adjusted so that the model accurately predicts a set of observations. The process can be time consuming and it is recommended to calibrate different variables separately, starting with runoff, because its accurate calibration is important for the calibration of the other processes (Arnold et al., 2012). Statistical criteria for goodness of fit, including the Nash-Sutcliffe Efficiency (NSE) coefficient and the coefficient of linear correlation, are used to identify if the model is sufficiently calibrated and validated. At the end of the process, it is also necessary to check the adjusted parameter values to verify that they are physically meaningful, as there is no automatic procedure that can substitute for physical knowledge (Arnold et al., 2012). Once calibrated, the model can be used for predictions and other uses.

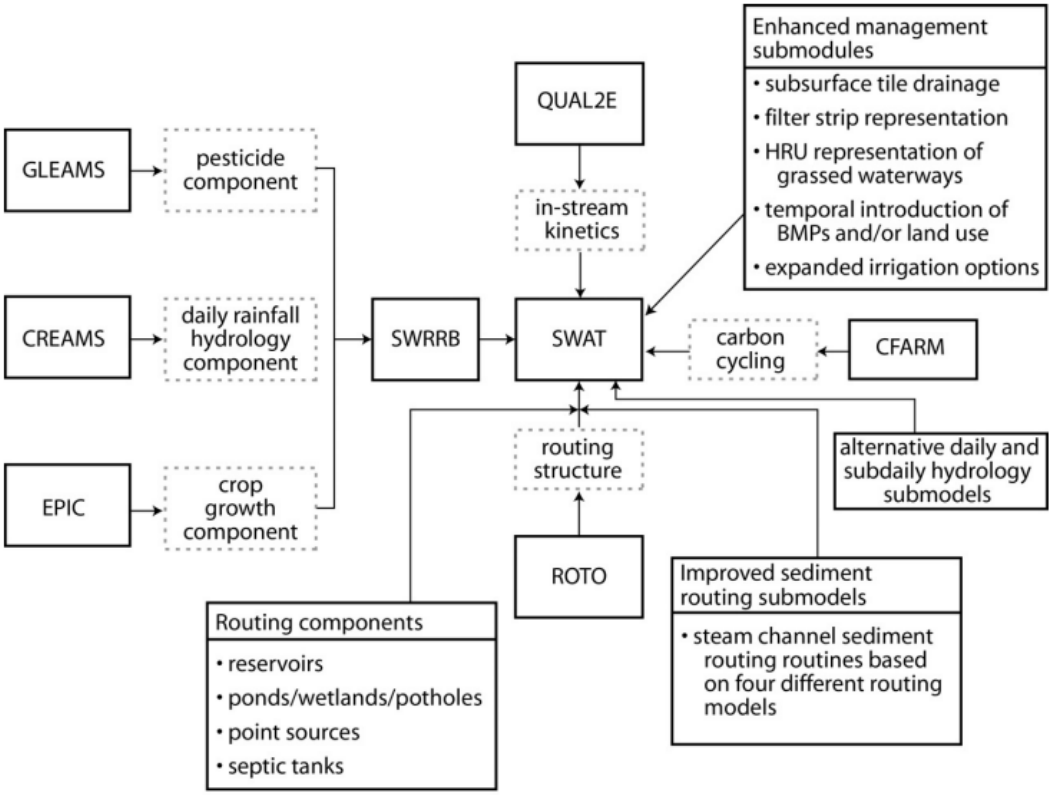

Figure 1-4. Development History of SWAT (Arnold et al., 2012)

1.4.3 Comparison of SWAT and HSPF

HSPF is a widely used hydrologic model for water quality assessments. Like SWAT, its use entails, at first, dividing a watershed into several sub-watersheds, but these sub-watersheds are then divided into pervious and impervious areas rather than HRUs (Mostaghimi, 2003). This simplification may make HSPF more computationally efficient than SWAT, which is important for large watersheds, but also less accurate in smaller watersheds. A few studies, that compared SWAT and HSPF are summarized here.

Nasr et al. (2003) compared the predictions of SWAT and HSPF on an agricultural catchment in Ireland. Their results indicated that SWAT and HSPF were both good at

predicting water volume and total phosphorus. They further reported that HSPF could predict better peak events for water volume than SWAT for their conditions.

Singh et al. (2005) simulated stream flow in the Iroquois River Watershed using both SWAT and HSPF. Their results indicated that both SWAT and HSPF provided good predictions on daily, monthly and annual bases, and that SWAT performed slightly better statistically than HSPF.

Mostaghimi et al. (2003) simulated the hydrology of an urbanizing watershed, Polecat Creek watershed in VA, using both SWAT and HSPF. Their results indicated that HSPF simulated hydrology and water quality slightly more accurately than SWAT. They also noted that SWAT was easier to use and more user-friendly than HSPF. This perspective was shared by other researchers who considered that SWAT made model implementation easier than HSPF (GLC, 2006).

The relative ease with which SWAT can be applied is partially due to the many extensions that have been developed for it over the years. For example, the SWAT Calibration and Uncertainty Program (SWAT-CUP) can be used for calibration and sensitivity analyses, and the ArcSWAT program can be used to format SWAT input data files directly from external sources using a GIS interface. This convenience, combined with a predictive accuracy comparable to that of HSPF, have contributed to the success of SWAT in the past decades.

1.4.4 Studies on CSAs

NonPoint Sources (NPS) of pollution are harder to identify than point sources because they are spatially extended and temporally intermittent (Niraula et al., 2013).

However, it has been observed that most of the times, only a small fraction of the area of a watershed contributes disproportionately to its pollutant yield (Niraula et al., 2013; White et al., 2009). The corresponding areas are called Critical Source Areas (CSAs) and have become easier to identify with the help of hydrologic models.

Niraula et al. (2013) identified CSAs in the Saugahatchee Creek watershed using two different hydrological models: SWAT and GWLF (Niraula et al., 2013). Their study area was located in the south US, in the state of Alabama, with an area of 570 km2. Using SWAT, they found that overall combined CSAs representing 6.5% of the watershed area, contributed 26.5% of sediments, 13.9% of total nitrogen and 23.1% of total phosphorus. Using the GWLF model, their identified CSAs occupied 5.6% of the watershed area, and contributed 23.1% of sediments, 12.7% of TN and 16.5% of TP. In other words, CSAs were found to produce 2 to 4 times more potential pollutants than an average watershed area (which would generate a fraction of total yield equal to the fraction of watershed area that it occupies).

Stone Environmental, Inc. identified phosphorus CSAs in the Vermont portion of the Missisquoi river basin (Stone Environmental, 2011). The area of their study watershed was 3105 km2. Their results showed that more than 50% of total phosphorus was generated in 10% of the watershed area, and 74% of total phosphorus was generated in 20% of the study area. Their CSAs produced between 3.5 and 5 times more phosphorus (per unit area) than the watershed average.

White et al. (2009) identified CSAs in six different watersheds in Oklahoma. The smallest watershed was 720 km2 and the largest was 1970 km2. Their results showed that, on average, the top 5% of watershed area contributed 50% of sediment yield and

34% of total phosphorus, which is between 7 and 10 times the per-area average for their watersheds.

Renkenberger et al. (2015) used SWAT to identify CSAs in an agricultural watershed on the eastern shore of Maryland. Their study area was the Greensboro watershed which is approximately 298 km2. Their results showed that 21% of the area contributed 31% of total runoff, 18% of the area contributed 46% of total suspended solids, 11% of the area contributed 31% total nitrogen and 13% of the area contributed 39% of total phosphorus. In other words, CSAs contributed between 1.5 and 3 times as much runoff, sediment and nutrients, per area, than average.

The takeaway from these studies is that CSAs have a high yield/area ratio, which means a high efficiency if remediation measures (BMPs) are implemented there as opposed to other areas of the watershed. If these areas are targeted, and BMPs are implemented there, water quality may be protected at a lower cost. Therefore, CSA identification is an important step in water quality improvement strategies for NPS pollution, prior to further management or regulatory decisions.

The identification of CSAs within a watershed requires at least a two-dimensional model so that spatial variability can be adequately represented. Assessing the impact of climate change on CSAs requires time scales in excess of decades which makes a continuous model more appropriate than an event-based one.

1.5 Climate Change Research

Climate data, including precipitation and temperature, play important roles in hydrological modeling. Rainfall drives hydrologic processes and temperature modulates chemical and biological processes through which potential pollutants are transformed.

Changes in climate are expected to produce modifications in watershed responses and commensurate changes in the results of hydrologic simulation of these watersheds. Future climate will depend not only on the response of the Earth system to changes in radiative forcing, but also on human responses in technology and policy (Moss et al., 2010). Climate models are used to predict possible future conditions based on these factors.

1.5.1 Global Climate Models and IPCC

The Intergovernmental Panel on Climate Change (IPCC) is the international organization that leads the assessments of climate change. It was set up in 1988, with the purpose of understanding the risk of human caused climate change and its potential impacts. In 1990, the first IPCC assessment report underlined the importance of human caused climate change, and a working group in the World Climate Research Program (WCRP) established the first phase of the Coupled Model Intercomparison Project (CMIP), which defined a standard method for studying the output of global Atmosphere-Ocean General Circulation Models (AOGCMs) (LLNL, n.d.). Climate forcings, such as atmospheric carbon dioxide concentration, could be adjusted in the CMIP AOGCMs to generate a variety of future climate scenarios, and the corresponding outputs were to be used to evaluate the potential impacts of policy decisions in a variety of sub-projects (LLNL, n.d.).

1.5.1.1 CMIP3 and SRES

Ten years after the phase 1 of CMIP, the working group collected the outputs from leading climate research centers around the world, and, in 2007, summarized them as a part of the phase 3 of the Coupled Model Intercomparison Project (CMIP3). In CMIP3, a set of standardized scenarios of future socio-economic development were applied to generate future climate forcings (LLNL, n.d.). In total, 23 models were created by more than ten countries and the resulting dataset provided for hundreds of peer-reviewed papers, and also played an important role in the IPCC 4th Assessment Report (Taylor et al., 2012).

The three major development scenarios in CMIP3 (A1B, A2 and B1) were described in a Special Report on Emissions Scenarios (SRES) and represent three future pathways for human activities (Houghton et al., 2001). Scenario A1B assumes a rapid technical and economic growth in the future, where population would reach a peak in mid-century, and it assumes that future energy sources would not be limited to fossil fuels. Scenario A2 assumes a highly regionalized future where technologic and economic growth are slowed due to the regionalization, and the population would keep increasing. Scenario B1 describes a convergent world, where, as in A1B, the population would reach a peak in mid-century, but due to globalization, the world has more possibilities to introduce clean technologies, which contribute to environmental sustainability. In each scenario, the anthropogenic emissions of CO_2, CH_4, N_2O and Sulphur dioxide were different, resulting in different future temperature and precipitation regimes (Houghton et al., 2001). The left-hand side portion of Figure 1-5 shows the global surface temperatures predicted to year 2100 by the CMIP3 models for the 3 main scenarios (averaged over

individual AOGCMs) (Knutti and Sedláček, 2013). CMIP3 was criticized for not separating anthropogenic and natural influences on climate and for not simulating separately the emission of greenhouse gases, aerosols and chemically active gases (Taylor et al., 2012). The related improvements were performed through phases 4 and 5 of the CMIP.

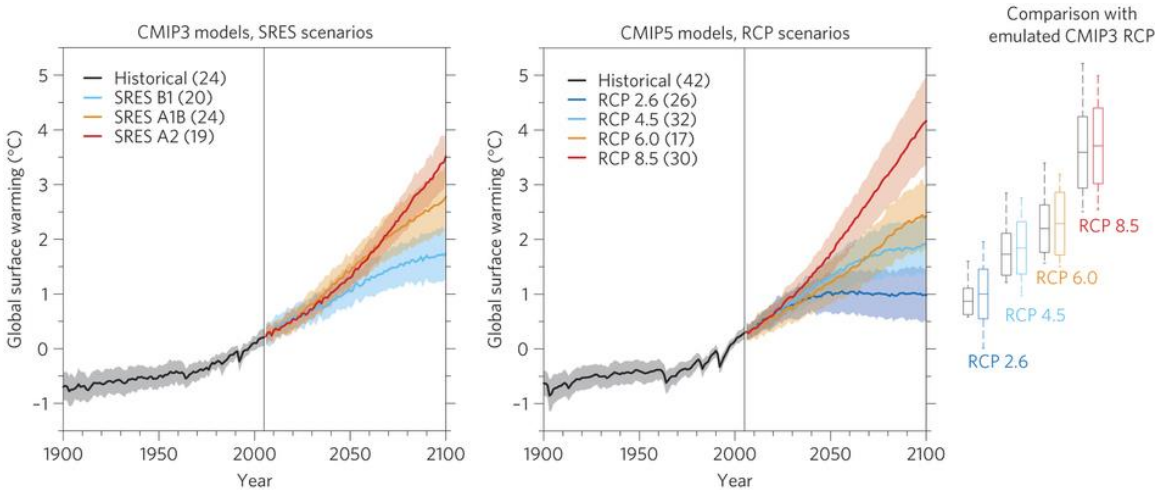

Figure 1-5. The Global Surface Warning Between CMIP3 and CMIP5 Scenarios

1.5.1.2 CMIP5 and RCPs

CMIP5 improved upon CMIP3 by simulating the emission of greenhouse gases, aerosols and chemically active gases, and by setting radiative forcing at year 2100 as the control factor in scenarios, instead of using economic development narratives (CIRC, n.d.). The CMIP5 scenarios are called Representative Concentration Pathways (RCPs) (Meinshausen et al., 2011) and are depicted in Figure 1-6. The four main CMIP5 scenarios are RCP2.6, RCP4.5, RCP6.0 and RCP8.5. For example, the red curve in Figure 1-6 corresponds to scenario RCP8.5, which represents a high emissions future, that would cause radiative forcing to reach approximately 8.5 W/m^2 at the end of 21 century. The RCP6.0 scenario assumes a medium high radiative forcing to 2150, and then

it would keep stable. The RCP4.5 show a medium radiative forcing to 2050, before stability. The RCP 2.6 show a peak of radiative forcing at 2020 at 3.0 W/m^2, and it would decrease to 2.6 W/m2 at 2100; which is also called the RCP3-PD scenario. Although scenarios changed from SRES storylines in CMIP3 to RCPs in CMIP5, the two sets of scenarios remain somewhat related as can be observed by comparing the left- and righ-hand sides of Figure 1-5. Overall, the range of surface warming predicted for RCPs in CMIP5 is slightly larger than for the SRES in CMIP3. RCP 8.5 predicts slightly more warming than SRES A2 and RCP2.6 predicts slightly less than SRES B1.

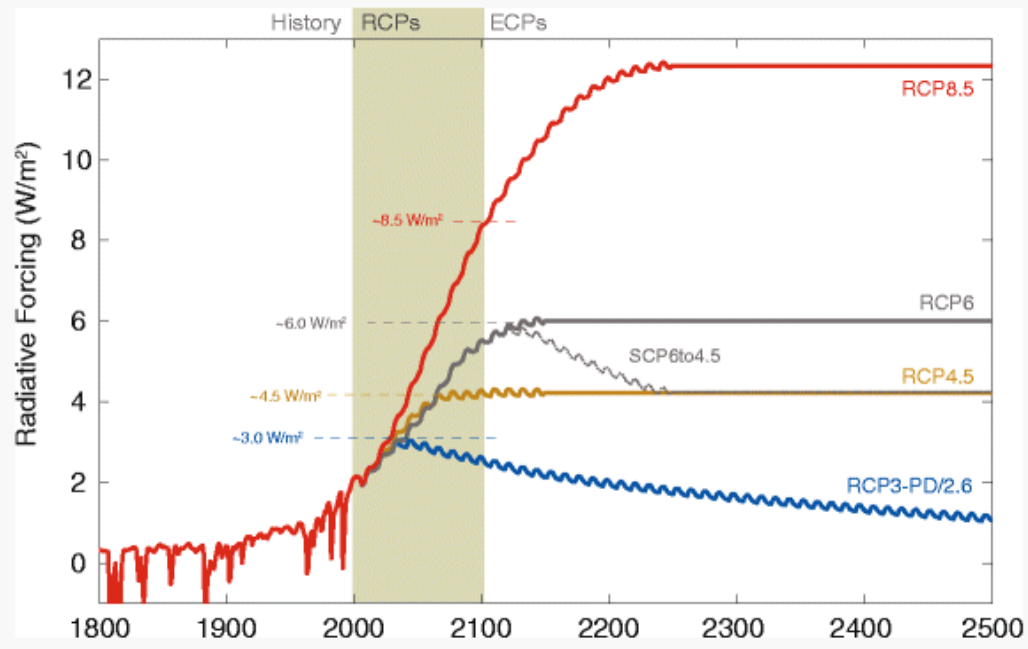

Figure 1-6. Radiative Forcing in Different Scenarios from 1800 to 2500

There were some additional improvements in CMIP5. Over 50 models from more than 20 modeling organizations were collected in CMIP5 (Taylor et al., 2012). The models were more comprehensive in CMIP 5, and were easier to use as well. For example, a project called Coordinated Regional Downscaling Experiment (CORDEX)

was applied to the output of most of AOGCMs to provide regionally downscaled climate data at high resolution (Taylor et al., 2012). Some of the updated CMIP 5 models also simulate the carbon cycle and atmospheric chemistry (CIRC, n.d.). The carbon cycle plays an important role in climate research and climate models, the related details will be presented in section 1.5.2.

1.5.1.3 Summary of GCM

CMIP3 data were released in 2007, and CMIP5 data were released in 2013. Therefore, the CMIP5 represents the latest climate change dataset at this time. The next generation, IPCC 6th assessment report will start in late 2017 and complete at the end of 2020. Due to the huge success achieved with CMIP3 on the 4th assessment report, CMIP3 is more widely applied than CMIP5 projects. For example, a website from TAMU allows researchers to download bias-corrected and downscaled datasets for nine CMIP3 models in SWAT input file format, for a given time period and location. CMIP5 datasets are not currently available on the TAMU's website for SWAT users and hence their use requires additional pre-processing (describe below in section 1.5.3).

As shown in Figure 1-5, future climate predictions vary substantially between AOGCMs and between scenarios but all models agree to an increase in global temperatures. Figure 1-7 maps averages of CMIP5 predictions of temperature and precipitation (for all available models and RCPs) over a 20-year interval at the end of 21st and 22nd centuries (Collins et al., 2013). The main trends in these predictions are for a world that is warmer in all areas but where some locations become wetter and others drier. For the United States, the northeast would have more precipitation, while the

southwest would become drier (Collins et al., 2013; NOAA, 2015). Precipitation intensity is also expected to increase in the northeast (Knutson et al., 2013).

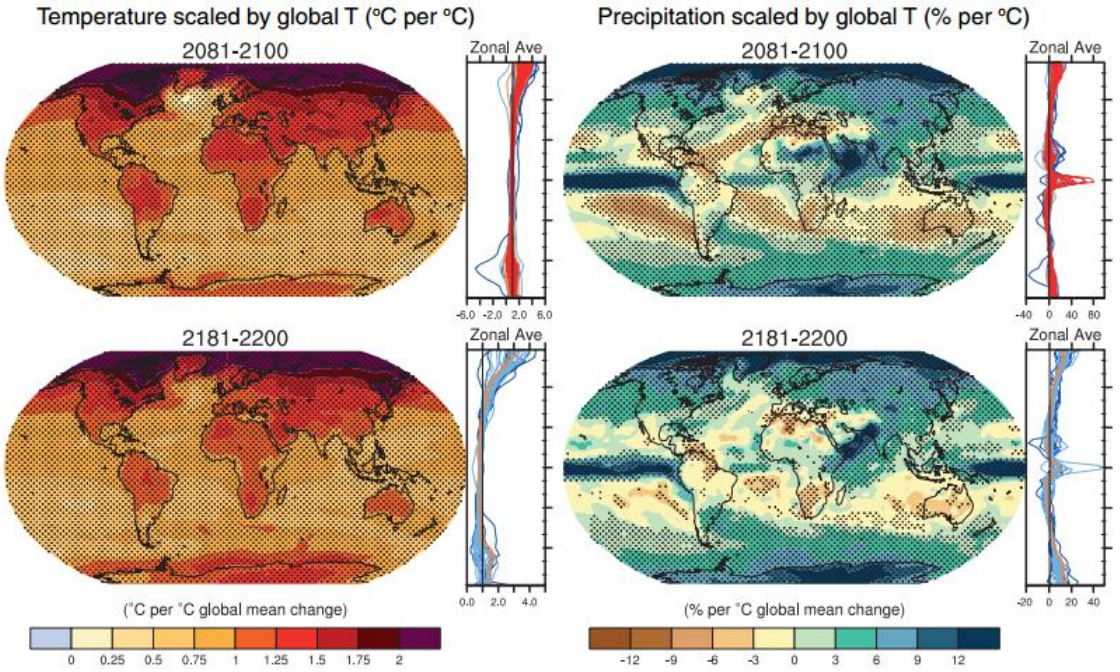

Figure 1-7. Global Temperature and Precipitation at the End of 21 and 22 Century

1.5.2 Carbon Cycle

Carbon dioxide is one of the main driving forces behind climate change. The global carbon cycle is depicted in Figure 1-8 which shows the relationships among carbon pools in the atmosphere, oceans and land biosphere (Solomon, 2007). In the figure, numbers in black indicate preindustrial levels, and red numbers indicate changes in those levels as of the 1990s. Fossil fuel burning is the main terrestrial source of atmospheric carbon. Part of this release is absorbed by the ocean, but the remainder stays in the atmosphere, and causes an increase of atmospheric carbon dioxide concentration. Furthermore, CO_2 emissions have increased by 80% between 1970 to 2004, and emissions of all greenhouse

gases have increased by approximately 70% which exacerbates the problem (Klein et al., 2008).

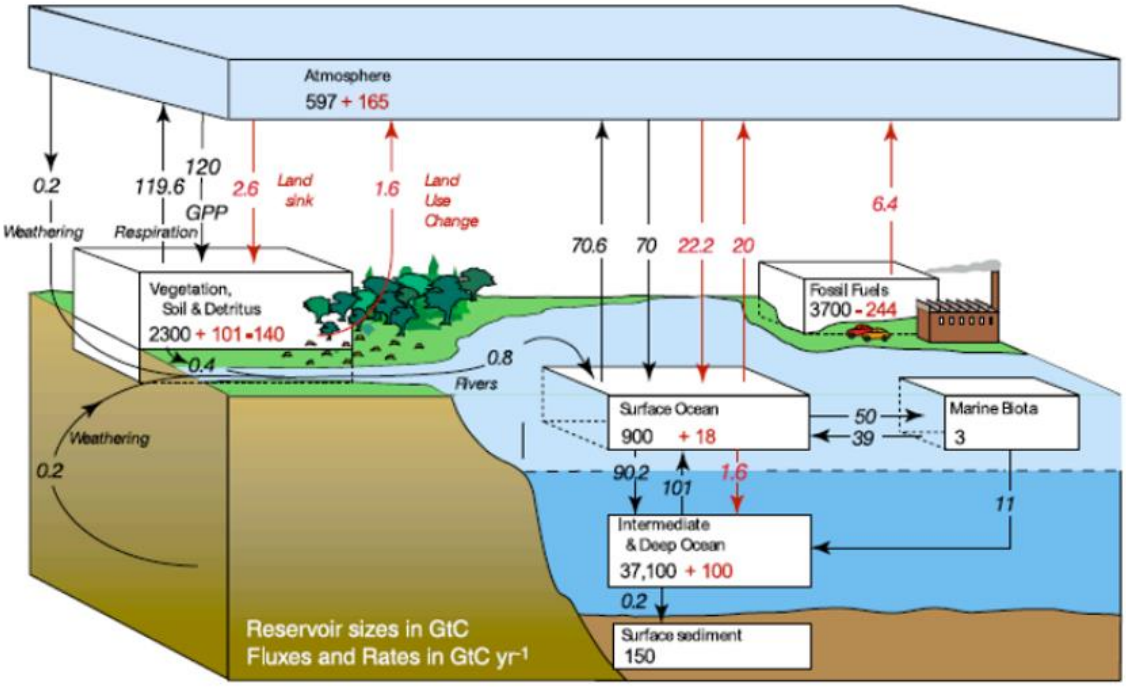

Figure 1-8. Components in the Global Carbon Cycle

The CMIP3 AOGCMs were driven by two carbon cycle models that used different mathematical formulations for the cycle's sub-components: BERN and ISAM. More specifically, the CCCMA-CGCM3.1, CNRM-CM3, IPSL-CM4 and MIROC3.2-medres models used the BERN model, and the GFDL-CM2.1 and MRI-CGCM2.3.2 used ISAM (IPCC, 2014). The predictions of BERN and ISAM were functions of SRES scenarios and are presented in Figure 1-9. The atmospheric CO_2 concentrations predicted by the models at year 2100 ranged from 500 to 900 ppm across the SRES scenarios. The difference in predicted CO_2 levels between scenarios are much larger than the difference between the two carbon cycle models for a given scenario, which means that, despite

their different formulations, the uncertainties between ISAM and BERN models were quite small.

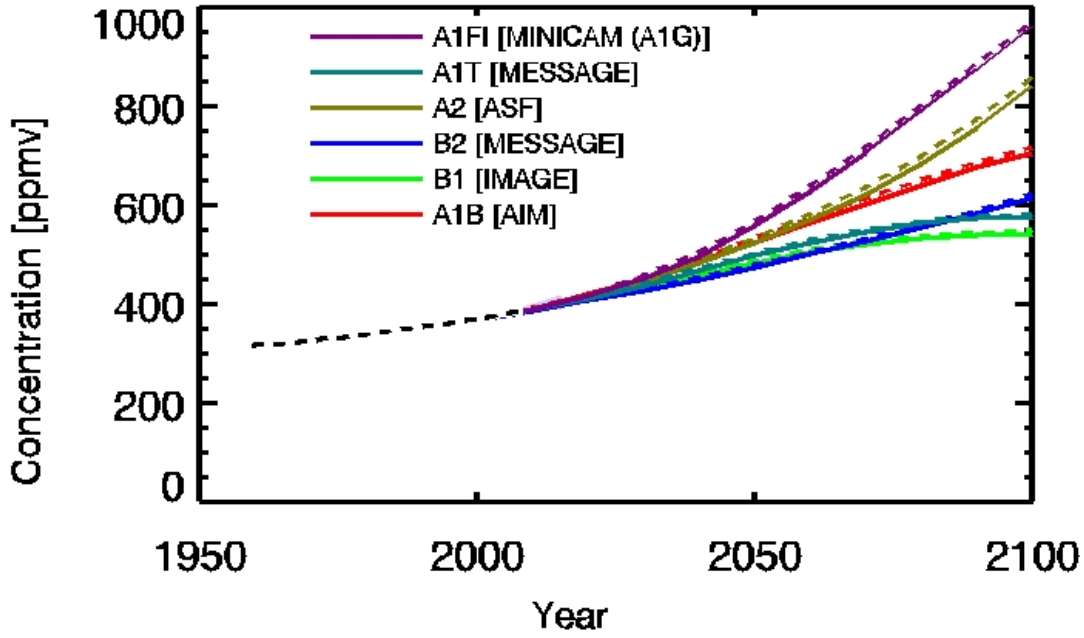

Figure 1-9. CO_2 Concentration from BERN and ISAM in Different CMIP3 Scenarios

In CMIP5, Representative Concentration Pathways (RCPs) were based on multi-gas emission scenarios from the literature and Earth System Models were used to adapt the rate at which carbon is removed from the atmosphere (eg. by vegetation) as a function of CO_2 concentration (Meinshausen et al., 2011). The result of these analyses was summarized by the Potsdam Institute for Climate Impact Research into one set of emission and concentration data for all AOGCMs to use (Meinshausen et al., 2011). The corresponding atmospheric CO_2 concentration data for the 4 main RCPs are shown in Figure 1-10 (PIK, n.d.) and, at year 2100, have a range of approximately 400 to 950 ppm, which is slightly briader than that used in CMIP3.It is also notable that in RCP2.6, CO_2

concentration reaches a peak near year 2050 and decreases slightly afterwards; a phenomenon that was not considered in CMIP3.

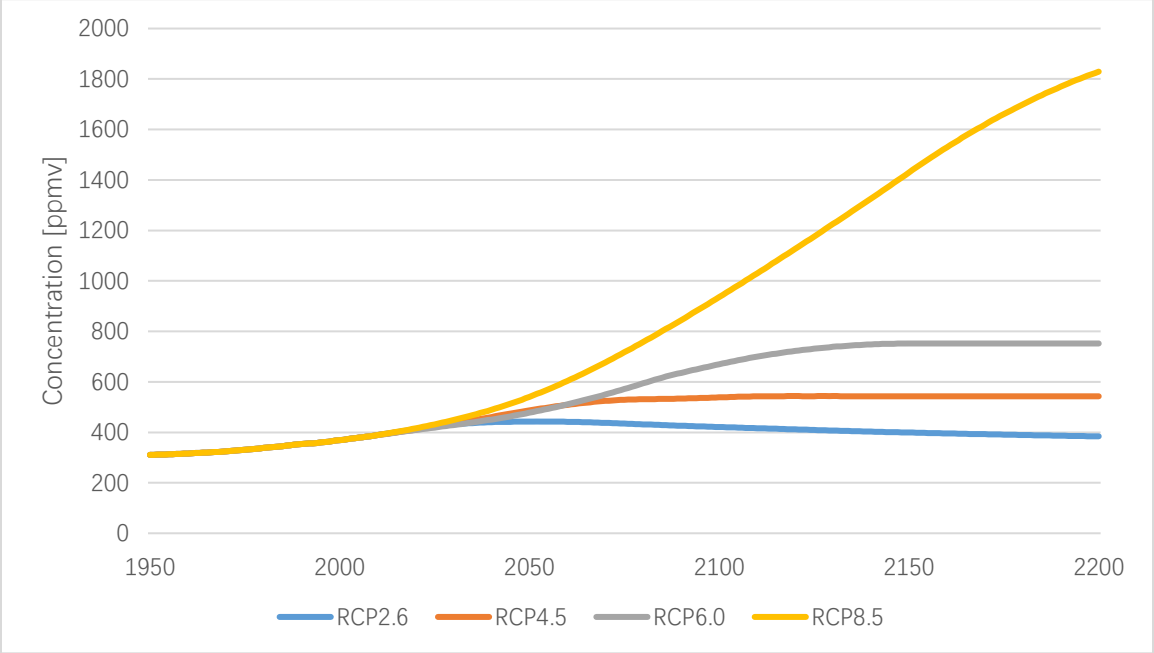

Figure 1-10. CO_2 Concentration in Different CMIP5 Scenarios from 1950 to 2200

1.5.3 Downscaled Climate Projections

AOGCMs predict future climate at a global scale that is not suitable for detailed hydrologic modeling at the watershed scale. Two major preparation steps are needed to transform these predictions into useable data: 1) downscaling, and; 2) bias correction.

1.5.3.1 Downscaled Data

Programs aimed at downscaling AOGCM predictions for hydrologic use started in 2007 (Brekke et al., 2013) and have resulted in several downscaled databases for both CMIP3 and CMIP5. The approaches are aimed at producing weather time series, with a spatial and temporal scale suitable for detailed hydrologic modeling, from the outputs of AOGCMs. Two major techniques were developed for this purpose: 1) the monthly Bias-

Correction and Spatial Disaggregation (BCSD), and; 2) the daily Bias-Correction and Constructed Analogs (BCCA) method (Brekke et al., 2013). The BCSD results in monthly mean values, which can be used for comparative analyses directly. The BCCA produces mean daily values, and is best suited for hydrology modeling with a daily time step.

In the latest CMIP5 dataset, quality assurance techniques were applied to the development of downscaled projections, and therefore, not all climate models were collected in the BCSD and BCCA CMIP5 Projection Ensembles (Brekke et al., 2013). One reason for quality issues, and exclusion from the ensembles, was a sensitivity to initial conditions in some of the models whereby small changes would produce widely different downscaled outputs in at least one scenario (Brekke et al., 2013).

1.5.3.2 Bias Correction

Bias correction is used to ensure that downscaled AOGCM predictions of past weather have the same statistics as observations of that past weather at the downscaling location. It is an important process because the predictions of hydrologic models are generally sensitive to bias in their forcing inputs, especially rainfall (Stocker et al., 2013). Bias-correction is commonly performed by comparing downscaling AOGCM predictions over historical timeframes to the Gridded Observed Meteorological Data, which was produced by the NOAA Cooperative Observer weather stations, and is also referred to as Reanalysis-1 data (Maurer et al., 2002; NOAA, n.d.). There are several bias correction approaches that are widely used. Some of the methods are very simple, such as simple scaling, but others may be very complex. Theoretically, all methods can correct the mean values, and the main difference among them relate to the other statistics, such as standard

deviation or percentiles. Among these methods, the distribution mapping method is the most favored because it can correct most of the statistical characteristics of downscaled predictions and has the smallest standard deviation (Teutschbein & Seibert, 2012). A schematic diagram of the method is shown in Figure 1-11. The daily precipitation is assumed to have a Gamma distribution in time, and the daily mean temperature is assumed Gaussian. The distribution of downscaled simulation data (gray dashed line) is adjusted to fit the observations (black dots) by adjusting the cumulative probability of simulated daily values. The method works well for both precipitation and temperature and has been accepted for correcting downscaled data for the BCCA and BCSD projections (Maurer et al., 2014).

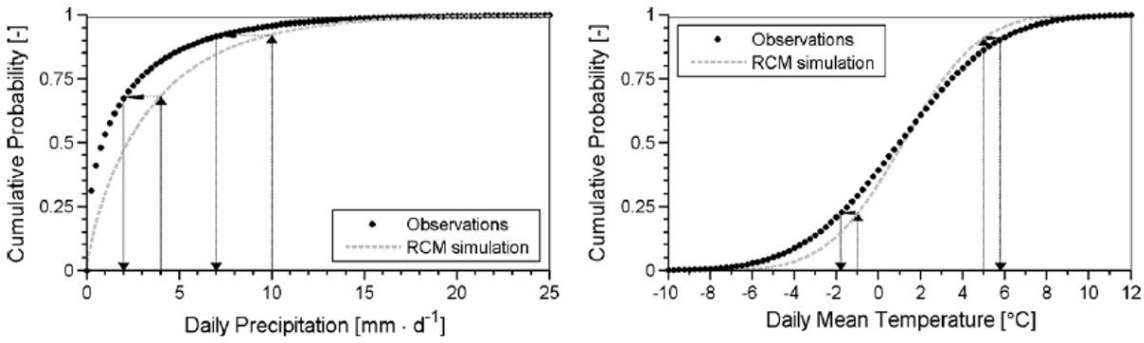

Figure 1-11. The Distribution Mapping Methods on Bias Correction of Daily Precipitation and Temperature.

1.5.3.3 Reanalysis Data

Reanalysis is the process by which weather data observed over an irregularly spaced network of meteorological stations is retrofitted to a synthetic grid with regular spacing. By placing observations on a spatial grid, the reanalysis can present a clearer picture of weather variations around large areas and also helps to produce interpolated

weather time series for arbitrary locations between grid points (NOAA, n.d.). As discussed earlier, the Reanalysis-1 dataset is one of the reanalysis products used to downscale and bias-correct AOGCM predictions. It was established in 1995 with a low horizontal resolution grid spacing of 2.5° in latitude and longitude (Kalnay et al., 1996; NOAA, n.d.). The Climate Forecast System Reanalysis (CFSR) is an updated version of Reanalysis-1, which covers the time period from 1979 to the present, and displays less bias and a smaller root-mean-square (RMS) error in several locations (Bao et al., 2013; NOAA, n.d.). The CFSR data are widely used in recent climate research and have sometimes been recommend for related fields such as hydrological modeling studies (Fuka et al., 2013; Dile & Srinivasan, 2014).

CFSR data help to simplify automated analyses of climate change and hydrology but do not always present advantages over actual weather station data. Roth & Lemann (2016), for example, noted that bimodal rainfalls were underestimated in CFSR data, while unimodal rainfall were overestimated significantly. Hydrologic modeling results were not as accurate with CFSR data than with weather station data in some studies (Roth & Lemann, 2016; Yang et al., 2014). In the paper by Radcliffe and Mukundan (2016), hydrological modeling results with CFSR data were good for one watershed but bad for another watershed. Therefore, reanalysis climate data may be necessary and perform well in some situations and perform poorly in others. Its adequacy to a particular watershed should be evaluated on a case by case basis..

1.5.4 Hydrologic Modeling with Climate Change

Studies of the hydrologic and water quality response of watersheds to climate change have started to appear in the last decade. Jha et al. (2006) performed a climate

change sensitivity assessment of the upper Mississippi river basin using SWAT with 6 CMIP3 AOGCMs and SRES scenario A2, for the end of the 21 century. The study focused on the effects of CO_2, temperature and precipitation on total water yield for the watershed. Their analysis illustrated how future precipitation could vary on a monthly basis for the different models. Under the assumption of 660 ppmv of CO_2, the six models predicted average annual water yields that differed from the historical baseline by -6% to 51% from 2061 to 2090. Their results underlined how the uncertainty in future response predictions can cause difficulties in drawing definitive conclusions on future stream flow impacts.

Schewe et al. (2014) performed a global assessment of water scarcity using five CMIP5 models and 11 global hydrological models. Their study focused on the relationships between global population and water resource. Their results indicated that the global mean temperature would increase by approximately 2 °C (by 2090) and that about 13% of the global population would face a discharge reduction greater than 20% by that time. Under scenario RCP8.5, the southwestern US would face a significant surface and sub-surface water reduction of 10 to 30%. In addition, upon comparisons of the five global climate models used in their study, the authors concludes that climate model uncertainty remained an important concern in hydrological modeling.

Jaeger et al. (2014) used SWAT to model dryland streams of the American Southwest in the Verde River Basin of Arizona, which is nearly 1600 km^2. Sixteen CMIP3 downscaled monthly models were used, and their results indicated that zero-flow days would increase by 27% by the year 2050. In addition, the extent of the river network

was predicted to diminish by an amount between 8% and 20% at early summer, in the future, which would cause significant stress on aquatic organisms.

Molina-Navarro et al. (2014) used SWAT to model the response of an 88 km^2 watershed in central Spain to 11 CMIP3 downscaled monthly models. Results showed that temperature would increase by 1.3°C to 3.9°C, and precipitation would decrease by 2.9% to 11.5%. Their predicted water quantity results showed a noticeable reduction of total flow of 25.8% to 52%. For NO3-nitrogen, the concentration remained the same but the total amount was decreased significantly because of the decrease in discharge. Phosphorus showed a significant increase (near 33%) in concentration, and a 13% increase in total amount in the worst scenario.

Verma et al. (2015) created a SWAT model of the Great Lakes Watershed, and subjected it to three CMIP3 downscaled models of future climate. Their study area was approximately 21500 km^2 in size. Their results showed a 2.9°C increase in temperature and a 3.2% decrease of precipitation from 2045 to 2055. Annual flow, TSS, N-NO3 and TP were predicted to decrease by 8.5%, 10.4%, 8.5%, and 9.9%, respectively, for this period. For the period of 2089 to 2099, the temperature would increase by 4.3°C and the precipitation would increase by 5.6%. Average annual flow, TSS, N-NO3 and TP were then predicted to increase by 9.7%, 19.6%, 3.5%, and 6.8% respectively, over this later period. The authors suggested that lengthening the crop cycles could help meet Total Maximum Daily Load (TMDL) guidelines in this later period where pollutant loadings increased.

Renkenberger et al. (2015) used SWAT and the GFDL AOGCM to evaluate how climate change may impact critical source areas (CSAs) of runoff, sediments, nitrogen,

and phosphorus in a 298 km^2 agricultural watershed of the Chesapeake Bay drainage basin. Yearly precipitation was predicted to increasing by 25 to 30% by the end of century. This resulted in increases of 56%, 79%, 56% and 52% in surface runoff, TSS, TN and TP, respectively. CSAs were predicted to expand substantially under future climate (SRES scenario A2) such that BMPs would be needed over practically the entire watershed to meet current day TMDLs.

El-Khoury et al. (2015) assessed how climate change would impact water quality variables in a 38000 km2 cropland watershed in Canada, using the Canadian Regional Climate Model 4.1, and SRES scenario A2. Climate change was predicted to result in increases of minimum and maximum temperatures of 1.21 and 1.55 °C at mid-century, along with an increase in precipitation of 3.5%. Their hydrologic modeling results showed an increase of 11.2% in annual streamflow while total nitrogen decreased by 20%, and total phosphorus increased by 28% in response to climate change.

Overall, the above studies demonstrated that climate change can have a significant impact on the hydrologic and NPS pollution response of a watershed at its outlet, and also on the spatial extent of CSAs. Predictions may however vary depending on the AOGCMs used to model future climate and it is important to consider this uncertainty in the related analyses.

1.6 Objectives

The goal of this study is to quantify how climate change is expected to affect the hydrologic and NPS pollution response of a suburban watershed in Maryland, and in particular, how it may affect the location and size of CSAs. The specific objectives are:

1. Develop a representative model of hydrologic and water quality processes in the study watershed.
2. Assess the impact of climate change on the hydrologic and NPS pollution response of the study watershed, at its outlet, including uncertainty.
3. Determine how climate change may impact the location and size of runoff and NPS pollution CSAs, identified using relative and fixed thresholds, in the study watershed.

The model of the study watershed will be developed using SWAT and calibrated against observed runoff and water quality samples. The predictions of 6 CMIP5 climate change models, over 4 RCP scenarios, downscaled and bias-corrected for the study area, will be used as inputs to the calibrated model to simulate the future response of the watershed, at its outlet, and compare it to that for current weather. Results obtained with individual climate models and scenarios will be compared with one another to assess the uncertainty in the future watershed response. CSAs will be identified at the HRU level from simulation results of current and future climate, using both relative and fixed thresholds. The location and size of CSAs will be compared between future and current weather, and across climate models, to determine how their characteristics may change in the future, and the certainty with which this change can be ascertained.

Results of this study will provide researchers, designers and policy makers a better understanding of how climate change is expected to impact the hydrologic and NPS response of a suburban watershed, in Maryland. The comparisons of multiple climate models will further enhance our understanding of the level of confidence that can be

given to future predictions. Results will also provide guidance on CSA identification techniques and help to identify robust strategies for the development of BMP allocation plans that remain effective at controlling runoff and NPS pollution, or at meeting TMDLs, into a future that involves climate variability.

Chapter 2: Materials and Methods

2.1 Study Area

The study area selected for this study is a small suburban watershed located in the town of Columbia, in Howard County, Maryland. The watershed drains into a man-made drainage reservoir, dug in 1966, and named Wilde Lake. The Wilde Lake watershed is located in the northern part of the Patuxent River basin and its outlet flows into a branch of that river as shown in Figure 2-1. The Patuxent River flows directly into the Chesapeake Bay.

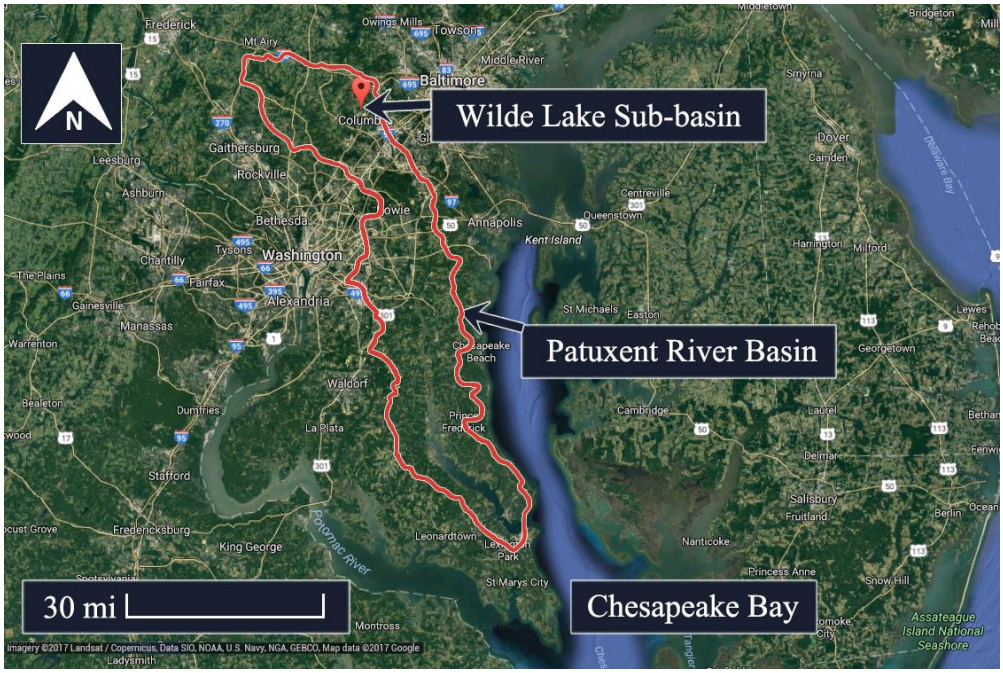

Figure 2-1. Satellite Map of Wilde Lake, Patuxent River and Chesapeake Bay Area

The Wilde Lake watershed has an area of approximately 1.9 square miles and is physically characterized by rolling hills with many woody stream valleys (Adams et al., 1985). The stream habitat was evaluated as poor in most of areas of the watershed, and some areas have severe erosion due to the failure of storm drain infrastructure from

excessive stormwater flows (Adams et al., 1985; CAWM, 2009). In 2007, Howard County started monitoring the watershed using chemical, biological, and physical techniques to aid in potential restoration efforts. The monitoring relied on grab water samples obtained during stormwater events that were analyzed for TSS, nitrogen, phosphorus, and heavy metals. In October 2012, a USGS monitoring station was installed in the watershed, upstream of the Lake, to continuously monitor stream flow, aggregate it on a daily basis and make it available online.

Table 2-1 summarizes various characteristics of the Wilde Lake watershed. Its average slope is relatively large at 7.5% which may favor the generation of surface runoff. Its land cover, however, consists mainly of low-density residential and forested areas, with a relatively low percentage (approximately 14%) of impervious zones, that can favor infiltration overall. The mean erodibility of soil is moderate at 0.3, suggesting that erosion may not be a problem everywhere in the watershed but may rather be localized in areas where the soil is more erodible than average.

Table 2-1. Summary of Wilde Lake Watershed Characteristics

Area (km^2)		5.1
Elevation (m)	Mean	125.06
	Min	90.98
	Max	152.32
Impervious Area (%)		14.5
Land Slope (%)	Mean	7.5
	Min	0.0
	Max	64.9
Dominant Land Use Types		Forest, Low-density Residential
Mean Soil Erodibility		0.3

The topography of the watershed is depicted in Figures 2-2 and 2-3. Elevations increase by approximately 60 meters from southeast to northwest and surface water is

expected to flow (on average) in the opposite direction, from the northwest towards the watershed outlet in the southeast. The land slope is below 5% in most of the watershed but increases substantially near streams where the potential for excess runoff generation and erosion is expected to increase.

Figures 2-4 and 2-5 depict the spatial distribution of land use and soil hydrologic groups in the watershed. The bulk of the watershed is occupied by low density residential land (peach color) and deciduous forest (light green). Medium and high density urban areas (orange and red) are found mainly near the southern boundary of the watershed. The urban areas are generally located where slopes are low while forested zones cover the steeper areas of the watershed. Most of the watershed in underlain by soils of hydrologic group B (blue color) which provides moderate infiltration. Some areas around streams are in hydrologic soil groups C and D which is less pervious and may generate more surface runoff, especially with steep slopes, but this should be partially compensated for by the forested land cover. Soils of hydrologic group D, with very low infiltration rate, are also found near the southeastern, southern and western boundaries of the watershed, under medium or high density residential areas, which may result in large amounts of surface runoff being generated there, despite relatively low slopes.

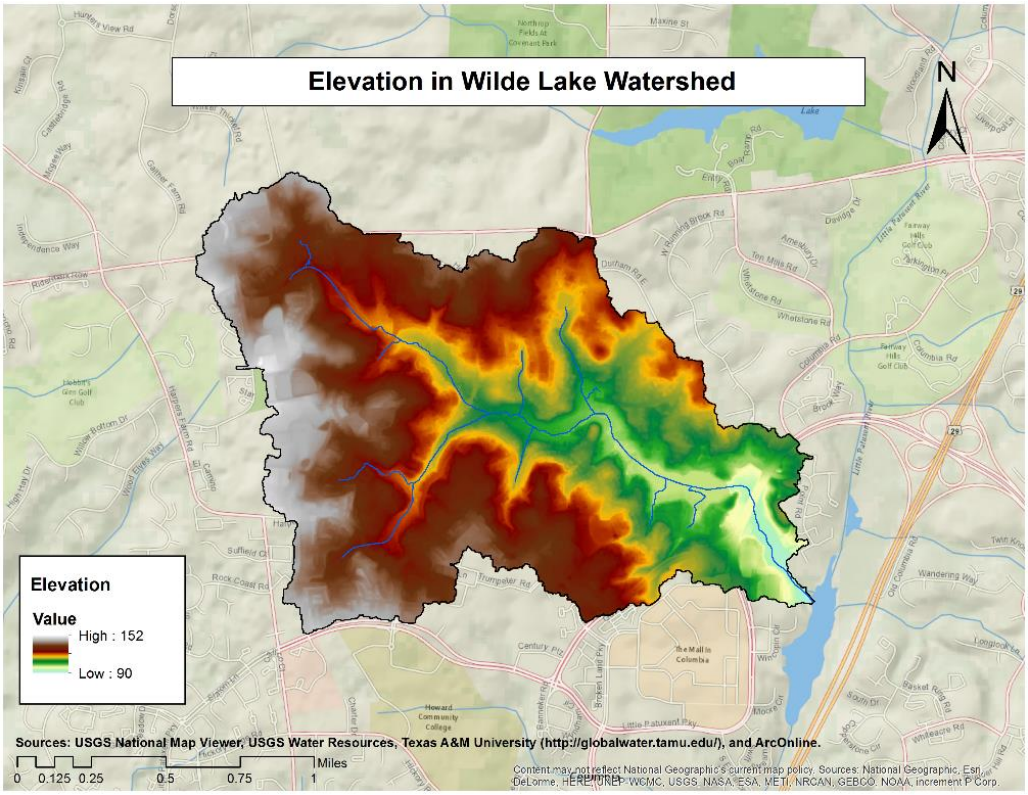

Figure 2-2. Elevation Map of the Wilde Lake watershed

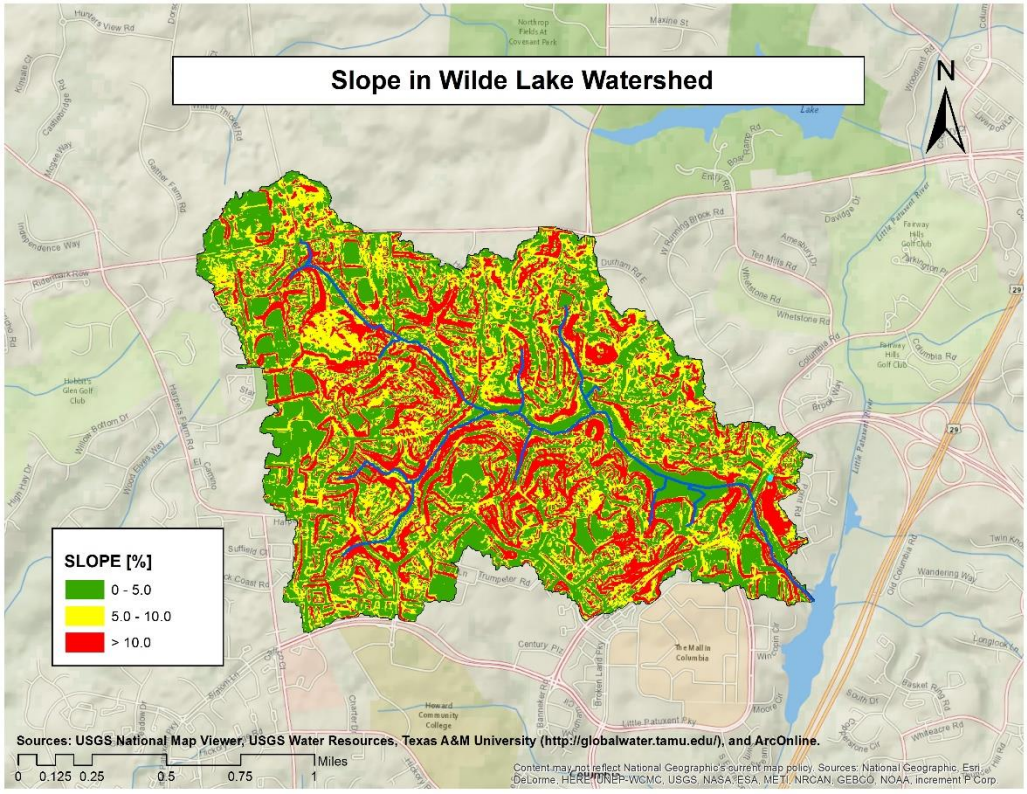

Figure 2-3. Slope map of the Wilde Lake watershed

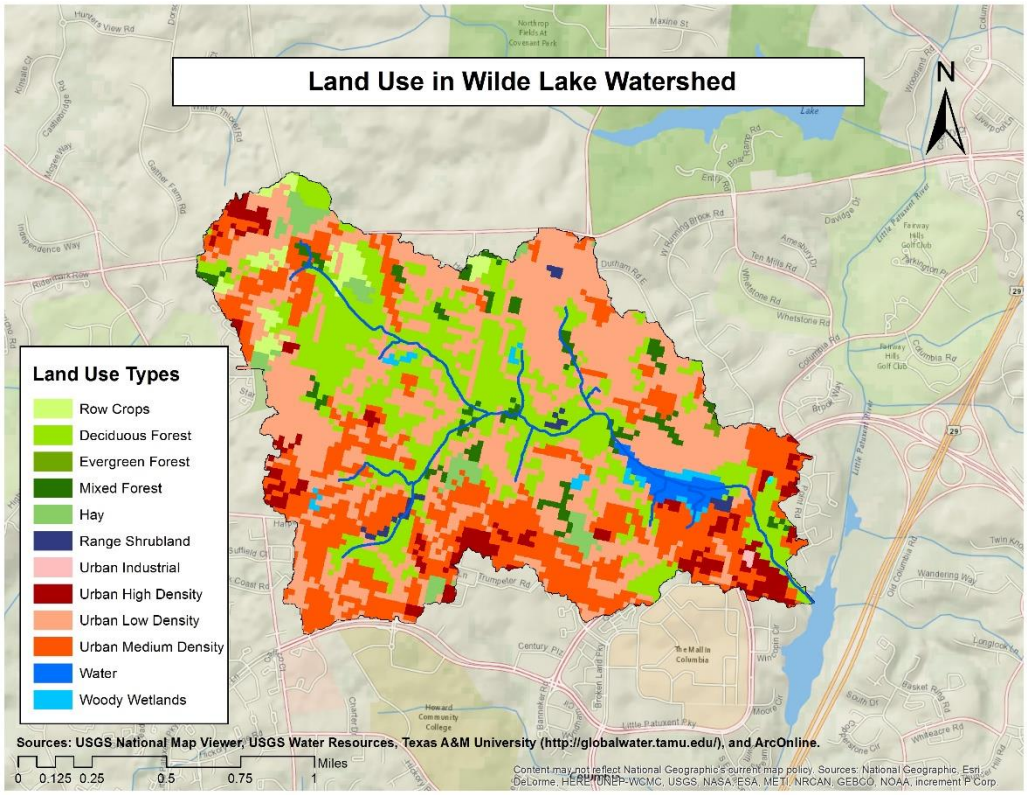

Figure 2-4. Land Use Map of theWilde Lake watershed

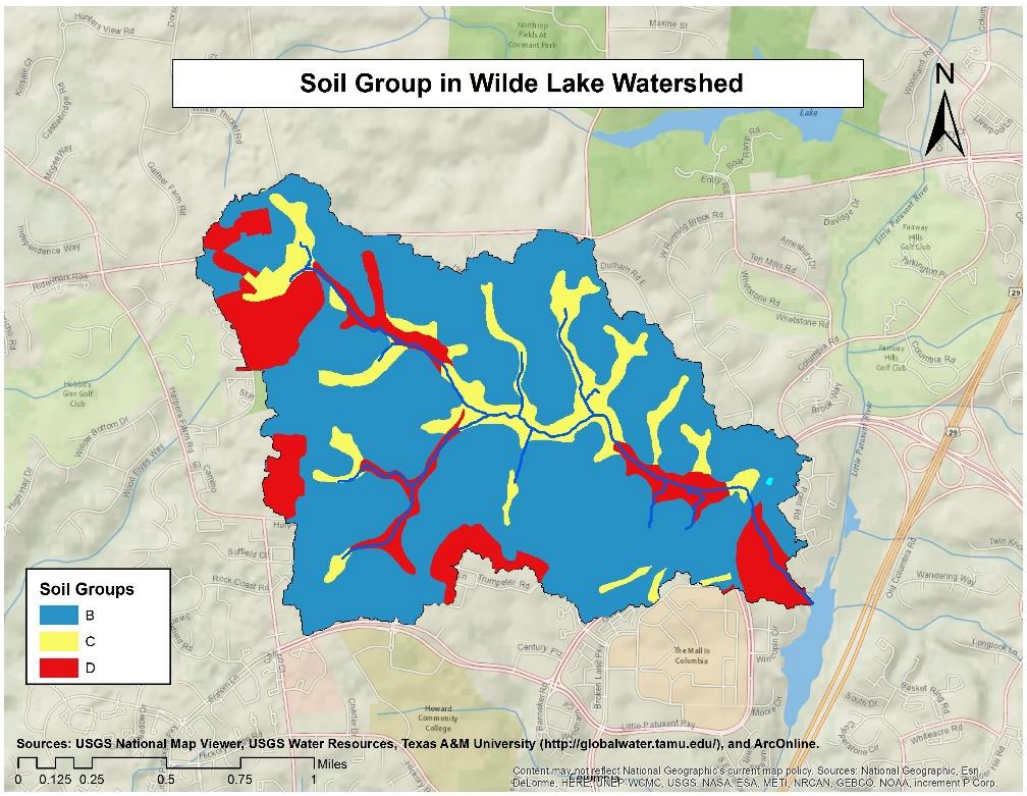

Figure 2-5. Map of Hydrologic Soil Groups in the Study Area

2.2 Software

Six software programs were used to accomplish the objectives of this study (Table 2-2). The main software program was the Soil and Water Assessment Tool (SWAT) which was used to develop the hydrologic model of the study watershed and to perform simulations of the watershed's response to current conditions and to predicted future climate conditions. In SWAT, a watershed is divided into sub-watersheds (sub-basin) which are further subdivided into Hydrologic Response Units (HRUs). HRUs are the smallest computational unit used in SWAT, and consist of sub-areas characterized by homogeneous land use, soil, slope, and management practices (Woznicki et al., 2011). In this study, the use of SWAT was divided essentially into three steps: 1) input file setup; 2) model calibration, and; 3) model prediction and analysis. The input files were prepared using ArcGIS and ArcSWAT, calibration was performed using SWAT-CUP, CMhyd was used to prepare climate change data for model predictions and RStudio was used to analyze the results. All software, excluding ArcGIS, were free to download and use. The free version of ArcGIS, for educational trial, was used in this study.

Table 2-2: Software Used in This Study

Software	Purpose	Source
SWAT	Model Development	Texas A&M University http://swat.tamu.edu/software/swat-executables/
ArcGIS	Spatial Analysis	ESRI http://www.esri.com/en/arcgis/products/arcgis-pro/Overview
ArcSWAT	Model Development	Texas A&M University http://swat.tamu.edu/software/arcswat/
SWAT-CUP	Model Calibration	Neprash Technology http://www.neprashtechnology.ca/downloads/
CMhyd	Bias Correction	Hendrik Rathjens http://swat.tamu.edu/software/cmhyd/
RStudio	Data Processing and Statistics Analyses	RStudio https://www.rstudio.com/products/rstudio/download/

ArcGIS is a Geographic Information System program developed by ESRI Inc. that is used to import, manage, process and display georeferenced spatial data. In this study, ArcGIS was used to manage the spatial input data required to perform SWAT simulations, for generating maps of the study watershed, and for producing output maps of simulation results.

The ArcSWAT program is a plugin for ArcGIS that is used as a domain-specific extension, specifically aimed at generating SWAT input data files from the GIS data stored in ArcGIS. Wang (2015) had previously generated the required SWAT input files for the Wilde Lake watershed using ArcSWAT and these input files were used in this study.

The SWAT Calibration and Uncertainty Programs (SWAT-CUP) is a software tool linked to the SWAT base program that incorporates a group of calibration algorithms. The algorithms include Sequential Uncertainty Fitting Ver. 2 (SUFI-2), Particle Swarm Optimization (PSO), Generalized Likelihood Uncertainty Estimation (GLUE), Parameter Solution (ParaSol), and Markov Chain Monte Carlo (MCMC) (Arnold et al., 2012). SWAT-CUP is used to calibrate, validate, and perform sensitivity and uncertainty analyses on SWAT. In this study, the SUFI-2 method implemented in SWAT-CUP was used for model calibration. This is a different calibration method than that used by Wang (2015) for the Wilde Lake watershed. It is a semi-automated method, which allows model parameters to be automatically adjusted, within manually selected ranges, by auto-calibration runs (Arnold et al., 2012; Abbaspour, 2015). SWAT-CUP can read and write SWAT input files directly and automatically runs SWAT with adjusted parameter values until the statistical termination criterion for the calibration is reached.

Climate Model data for hydrologic modeling (CMhyd) is a software program used to perform bias correction of climate change projections of temperature and precipitation. Such corrections eliminate systematic model errors due to limited spatial resolution, discretization and spatial averaging within grid cells that remain after downscaling AOGCM predictions (Ehret et al., 2012; Rathjens et al., 2016). In this study, CMhyd was used to bias-correct downscaled CMIP5 climate data for the study area.

RStudio is an open-source development environment for R, a programming language for statistical computing and graphics, especially suited for dealing with big data (Rossiter, 2012). Due to the large amount of input data and simulation outputs produced in this study, RStudio was used for statistical analyses of the climate change and the watershed simulation outputs. It was also used to develop scripts to automate some of the time consuming and repetitive data processing tasks, performed repeatedly for each climate model and scenario, in this study.

2.3 SWAT Input Data

2.3.1 Spatial Data

The spatial data used to develop the model of the Wilde Lake watershed were obtained from databases managed by the US Federal Government. Table 2-3 lists the types, versions and sources for these data. The spatial data included a Digital Elevation Model (DEM), landuse and land cover maps, hydrography and soil maps. These data were acquired, for the Wilde Lake watershed, and converted to SWAT input files (using ArcSWAT) in previous work by Wang (2015). These input files were used directly in the

present study but the objectives, calibration approach and watershed response analyses performed here differ from those of that prior study.

Table 2-3. Spatial Input Data Sources

Data Name	Data Version/Type	Data Sources
Elevation DEM	1/9, 2008, Wilde Lake	The national map viewer http://viewer.nationalmap.gov/viewer/
Land Cover	2006	
Soil	Shape Files	USDA http://soildatamart.nrcs.usda.gov/

2.3.2 Climate Data

This study used both observed and synthetic weather data to drive SWAT simulations of the Wilde Lake watershed. Observed weather data was used for simulations under current conditions and synthetic data was used for climate change analysis. The sources of these data are listed in Table 2-4. For observed data, both the CFSR and a local NOAA weather stations were initially used, such that the particular dataset generating the most accurate simulations of observed watershed behavior could be selected for the remainder of the study. For climate change analysis, downscaled CMIP5 data were downloaded from the Program for Climate Model Diagnosis and Intercomparison (PCMDI) at Lawrence Livermore National Laboratory (LLNL, n.d.). Data from 6 AOGCMs and 4 RCPs, downscaled to the geographical location of the study watershed, were obtained from that source and bias-corrected against observations using CMhyd (specific models and methods are detailed below in section 2.5 of this document).

Table 2-4. Climate Data Used in SWAT Input Files in Calibration and Validation

Data Name	Data ID	Location	Data Used
Baltimore Washington International Airport, MD	USW00093721	39.167°, -76.683°	Daily Precipitation Daily Max/Min Temperature Jan 1, 1961 to Dec. 31, 2015
CFSR Climate Data		39.185°, -76.875°	Daily Precipitation Daily Max/Min Temperature Jan 1, 1979 to Dec. 31, 2013
CMIP5 Climate Model Data	CMIP5*	39.125° to 39.250°, -76.875° to -76.75°	Daily Precipitation Daily Max/Min Temperature Jan 1, 1961 to Dec. 31, 2099

* Further information on CMIP5 models is presented in section 2.5

2.3.3 Hydrologic and Water Quality Data

Observed data were needed to calibrate the Wilde Lake watershed model for surface runoff (SurfQ), total suspended sediment (TSS), total nitrogen (TN) and total phosphorus (TP). Daily discharge data was obtained from the USGS gauging station (#01593370) located at Lat 39°13'32.8", long 76°52'12.2", which monitors the Little Patuxent River Tributary, upstream of the Wilde Lake, and has been operating since October 2012. Water quality data was obtained from grab samples analyzed for constituent concentrations by the Columbia Association at the Wilde Lake NPDES monitoring site, during stormwater events, from 2007 to 2015. The author pre-processed the data to estimate watershed yield for the sampled stormwater events so that they could be used for calibration by SWAT-CUP.

Observation data are commonly separated by time period into two datasets, one for calibration and another for the validation (Arnold, 2012). In this study, the data from calendar years 2009 to 2014 were selected to form the calibration dataset, and those from calendar years 2005 to 2008, and 2015, were selected for model validation. As shown in

Figure 2-6, with this temporal division, there are approximately 70% of stream flow observations in the calibration period and the remaining 30% are in the validation period. Similarly, for the water quality data, there are approximately 71% of data points in the calibration period, and the remaining 29% are in the validation period.

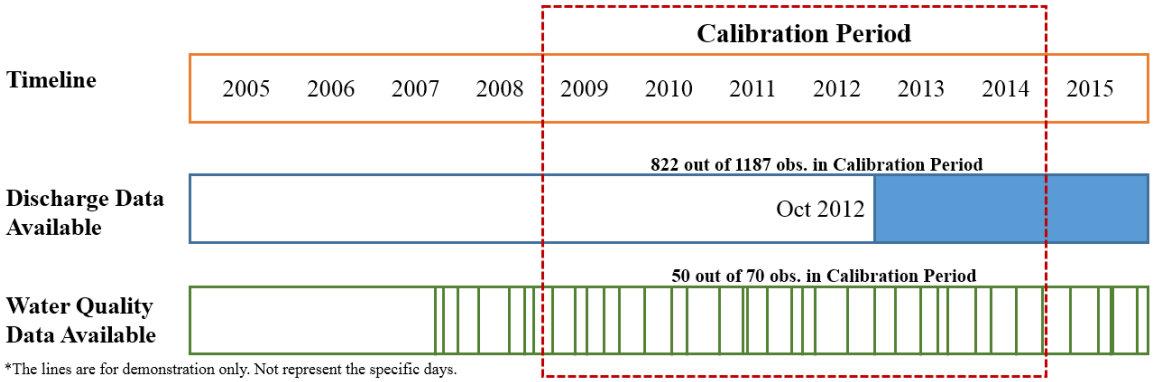

Figure 2-6. Calibration and Validation Periods Used in this Study

It is generally important to have the similar weather conditions in the calibration and validation periods (Arnold et al., 2012; Gan et al., 1997). Figure 2-7 presents the yearly total precipitation, in millimeters, for both periods (green bars for calibration and blue bars for validation). The mean yearly precipitation over both periods is 1182.7 mm (orange line) and both periods include some dry and wet years. The average yearly precipitation for the selected calibration period is 1221.8 mm, and that for the validation period is just 10% lower, at 1135.7 mm.

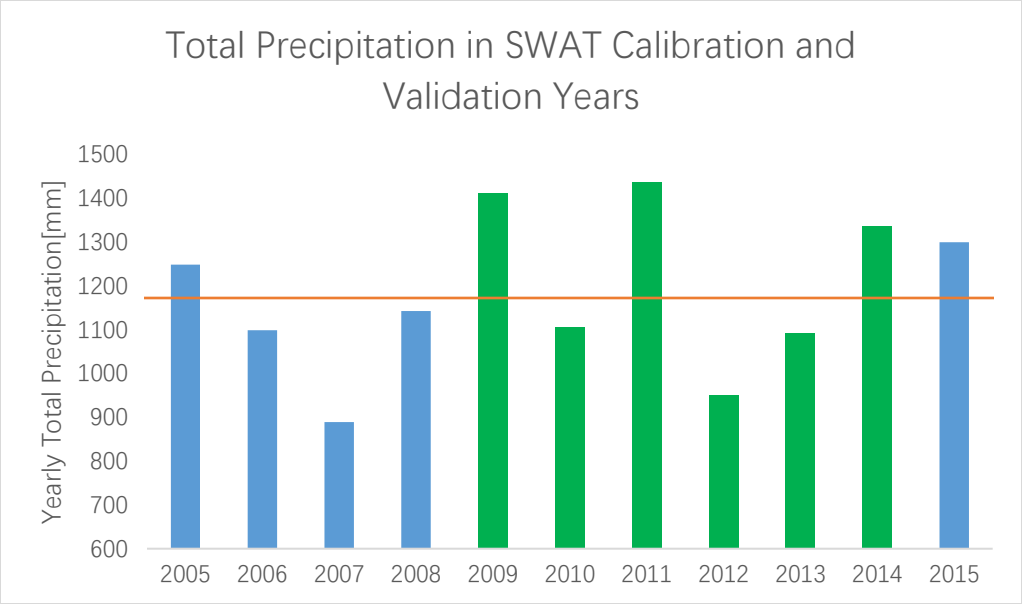

Figure 2-7. Total Precipitation in SWAT Calibration and Validation Years

2.4 Methods for Objective 1: SWAT Model Development

The first objective of this study is to develop a representative model of the hydrologic and water quality response of the Wilde Lake watershed. This typically entails the development of spatial data input files, followed by calibration of model parameters and validation of the model against observed data. In this study, SWAT was selected as the hydrologic modeling software with which to develop the model of the Wilde Lake watershed and a set of input files, developed previously by Wang (2015) were available to get the process started. Accordingly, model development activities were focused on parameter calibration and model validation.

Model calibration and validation were performed using the SWAT-CUP software program. The flowchart in Figure 2-8 shows the steps used in calibration. A two-step process was used where parameters related to streamflow were calibrated first and the

resulting model was then calibrated for water quality. SWAT-CUP used the SUFI-2 method to automatically generate parameter update values, and then ran SWAT with those values, and calculated goodness of fit statistics for the results, including the Nash–Sutcliffe Efficiency (NSE). It repeated this process iteratively until either a maximum number of iterations was exceeded, or the target accuracy was reached. Goodness of fit statistics and parameter values were checked manually at the end of the process to verify model accuracy and whether identified parameters were physically reasonable.

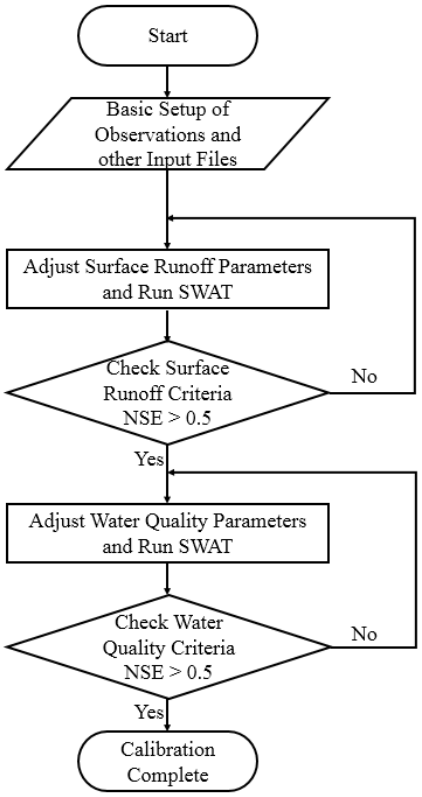

Figure 2-8. Steps of Calibration Processes in this Study

2.4.1 Parameter Selection

The selection of which parameters to include in the calibration set was guided by literature sources (Piniewski, 2014; Wang, 2015; Malagò et al., 2015). A total of 28

parameters were chosen for calibration: 9 parameters were used to adjust runoff and the other 19 parameters were used to calibrate water quality. Table 2-5 lists all of the selected parameters, along with their meanings and grouping methods. The parameters for different model units with similar characteristics are estimated together rather than separately to reduce the number of free parameters. The initial values and range for these parameters were determined from the literature (Piniewski, 2014; Wang, 2015; Malagò, 2015), with the additional consideration that wider ranges can help the search algorithm find better solutions (Dile et al., 2016). Therefore, the initial range of these parameters were kept as large as possible, within a physically meaningful range, based on the literature review.

Table 2-5. Model Parameterization

Model Input	Meaning	Grouping Method	Sub-parameter Numbers
ADJ_PKR.bsn	Peak rate adjustment factor for sediment routing in the subbasin		1
ALPHA_BF.gw	Baseflow alpha factor	Land Use	12
BC1_BSN.bsn	Rate constant for biological oxidation of NH3		1
BC2_BSN.bsn	Rate constant for biological oxidation of NO2 to NO3		1
BC3_BSN.bsn	Rate constant for hydrolosis of organic nitrogen to ammonium		1
BIOMIX.mgt	Biological mixing efficiency	Land Use	3
CANMX.hru	Maximum canopy storage	Land Use	12
CDN.bsn	Denitrification exponential rate coefficient		1
CH_N1.sub	Manning's n value for the tributary channel	Sub-Basin	20
CH_N2.rte	Manning's n value for the main channel	Sub-Basin	20
CH_ONCO_BSN.bsn	Channel organic nitrogen concentration in basin		1
CMN.bsn	Rate factor for humus mineralization of active organic nutrients		1

CN2.mgt	Initial CSC runoff curve number for moisture condition II	Land Use	12
EPCO.hru	Plant uptake compensation factor	Land Use	12
ERORGN.hru	Organic N enrichment ratio for loading with sediment	Land Use	12
ESCO.hru	Soil evaporation compensation factor	Land Use	12
GW_REVAP.gw	Groundwater "revap" coefficient	Land Use	12
HLIFE_NGW.gw	Half-life of nitrogen in shallow aquifer		1
HLIFE_NGW_BSN.bsn	Half-life of nitrogen in groundwater		1
N_UPDIS.bsn	Nitrogen uptake distribution parameter		1
NPERCO.bsn	Nitrogen percolation coefficient		1
OV_N.hru	Manning's n value for overland flow	Land Use	12
P_UPDIS.bsn	Phosphorus uptake distribution parameter		1
PHOSKD.bsn	Phosphorus soil partitioning coefficient		1
PRF_bsn.bsn	Peak rate adjustment factor for sediment routing in the main channel		1
PSP.bsn	Phosphorus availability index		1
USLE_K(1).sol	USLE equation soil erodibility factor	Soil Group	3
USLE_P.mgt	USLE equation support partice factor	Land Use	12

2.4.2 Statistical Evaluation

SWAT-CUP provides twenty goodness of fit statistics with which to evaluate calibration and validation results. In this study, the Nash-Sutcliffe Efficiency (NSE) coefficient was selected as the main evaluation statistic, with the criterion that NSE>0.5 indicates a satisfactory model (Arnold et al., 2012). Three other statistics were evaluated after the calibration to gain additional insights into the results: the Pearson Correlation Coefficient (*r*), Mean Square Error (MSE), and Percent Bias (PBIAS). These goodness of fit statistics are defined below in equations (7) to (10).

$$NSE = 1 - \frac{\sum_{i=1}^{n}(\hat{Y}_i - Y_i)^2}{\sum_{i=1}^{n}(Y_i - \bar{Y})^2} \quad \text{..... (7)}$$

$$r = \frac{\sum_{i=1}^{n}(\hat{Y}_i - \bar{Y})^2}{\sum_{i=1}^{n}(Y_i - \bar{Y})^2} \quad \text{..... (8)}$$

$$MSE = \frac{1}{n} \cdot \sum_{i=1}^{n}(\hat{Y}_i - Y_i)^2 \quad \text{..... (9)}$$

$$PBIAS = \frac{\sum_{i=1}^{n}\hat{Y}_i - \sum_{i=1}^{n}Y_i}{\sum_{i=1}^{n}Y_i} \quad \text{..... (10)}$$

2.4.3 Calibration and Validation

SWAT-CUP was used to perform runs of SUFI-2 iterations. The calibration stopped when goodness-of-fit statistics stopped improving. In each iteration, parameters were automatically updated (within the initial range) and the SWAT main program was executed 250 to 500 times. Goodness-of-fit statistics were calculated after each run and a new set of iterations, using different initial values or ranges, were performed if these statistics were unsatisfactory. More runs and iterations can generally improve a calibration, but simulations with a daily time-step can be costly. For the settings in this study, each iteration took 24 to 48 hours.

In the water quality step of the calibration process, observed data were available in the form of concentrations ($M \cdot L^{-3}$) of sediments, nitrogen and phosphorus, obtained from grab samples during storm event. These data had to be converted to daily yields ($M \cdot T^{-1}$) so that SWAT-CUP could compare them to the values it extracts automatically from SWAT output files (output.hru). Streamflow had not been reliably measured when the samples were obtained and therefore, simulated streamflows, predicted from the first step

of the calibration process (where parameters related to runoff were calibrated) were used to convert measured concentrations into daily yields for the water quality calibration step.

Both CFSR reanalysis data and NCDC weather station data were used as driving forces during calibration, to assess which dataset, if any, produced the most accurate simulations. At the end of calibration, goodness of fit statistics resulting from the use of the two weather time series were compared to one another, and the weather dataset that produced the best statistics was selected for the remainder of the analysis.

Calibration was complete once goodness-of-fit statistics were stable and SWAT-CUP was used to evaluate the calibrated watershed model against the validation dataset. The validation method in SWAT-CUP is essentially the same as for calibration but a single iteration, without parameter update, is used.

2.5 Methods for Objective 2: Climate Change Impacts on Stream Water Quantity and Quality

The second objective of this study was to assess the impact of climate change on the hydrologic and NPS pollution response of the study watershed, at its outlet. This was performed by subjecting the calibrated SWAT model of the Wilde Lake watershed to synthetic precipitation and temperature time series predicted by downscaled CMIP5 climate models. This section presents the method used to select climate models for this analysis, the approach used to adjust CO_2 concentration in the watershed model, the bias-correction of the downscaled climate time series, and how watershed simulations were performed and analyzed.

2.5.1 Selection of Climate Models

A subset of the more than 50 AOGCMs included in CMIP5 were selected to perform climate change analyses in this study. The selection process was aimed at ensuring that the selected models were relatively accurate for eastern U.S. and provided a broad range of possible future climates. The analysis of Knutti et al. (2013), on the family trees to which CMIP5 AOGCMs belong, and on the accuracy with which these models can predict historical climate, was a key resource in this process. Those researchers demonstrated, for example, that AOGCMs developed from the same institute often produce very similar predictions of future climate. Accordingly, accounting for future climate uncertainty requires a selection of models that are widely separated in the branches of the family tree that they developed by hierarchical clustering of AOGCMs. Following this principle, and focusing on models for which at least 3 RCPs were available, a total of six models, developed by six different institutions, all of which had been doing climate change modeling research for years, and all of which had former versions of their climate models in CMIP3, were selected for this study. The models are listed in Table 2-6.

The selected models are composed of different sub-process models and involve differing coupling methods between these sub-models. For example, the IPSL-CM5 is composed of the LMDZ atmospheric physics sub-model, Orchidée continental model, Nemo ocean model, LIM sea ice model, INCA aerosol chemistry model, and the OASIS coupler (ISPL, n.d.). The CNRM-CM5.1 on the other hand, includes the atmospheric model ARPEGE-Climat, continental model SURFEX, ocean model Nemo, sea ice model GELATO, and the coupler is OASIS as well (Voldoire et al., 2013). Only the ocean model

and the coupler are the same between IPSL-CM5 and CRNM-CM5.1, even though both models were developed in France. In addition, IPSL-CM5 uses a separate aerosol chemistry model, while CNRM-CM5.1 uses a formulation that is incorporated in its atmospheric model. Overall, the selected models are relatively far from one another in the genealogical tree presented by Knutti et al. (2013) and have only small similarities with each other.

Table 2-6. CMIP5 Climate Models Selected for this Study

Model No.	Name	Country	Institution	RCPs Available
1	CanESM2.5	Canada	Canadian Centre for Climate Modelling and Analysis	26, 45, --, 85
2	CNRM-CM5.1	France	Centre National de Recherches Météorologiques—Groupe d'études de l'Atmosphère Météorologique and Centre Européen de Recherche et de Formation Avancée	--, 45, --, 85
3	GFDL-CM3	United States	Geophysical Fluid Dynamics Laboratory, NOAA	26, --, 60, 85
4	IPSL-CM5A-MR	France	Institute Pierre Simon Laplace	26, 45, 60, 85
5	MIROC5	Japan	Center for Climate System Research	26, 45, --, 85
6	MRI-CGCM3	Japan	Meteorological Research Institute	26, 45, 60, 85

Figure 2-9 shows the normalized distance between historical observations of temperature and precipitation and predictions of CMIP5 AOGCMs over the same time period (Knutti et al., 2013). Lower values indicate a more accurate model for that period and the solid line represents the mean distance for CMIP5 models (the dashed line is the median). The models selected for this study are identified by rectangular boxes. Half of them are more accurate than average and the other half is slightly less accurate than average at predicting the historical period, but none is a member of the bottom 6 CMIP5

models that appear to be much less accurate than the others. Overall, based on their spread through AOGCM genealogy and their accuracy at predicting historical climate, the selected climate models are believed to form a diverse and rational group for evaluating climate change impacts on watershed hydrology in this study. Downscaled weather time series for these 6 models were downloaded from the Lawrence Livermore National Laboratory (LLNL) online database.

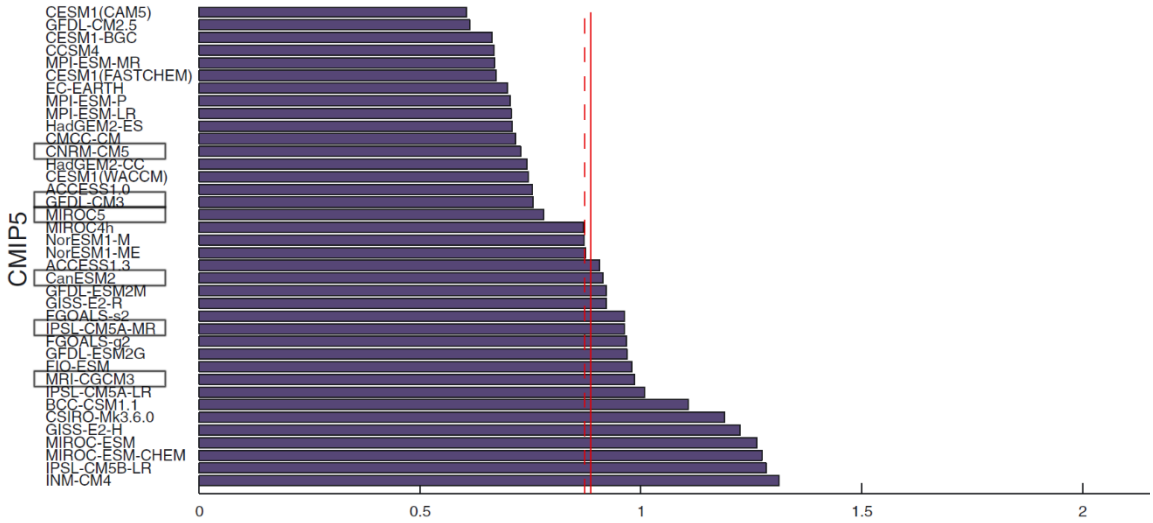

Figure 2-9. The Root Mean Square of Temperature and Precipitation to the Observations (Knutti et al., 2013)

2.5.2 Future atmospheric CO_2 concentration in SWAT

Atmospheric CO_2 concentration are not dynamic in the current version of the SWAT model, rather, a single value is used. Accordingly, for each future climate scenario simulated in this study, a fixed value of atmospheric CO_2 concentration was set. For simulations under future climate, they were selected as the average value for each RCP, from 2016 to 2099. For simulations under current climate, the historical value was averaged from 1961 to 2015. The resulting atmospheric CO_2 concentration values used in

SWAT, in this study, are shown in table 2-7. These values were entered manually in SWAT's ".sub" input file for each of the corresponding simulations.

Table 2-7. CO_2 Concentration used in SWAT Modeling of Various Climate Scenarios

SWAT Model Periods	Calibration/ Validation	Historical	RCP2.6	RCP4.5	RCP6.0	RCP8.5
CO_2 [ppmv]	380	352	432	490	516	616

2.5.3 Bias-Correction of Precipitation and Temperature

Downscaled CMIP5 AOGCM precipitation and temperature time series were obtained from LLNL over the latitudinal-longitudinal area bounded by 39.125° to 39.250° and -76.875° to -76.75°, respectively. These downloaded data were bias-corrected to CFSR but not to NCDC observations. In this study, both weather datasets were used for model calibration and it was therefore necessary to also bias-correct the CMIP5 time series against historical NCDC data.

In this study, bias-correction was performed using the CMHyd software program, which implements several bias correction methods. The method of distributing mapping, described earlier in section 1.5.3, was used for this purpose. The bias-correction was based on NCDC weather from the BWI airport station for the historical period from Jan 1961 to Dec 2000. CMHyd was also used to compute the statistics of the bias-corrected CMIP 5 data and compare them to those of the observed historical data to verify the correctness of the bias-correction process. Once the bias-correction coefficients had been established from historical data, for each AOGCM, they were applied to the bias-correction of future climate predictions by that same AOGCM. After successful bias-correction, a Rstudio script was used to batch convert the format of the output files

produced by CMHyd to the input file format of SWAT, such that the bias-corrected time-series were ready to use in simulations of the future response of the study watershed to climate change.

2.5.4 Watershed Simulations

The calibrated SWAT model of the Wilde Lake watershed was run with each of the bias-corrected CMIP5 precipitation and temperature time series as input. Runs were performed separately for each of the 6 climate models and 2 to 4 RCP scenarios per model (RCP2.6, RCP4.5, RCP6 and RCP8.5). The CO_2 levels were adjusted for each run, as described earlier. The simulations of watershed response, driven by CMIP5 data, were performed for both the historical period of 1965 to 2015 and the future period of 2016 to 2099 (with the various RCPs).

After each run, the SWAT output files output.hru and output.rch were saved in a separate folder. The output.rch file contains the summarized yearly mean surface runoff in cubic meters per second, yearly total suspended solids in tons, total nitrogen and total phosphorus in kilograms in each watershed reach. There is one reach (or main channel) per sub-basin of a watershed (Arnold et al., 2011). In this study, for the assessment of the impact of climate change on in-stream variables, the data for the reach at the outlet of the watershed (reach 20) was extracted. Four main output variables, listed in Table 2-8, were obtained and analyzed for this reach.

For each climate model and scenario, outlet values predicted under future climate were compared to those predicted using the same climate model during the historical period, and expressed as a percentage change from that period. Percent changes were

aggregated by RCP scenario, by averaging across climate models, and the standard deviations of the percent changes used to calculate those averages were computed to quantify uncertainty in each scenario-aggregated future response prediction.

Table 2-8. Output Variables in Reach

Parameter Name	Units	Definition
FLOW_OUT	cms	Average daily stream flow out of reach during time step.
SED_OUT	tons	Sediment transported with water out of reach during time step
TOT N	kg	Total nitrogen in surface runoff
TOT P	kg	Total phosphorus in surface runoff

2.6 Methods for Objective 3: Climate Change Impacts on On-land Variables and CSA Identification

The results of the models runs used to assess the impact of climate change on the study watershed's outlet response were also used to assess its impact on runoff and NPS pollutant generation at the land surface, and on CSAs. The analysis focused on the contents of SWAT's output.hru files, which were saved in separate folders at the end of each simulation. This section describes the methods used to process data from these files, the approach used to assess the response of the watershed's surface to current and future weather, and the steps used to analyze the impact of climate change on CSAs. The analysis was focused on comparing watershed conditions in two future time horizons: mid-century (2040-2059) and end-century (2080-2099), to conditions during a historical baseline (1970-1989) representing current weather.

2.6.1 Post-processing of SWAT Model Outputs

The output.hru file contains the model predictions of yearly surface runoff in millimeter, sediments in tons per hectare, and nitrogen and phosphorus in kilograms per hectare, as generated by each individual HRU in the watershed model. The variables extracted from the output.hru files in this study are shown in Table 2-9. The amount of surface runoff generated by each HRU was found in the variable SURQ_GEN, and the sediment yield was obtained from SYLD. For total nitrogen and phosphorus, the yields of individual species of these nutrients were added together using equations (11) and (12).

$$\mathrm{TN} = \mathrm{ORGN} + \mathrm{NSURQ} + \mathrm{NLATQ} + \mathrm{NO3GW} \quad \cdots\cdots (11)$$

$$\mathrm{TP} = \mathrm{ORGP} + \mathrm{SEDP} + \mathrm{SOLP} + \mathrm{P\_GW} \quad \cdots\cdots (12)$$

Table 2-9. Simulation Output Variables Defined on the Basis of HRUs

Parameter Name	Units	Definition
Area	ha	The surface area of each HRU
SURQ_GEN	mm	Surface runoff generated in HRU
SYLD	tons/ha	Sediment from the HRU that is transported into the main channel.
ORGN	kg/ha	Organic nitrogen transported out of the HRU and into the reach.
NSURQ	kg/ha	Nitrate transported with surface runoff into the reach.
NLATQ	kg/ha	Nitrate transported by lateral flow into the reach
NO3GW	kg/ha	NO3 transported into main channel in the groundwater loading from the HRU
ORGP	kg/ha	Organic phosphorus transported with sediment into the reach.
SEDP	kg/ha	Mineral phosphorus adsorbed to sediment transported into the reach.
SOLP	kg/ha	Soluble mineral forms of phosphorus transported by surface runoff into the reach.
P_GW	kg/ha	Soluble phosphorus transported by groundwater flow into main channel.

Where appropriate, the values of the above variables were mapped to display the spatial distribution of constituent yields within the study watershed. Additionally, spatially averaged values of the yields of each constituent were calculated using equation (13) to provide and overall perspective on watershed behavior. These overall values made it easier to compare the watershed's response to current and future climates in some cases.

$$\text{Average per area Yield} = \frac{\sum_{i=1}^{n}(\text{Yield}_i \cdot \text{Area}_i)}{\sum_{i=1}^{n}(\text{Area}_i)} \quad \cdots\cdots\cdots\cdots\cdots\cdots\cdots\cdots\cdots\cdots \quad (13)$$

2.6.2 Watershed Response to Current and Future Climate

The response of the study watershed to current climate (historical baseline) was determined from simulation results obtained using observed weather data. These results were summarized as watershed wide statistics on runoff generation, and sediment and nutrient yields on a per-area basis. Results were also mapped to assess the spatial variability of constituent generation within the basin and provide explanations for this variability.

The response of the watershed to synthetic weather data produced by the CMIP5 models for the historical baseline were summarized in terms of watershed-wide per-area yields and compared to those obtained with measured rainfall. This was done to assess the degree to which those bias-corrected models may produce responses that either match or deviate from that which characterized the period. Comparisons were performed for the 4 constituents and expressed as the percentage of deviation in yield resulting from the application of each model's synthetic climate data.

The response of the watershed to the 4 future climate scenarios was assessed by aggregating watershed-wide surface yields across AOGCMs for each RCP. Changes in yields were expressed as percentages relative to the historical baseline for each climate model and RCP, and both the average and standard deviations of these percentage changes were computed for each future scenario. This analysis was performed to quantify both the expected changes in watershed response as a function of future climate scenario, for each surface constituent, and to assess the level of uncertainty that characterizes these expected changes.

2.6.3 Climate Change Impacts on CSAs Identified with Relative- and Fixed-Thresholds

In this study, a relative threshold approach was used to identify CSAs from current climate. To extend CSA identification into the future, both a relative threshold and a fixed threshold (based on current climate) were used. In both methods, HRUs are first sorted in order of their per-area yield of each constituent and then the top yielding HRUs are defined as hotspots, for their respective constituents. In the relative threshold approach, a percentage of HRUs, for example 20%, are selected as the CSAs (eg. the top 20% of HRUs in terms of per-area sediment yield). In the fixed threshold approach, on the other hand, all the HRUs that generate more than a pre-selected per-area yield are tagged as CSAs. The two methods are interchangeable under stationary conditions (statistics consistent in time) but their application to CSA identification under climate change may reflect different assumptions about the nature of the constituent which CSA identification is meant to help control. For example, if one's goal is to identify CSAs to help control a constituent whose concentration should not exceed pre-set levels in a water body, and if

climate change is assumed to result in proportional changes in water yield and in the yield of that constituent, then the same relative threshold used to identify CSAs under current conditions should be effective for identifying CSAs under climate change. However, if it is the total quantity of that constituent entering water bodies that should be controlled, irrespective of the amount of runoff that accompanies it (as suggested by TMDLs) then the same yield threshold used to identify CSAs today, rather than a relative value, should be most applicable to the identification of CSAs under climate change.

CSAs were identified under current climate using relative thresholds of 10%, 20%, 30% and 40%. The percentage of watershed area occupied by CSAs and the percentage of the total watershed yield of each constituent produced by these hotspots were tabulated at the 4 threshold levels to assess the advantage that may be gained by implementing BMPs over these CSAs under current climate in the study watershed. Mass/Area ratio curves were also produced for this purpose.

CSAs were identified from the results of all simulations of watershed response to future climate models and scenarios using the same 10% to 40% thresholds used for current climate (relative threshold approach). This means that the same number of top-yielding HRUs constituted the future climate CSAs as were present in current climate hotspots, but the specific HRUs included in the critical set could differ due to differences in rainfall and temperature regimes. HRUs that were present in both future and current climate CSAs were counted and divided by the total number of HRUs in the CSAs for each targeting level and each climate model and scenario. Results were expressed as the percentage of HRUs that are part of CSAs under current conditions and that would remain hotspots under future climate. The minimum value of this percentage and its

median were identified for each constituent, across all future scenarios and models, to determine the degree to which CSAs identified by relative thresholds would be robust against climate change in the study watershed.

The lowest per-area yields of HRUs identified as CSAs under current climate, at the 10% to 40% targeting levels, were used as fixed thresholds to identify CSAs for all constituents from simulation results obtained under future climate (fixed threshold approach). The changes in the number of HRUs included in CSAs were computed for each climate model, constituent and threshold level for the worst-case RCP 8.5 scenario to place an upper bound on CSA variability. The percentage of watershed area occupied by threshold-defined CSAs was computed for all future climate models and scenarios, and the average and standard deviation of these results were tabulated for the 4 thresholds and constituents at baseline, mid- and end-century to assess both expected change and uncertainty of future CSAs. This analysis was repeated from the mildest (RCP 2.6) to worst-case (RCP 8.5) future scenarios to determine upper and lower bounds on expected CSA changes when a fixed threshold is used in this suburban study watershed.

Chapter 3. Results and Discussion

3.1 Results for Objective 1: SWAT Model Development

Figure 3-1 shows how the Wilde Lake watershed model was divided into 20 sub-basins, including 1334 HRUs, in ArcSWAT. The SWAT model input files were generated by ArcSWAT in ArcGIS interface (Wang, 2015). The USGS gauging station and measurement of water quality variables are at reach 11. Totally 169 parameters from these input files were calibrated in the model setup section.

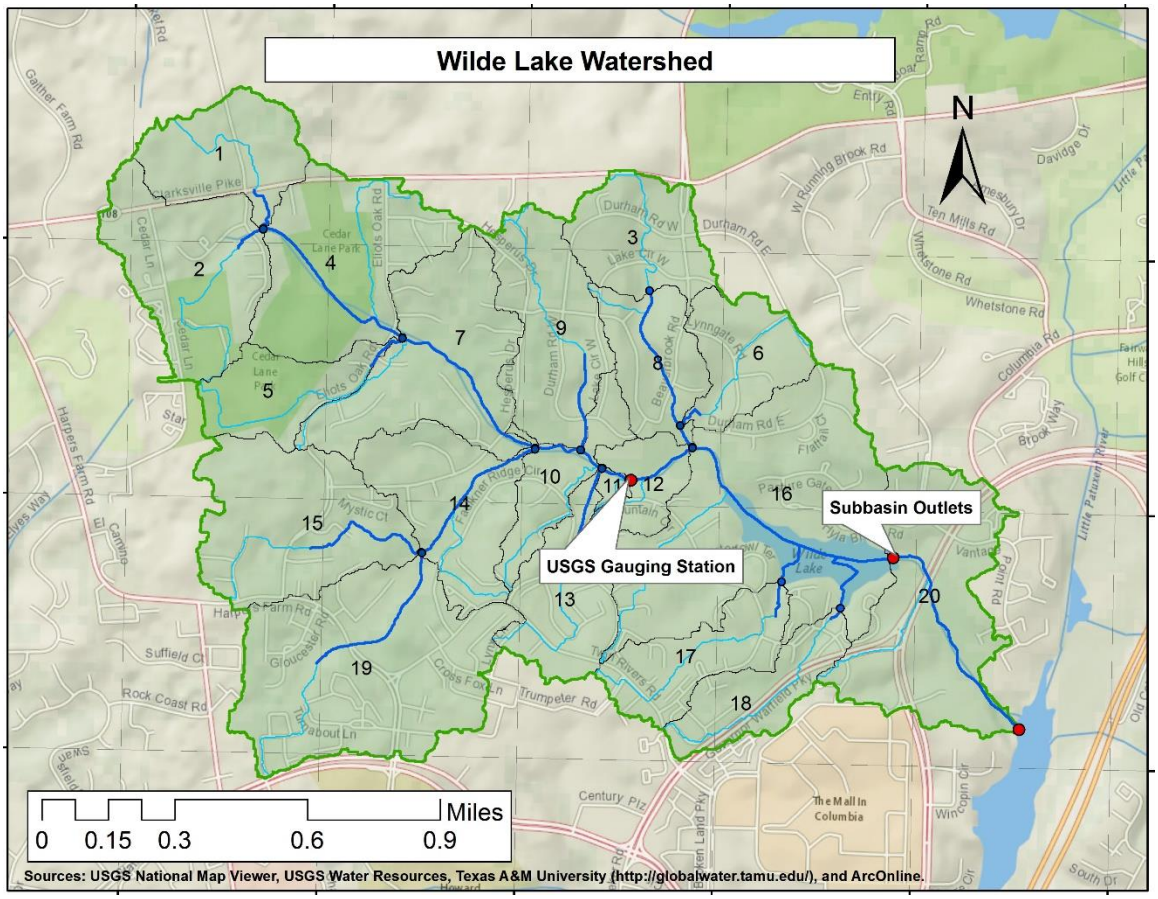

Figure 3-1. Watershed and the Sub-watersheds in Wilde Lake Watershed

3.1.1 Calibration with CFSR and NCDC

As is stated, CFSR and NCDC are two different data sets. Although the climate scientists recommend the CFSR data because they are adjusted, many water resource research show a poorer calibration results with CFSR.

Table 3-1 shows the calibration results of the first step, the calibration of surface runoff at Wilde Lake. The CFSR climate data is available until Jul-2014, so the calibration end year is 2013, while the NCDC calibration end year is 2014. The data shows that CFSR results show the worse calibration with NSE of 0.61 and person's r of 0.61. The NCDC calibration show the NSE of 0.66 and r of 0.82. Because the NCDC has an additional calendar year, the statistics of the years of 2009-2013 are computed as well and shown in the last column. The results show the NCDC calibration of 2009-2013 would have an NSE of at least 0.84 and r of 0.93, which is much higher than with CFSR data. Therefore, in this study, all subsequent analyses were performed using NCDC climate data.

Table 3-1. The statistics of Calibration results with CFSR and NCDC observations

Statistics	NCDC (2009-2014)	CFSR (2009-2013)	NCDC (2009-2013)
r	0.82	0.61	0.93
NSE	0.66	0.61	0.84
Bias [%]	-24.1	1.9	-31.4
MSE	0.012	0.010	0.004

3.1.2 Values of Parameters

With the NCDC climate data, the values of 169 model parameters were calibrated after dozens of iterations. 137 parameters were used for surface runoff calibration and 32 for TSS, TN and TP calibration. For most of parameters, the calibration grouping was by

land use, and a few of them were calibrated by sub-basin. Several parameters were defined at the whole basin level, so there was no grouping methods. The fitted values are shown in Tables 3-2 and 3-3. Detailed values for all 169 parameters are shown in the Appendix A.

Table 3-2. Fitted Parameters in Stream Flow

Model Input Parameter	Type of Change	Fitted Values	Sub-parameters	Grouping Method
ALPHA_BF.gw	Replace	0.004 to 0.198	12	Land Use
CANMX.hru	Relative	-1.00 to 0.42	12	Land Use
CH_N1.sub	Replace	0.011 to 0.018	20	Sub-basin
CH_N2.rte	Replace	0.031 to 0.120	20	Sub-basin
CN2.mgt	Relative	-0.46 to 0.37	12	Land Use
EPCO.hru	Replace	0.71 to 1.00	12	Land Use
ESCO.hru	Replace	0.47 to 1.00	12	Land Use
GW_REVAP.gw	Replace	0.003 to 0.024	12	Land Use
HLIFE_NGW.gw	Replace	1.07	1	
OV_N.hru	Relative	-0.50 to 0.43	12	Land Use
USLE_P.mgt	Replace	0.011 to 0.087	12	Land Use

Table 3-3. Fitted Parameters in Water Quality

Model Input Parameter	Type of Change	Fitted Values	Sub-parameters	Grouping Method
ADJ_PKR.bsn	Replace	0.54	1	
BC1_BSN.bsn	Replace	0.68	1	
BC2_BSN.bsn	Replace	0.85	1	
BC3_BSN.bsn	Replace	0.14	1	
BIOMIX.mgt	Replace	0.03 to 0.72	3	Land Use
CDN.bsn	Replace	2.00	1	
CH_ONCO_BSN.bsn	Replace	7.39	1	
CMN.bsn	Replace	0.0006	1	
ERORGN.hru	Replace	6.65 to 15.00	12	Land Use
HLIFE_NGW_BSN.bsn	Replace	133.5	1	
N_UPDIS.bsn	Replace	50.20	1	
NPERCO.bsn	Replace	0.25	1	
P_UPDIS.bsn	Replace	109.80	1	
PHOSKD.bsn	Replace	39.67	1	
PRF_bsn.bsn	Replace	0.766	1	
PSP.bsn	Replace	0.52	1	
USLE_K(1).sol	Relative	-0.44 to -0.15	3	Soil Group

3.1.3 Results of Calibration and Validation

Daily stream discharge observations were gathered from the USGS gauging station located at Little Patuxent River Tributary above Wilde Lake (#01593370). These data are from Oct 2012 to Dec 2015. Totally 70 data points of measurements of total suspended sediments, total nitrogen, and total phosphorus from 2007 to 2015 were obtained from the NPDES monitoring group at Columbia Association. The calibration period of SWAT-CUP was set as 2009 to 2014, and the validation period is 2005 to 2008 and 2015. The statistics including Nash-Sutcliffe Efficiency (NSE), Pearson Correlation Coefficient (r), Mean Square Error (MSE), and Percent Bias (PBIAS) in both calibration and validation periods. The calibration statistics are shown in the Table 3-4.

Table 3-4. The statistics of the Calibration Periods 2009-2014

Statistics	Runoff	TSS	TN	TP
r	0.82	0.84	0.66	0.86
NSE	0.66	0.54	0.41	0.71
PBIAS	-24.1	85.7	15.0	21.8
MSE	0.012	5.4	360	8.7

In the first step, the calibration of surface runoff showed statistics results of NSE at 0.66 and PBIAS at -24.1. Based on the criteria in Table 3-5, the calibration of streamflow with a NSE at 0.66 is a good performance, while the PBIAS is in satisfactory level. The criteria are recommended by TAMU for the monthly calibration (Moriasi et al., 2007).

Figure 3-2 and 3-3 show the best simulation results of surface runoff at Wilde Lake. The blue lines are the observations and the red lines are the simulations. It is shown in the table that the simulations are 24.1% under predicted when calculating the mean values. This figure indicated that many data points from Oct 2013 to Apr 2014 have an

over estimation relative to the observations, and the other periods such as the Oct 2013 to Mar 2013 shows an under estimation. There is no problem to have some data points under estimated and other over estimated as long as it is not partial biased. However, it is hard to identify whether it is locally-biased because it contains only 2 and a quarter years in the calibration period.

Table 3-5. Performance Rating of SWAT Modeling on Monthly Time-step (Moriasi et al., 2007)

Performance Rating	NSE	PBIAS [%]		
		Streamflow	Sediment	Nutrient
Very good	0.75<NSE<1.00	PBIAS<±10	PBIAS<±15	PBIAS<±25
Good	0.65<NSE<0.75	±10<PBIAS<±15	±15<PBIAS<±30	±25<PBIAS<±40
Satisfactory	0.50<NSE<0.65	±15<PBIAS<±25	±30<PBIAS<±55	±40<PBIAS<±70
Unsatisfactory	NSE<0.50	PBIAS>±25	PBIAS>±55	PBIAS>±70

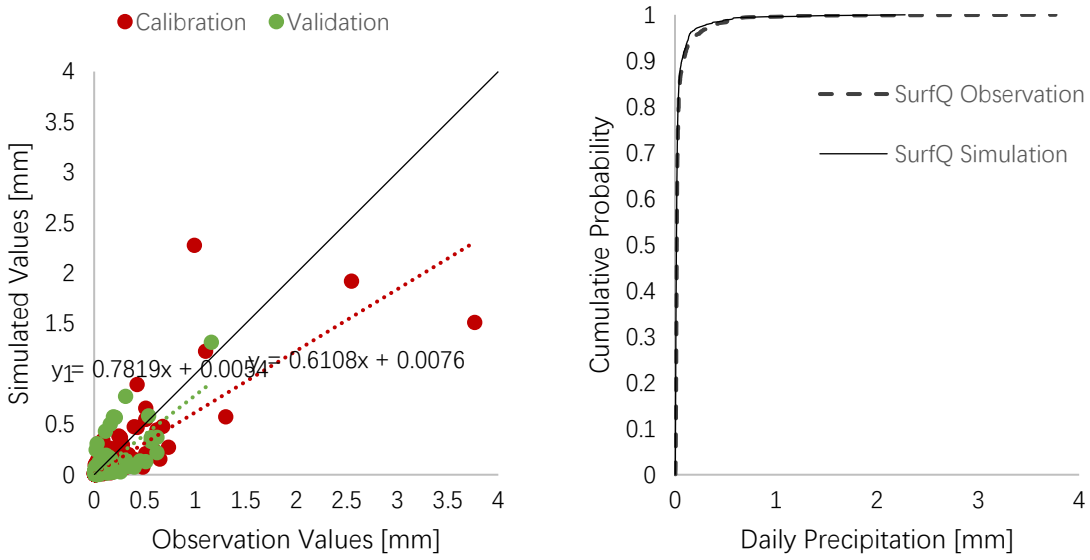

Figure 3-2. The Daily Observation and Simulation of Surface Runoff for Calibration and Validation Period (Left) and Cumulative Distribution of Daily Simulation and Observation (Right)

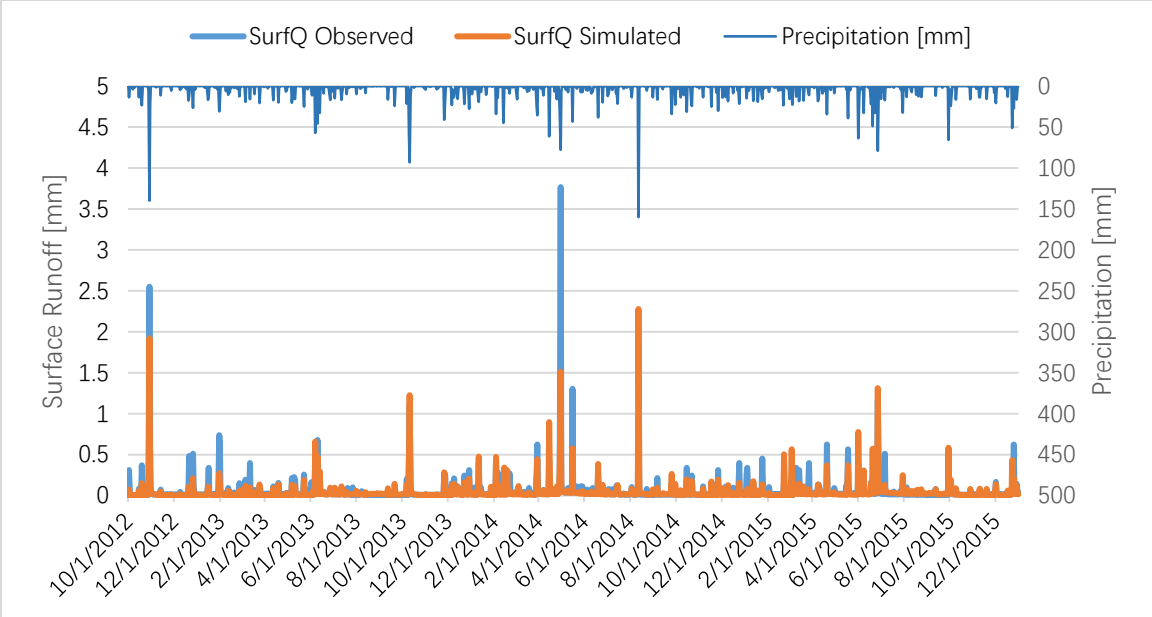

Figure 3-3. The Observed and Simulated Surface Runoff and Precipitation for Calibration and Validation Period

The calibration of parameters related to TSS, TN and TP would not cause the change of the calibrated runoff. However, some parameters would affect each other within the water quality calibration step. For example, the parameter USLE_K is a parameter related to the soil erosion, which would mainly affect the TSS, but it would also cause slight changes on TN and TP in test runs. Therefore, the second step calibrates all water quality variables TSS, TN and TP together.

The calibration and validation results of TSS, TN and TP are shown in the Table 3-4 as well. TSS has a satisfactory NSE at 0.54 with a large bias of 85.7%. This bias value is much higher than the satisfactory criteria of 55%, which means an over estimation in the SWAT model. The TN shows an unsatisfactory NSE at 0.41 with a good bias at 15%. The TP shows a good NSE at 0.71 with a very good bias at 21.8%. The X-Y plots and time series plots of the calibration results on TSS, TN and TP are shown in Figure 3-4 to 3-6. Although all three water quality variables are over estimated, they show different

patterns. For the TSS, most of days with moderate-low observations have an over estimation, the moderate-high observations match the estimation pretty well. For the TN, only two highest observations match the estimations, the moderate and the low values do not match. The TP are good on most of observations, only bad on several observations, and it is the best-calibrated variable among the water quality variables.

The statistical results at validation periods are shown in the Table 3-6. The NSE for all four variables are decreased, and the changes ranging from 0.14 to 0.27. The bias for the surface runoff, TSS and TN decreased as well, which means they are less biased and have a relative accurate mean value in the validation periods. The TP at validation periods shows a higher bias, while it is still in the acceptable range according to the Table 3-5 (Moriasi et al., 2007).

Table 3-6. The Statistics at the Validation Period

Statistics	Runoff	TSS	TN	TP
R	0.76	0.68	0.48	0.80
NSE	0.52	0.27	0.23	0.44
PBIAS	-10.6	-40.1	-7.3	-33.3
MSE	0.0053	140	2700	92

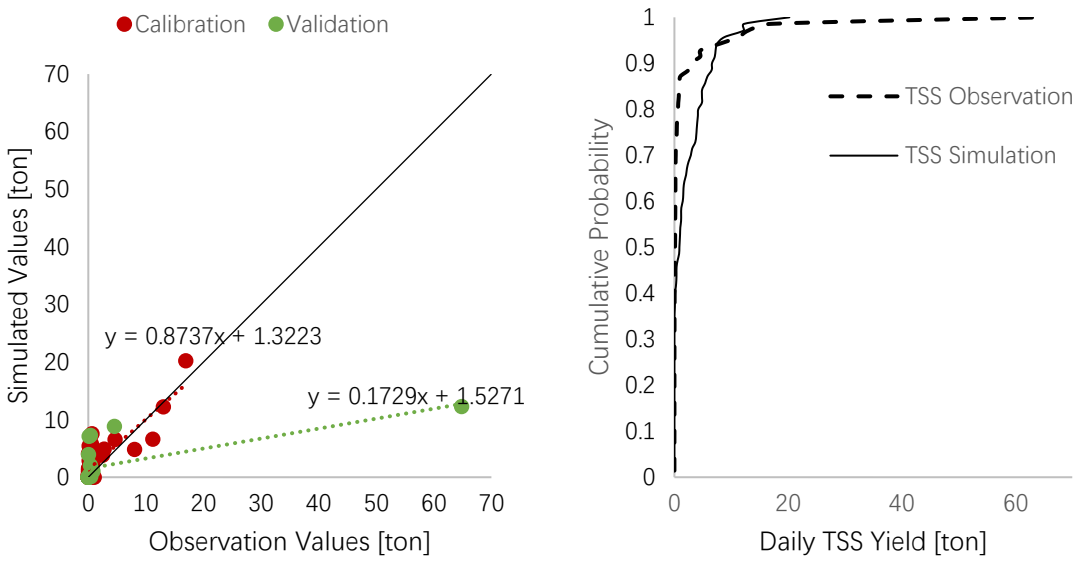

Figure 3-4. The Daily Observation and Simulation of Total Suspended Solids for Calibration and Validation (Left) and Cumulative Distribution of Daily Simulation and Observation (Right)

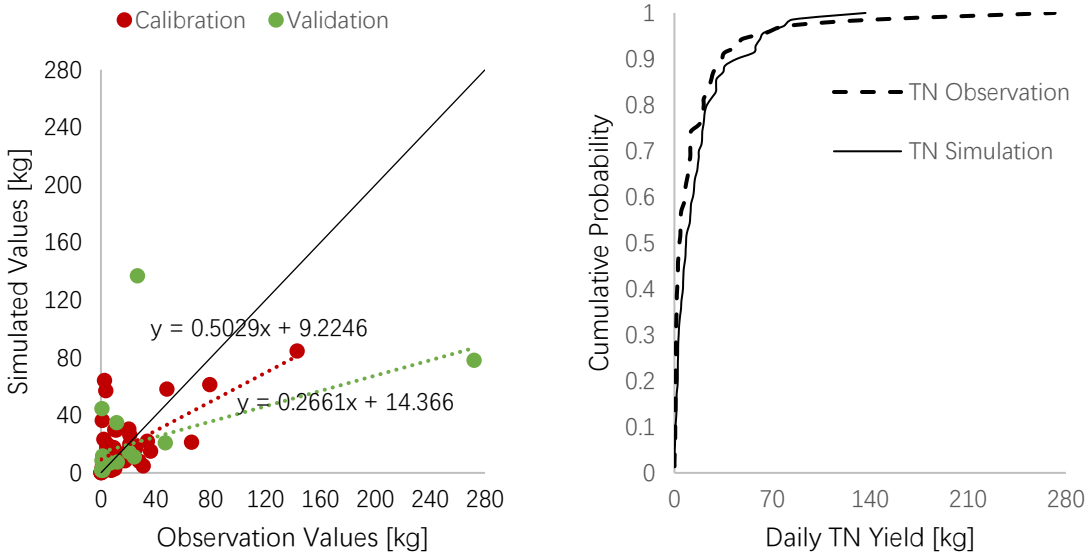

Figure 3-5. The Daily Observation and Simulation of Total Nitrogen for Calibration and Validation (Left) and Cumulative Distribution of Daily Simulation and Observation (Right)

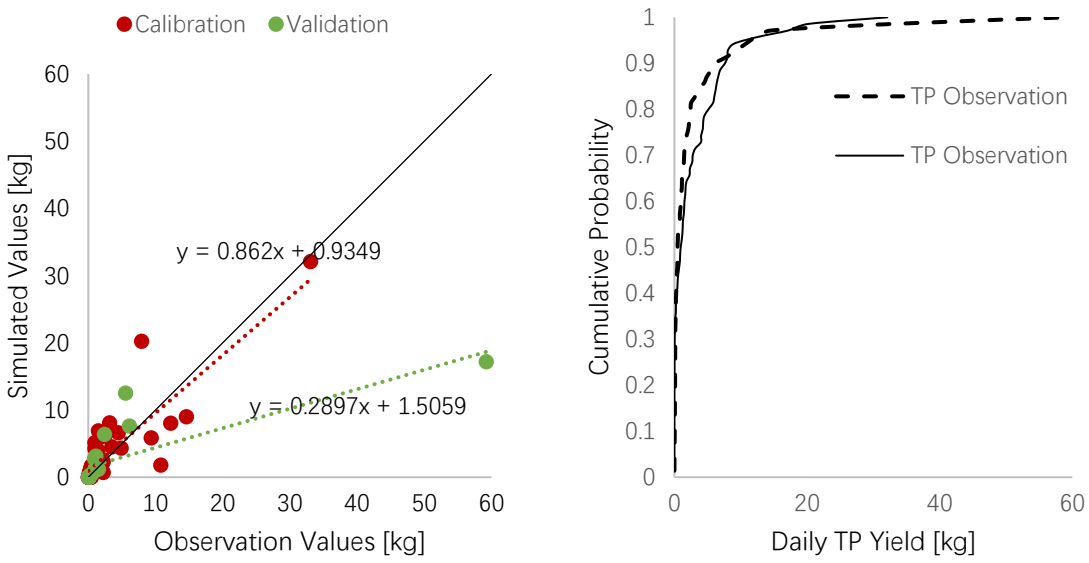

Figure 3-6. The Daily Observation and Simulation of Total Phosphorus for Calibration and Validation (Left) and Cumulative Distribution of Daily Simulation and Observation (Right)

Figures 3-4 to 3-6 show the observations and estimations for the validation periods. It is clear that there is one extreme observation of TSS, TN and TP. The values are more than twice of the highest observations in calibration periods. Due to the lack of data variance, one single extreme events with a poor estimation can influence the statistic significantly, and this is the reason for relative poor validation statistics. One interesting thing is the sign of bias for the TSS, TN and TP was changed between calibration and validation. It is possible to represent a local bias between calibration and validation years, but it may also be caused by the imprecise observation measurements. The observations were in units of concentration, such as mg/L, and there are uncertainties associated with using these point values to represent the total yield in a whole day, which may be an indirect reason for the poor statistics for TSS, TN and TP in the validation period.

Other than the extreme data point, it is also normal to have the validation periods with a poorer statistics than the calibration periods (Moriasi et al., 2007). This is mainly

because the calibration periods and validation periods were split with calendar years, which are mutually independent. The parameters calibrated based on the calibration periods may perform poorer in the validation period due to the difference between years. A good statistics on validation periods indicates the calibrated model not only can work on calibration periods, but also would perform well on other years consistently. Therefore, the slightly poorer statistics of validation in this study is acceptable.

Moreover, there is an issue related to the evaluation criteria. The criteria used and recommended by SWAT are based on the monthly time-step, and may not apply directly to the daily time-step of the present study. Based on the criteria, Moriasi et al. (2007) also pointed out that the model simulations are generally poorer for a shorter time-step, like daily time-step, than a longer one, like a monthly or yearly time step. The extreme stormwater events in single days can be diluted into the whole month when using monthly time-step, and the seasonal biases can be neutralized in the yearly time-step, which may lead to easier and better calibrations.

It may work to use some random observations to represent the whole month or year. However, in this study, the TSS, TN and TP were measured during stormwater flow events, not randomly. Moreover, the record only include one or two observations in each month. Therefore, it is impossible to calibrate them in a monthly or yearly time-step due to the lack of observations.

3.1.4 Summary

The hydrological model produced by SWAT in Wilde Lake area is considered as satisfactory based on the current information. The surface runoff is good on both calibration and validation at the daily time-step. NSE of the surface runoff is 0.66 and

0.51, and the PBIAS is -24.1% and -10.4% for the calibration and validation period respectively. The complete discharge data from the USGS station contributes to the good performance of model simulation on surface runoff.

The water quality variables perform worse than the surface runoff, which may be caused by the uncertainties of the observation measurements, and estimation of water quality parameters. The TSS NSE of 0.54 with a bias of 85.7% in the calibration period, shows a strong correlation coefficient of 0.84. However, in the validation period, it has a negative bias of -40.1% with a NSE of 0.27. The nitrogen has the NSE at 0.41, and phosphorus has NSE at 0.71, while both bias are below ±25%, which is considered as good results. The validation shows a slight lower statistics on NSE with a better bias performance, which is reasonable and acceptable due to the extreme values. The change of sign of PBIAS indicates some uncertainties were observed in calibration and validation periods, which may related to the observation data and the bias among years.

Overall, for all four variables, the calibrated model on Wilde Lake is statistically satisfactory in the calibration/validation process. Although there is a relatively high bias to the observations due to the limitations, parameter values are rational and in the range consistent with that found by Wang (2015) and Renkenberger et al. (2015). It is still good enough and capable to be used for modeling future yields and compare the changes under the climate change to the historical baseline.

3.2 Results for Objective 2: Climate Change Impacts on Stream Water Quantity and Quality

The second objective in this study is to identify the total surface runoff as well as the in-stream water quality variables at the outlet of the Wilde Lake in the historical baseline and the future. All works are based on the calibrated SWAT model generated in this research. The downloaded downscaled climate data were processed by the CMHyd program to correct the bias based on historical observations from NCDC.

The climate change data were used in the SWAT model, with daily precipitation and temperature for the period of Jan 2016 to Dec 2099. After the SWAT model was executed for both historical and future periods, the output data at Wilde Lake outlet was extracted and analyzed.

3.2.1 Climate Data and Bias-Correction

Nineteen (19) future climate scenarios were used for the prediction, the detailed information is shown in the section 2.5.1. Additionally, one set of NCDC historical data obtained from NOAA, was used for the bias correction and generating historical baseline.

Figure 3-7 shows the statistics of historical data, and Figure 3-8 shows the statistics of one test model GFDL-CM3 at RCP8.5. The time period used for the statistical analyses is 1961 to 2000. There is no significant difference on the yearly mean value between NCDC and modeled data, although the monthly distribution is significantly different. The standard deviation of climate model is slightly higher than the observations. However, the biggest problem is the precipitation intensity. The climate model only has one third of the precipitation intensity of the NCDC observation. This is caused by the climate models themself. The climate model would normally generate a

relative smoother curve, and this would contribute less extreme values such as zero values than them in the real life. As is also shown wet day probability plot in the Figure 3-7, there are only about 30% of days at Wilde Lake are wet days, which means about 70% of days are days with no precipitation. However, in the historical period of the climate model, only about 30% of days are rain-free days. This indicates that, the most important consideration for the bias correction of precipitation is the intensity and frequency of occurrence, rather than the mean and standard deviation.

To fix this, CMHyd program was executed. The statistics of bias-corrected historical data from the climate model are shown in Figure 3-9. This figure shows that the wet day probability and the precipitation intensity is almost the same between the NCDC observation and the climate model GFDL-CM3 at historical period. The slightly difference between them is caused by the difference of location coordinate.

Although the intensities at historical time period are the same in the monthly time-step, the future time period is still significantly different from historical time period. And this is exact how the climate model works. As with the precipitation, the temperature data were also bias corrected with the distributing mapping methods as is stated in the section 1.5.3.2.

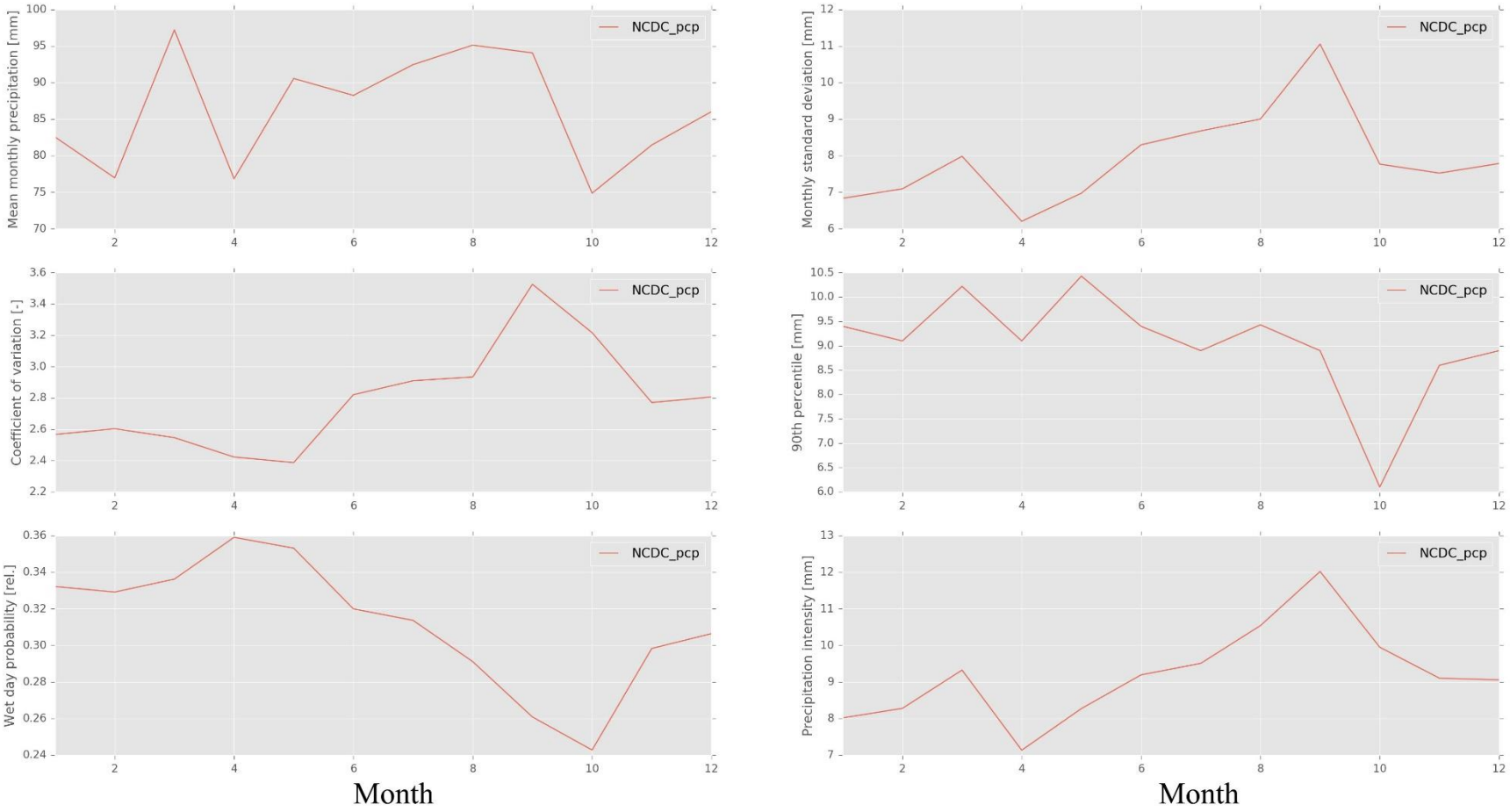

Figure 3-7. Statistics of Precipitation at NCDC Observation Climates at Historical Periods from 1961 to 2000

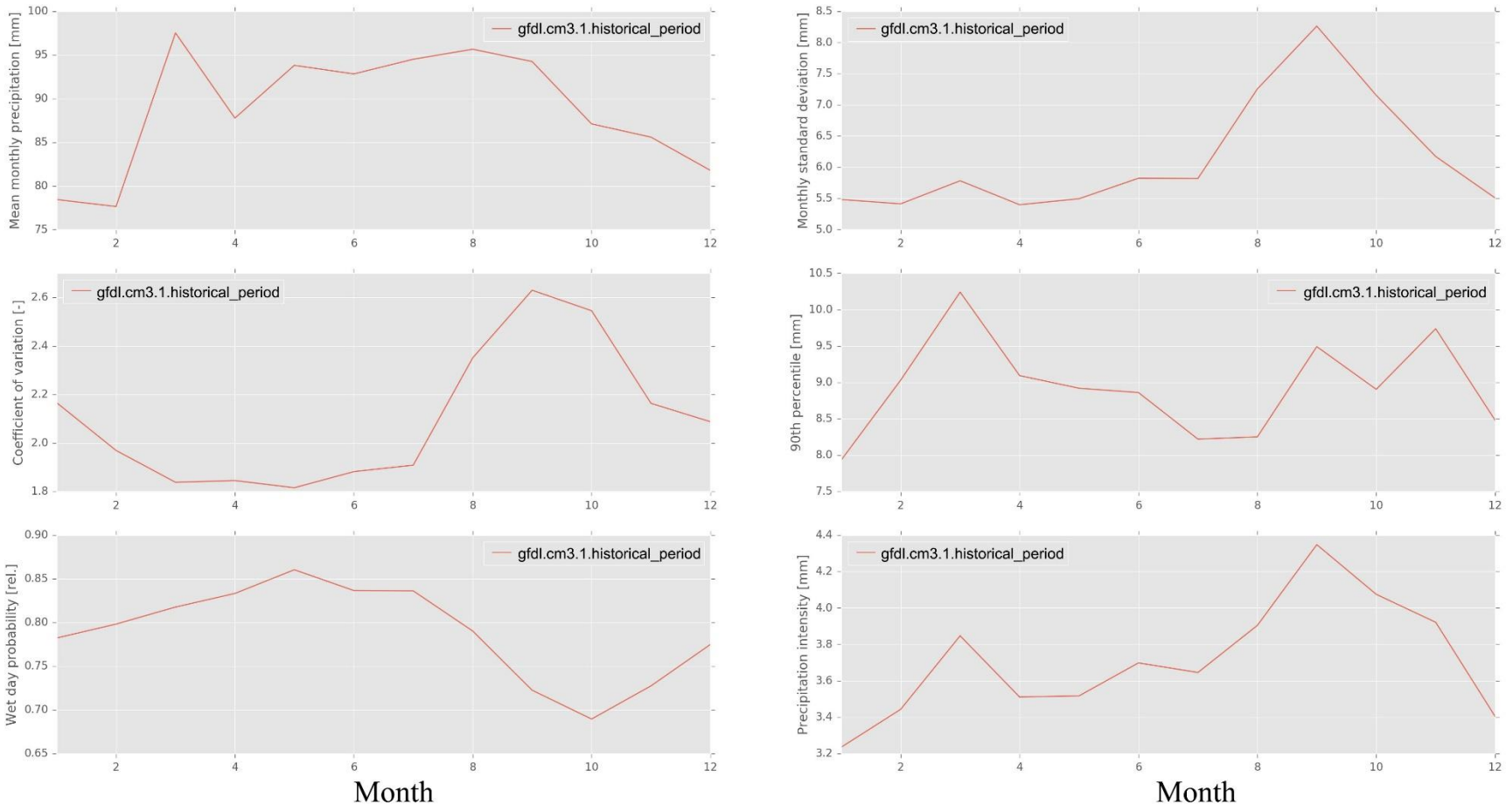

Figure 3-8. Statistics of Precipitation of GFDL-CM3.1 Periods at Historical Periods from 1961 to 2000 before Bias-Correction

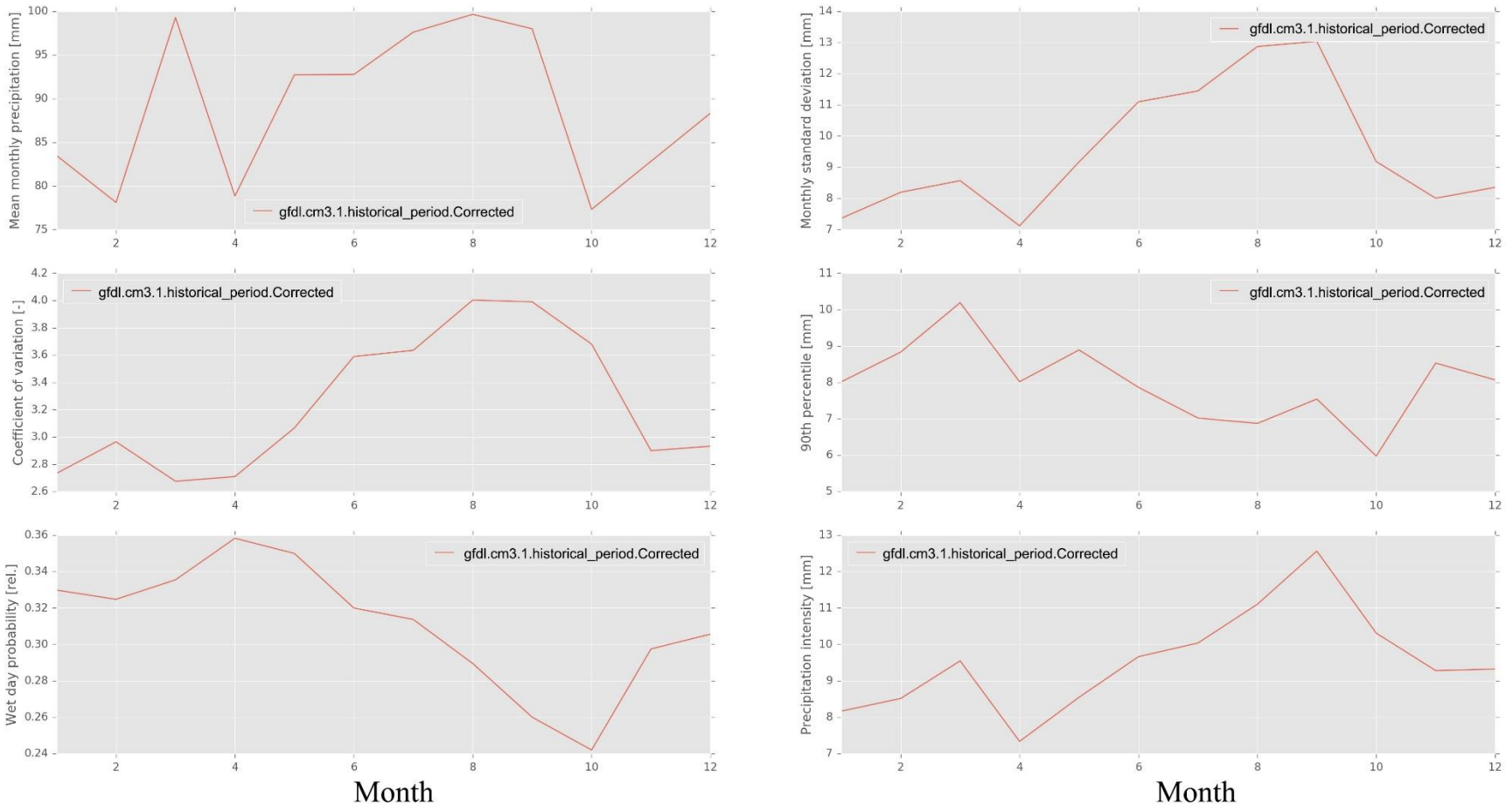

Figure 3-9. Statistics of Precipitation of GFDL-CM3.1 Periods at Historical Periods from 1961 to 2000 after Bias-Correction

3.2.2 Climate Change Input Data

Before running and analyzing the models, statistics of the input files are analyzed and shown in the Table 3-7. At the sections of the input file analyses and the output analyses for the future, the end-century period is used from 2080 to 2099. The historical baseline is from 1970 to 1989.

The results in the table shows that all climate models in the future have a higher average precipitation and a higher standard deviation than the historical period. And only two models have a lower 95the percentile than the historical data. Therefore, all models at all RCPs suggest more average rainfall than the historical baseline, and it is highly possible to have more extreme stormwater events in the future at Wilde Lake area.

Table 3-7. Statistics of Future Daily Precipitation (mm) From 2080 to 2099

Model	Average	SD	Percentile			
			50th	75th	90th	95th
NCDC Historical Baseline	2.93	8.20	0.00	1.00	9.90	18.46
Model1_RCP2.6	3.45	10.79	0.00	1.52	9.67	20.23
Model1_RCP4.5	2.94	9.96	0.00	0.95	7.86	16.64
Model1_RCP8.5	3.31	10.17	0.00	1.64	9.26	19.32
Model2_RCP4.5	3.09	10.05	0.00	0.62	8.68	19.11
Model2_RCP8.5	3.41	11.37	0.00	0.87	9.09	20.53
Model3_RCP2.6	3.55	10.67	0.00	1.52	10.13	21.24
Model3_RCP6.0	3.66	10.40	0.00	1.70	11.29	22.20
Model3_RCP8.5	3.79	10.83	0.00	1.85	10.90	21.87
Model4_RCP2.6	2.97	9.61	0.00	0.00	8.37	18.61
Model4_RCP4.5	3.82	12.06	0.00	0.86	10.99	23.78
Model4_RCP6.0	3.20	10.14	0.00	0.00	8.64	20.23
Model4_RCP8.5	3.72	12.49	0.00	0.00	10.30	23.07
Model5_RCP2.6	3.40	10.62	0.00	1.21	9.07	20.20
Model5_RCP4.5	3.31	10.79	0.00	0.97	8.95	19.50
Model5_RCP8.5	3.55	11.36	0.00	1.07	9.77	21.70
Model6_RCP2.6	2.73	9.24	0.00	0.00	7.24	16.43
Model6_RCP4.5	3.22	10.58	0.00	0.45	8.73	19.43
Model6_RCP6.0	3.10	9.96	0.00	0.48	8.72	18.96
Model6_RCP8.5	3.54	10.89	0.00	0.89	10.79	21.13

The Table 3-8 shows the relative increase of daily mean precipitation comparing to the historical data. It can be concluded that the difference between climate models is larger than the differences between RCPs. Especially, the RCP2.6, RCP4.5 and RCP6.0 has a similar mean daily precipitations, but the RCP8.5 has a significant higher average precipitation. This is corresponded to the radiative forcing Figure 1-6 that the changes between RCP2.6, 4.5 and 6.0 is small within the 21 century.

Table 3-8. The Change of Precipitation in End-century relative to their historical baseline

	Model1	Model2	Model3	Model4	Model5	Model6	Avg(SD)
RCP2.6	24%		28%	-6%	17%	-4%	12% (16%)
RCP4.5	6%	6%		21%	14%	14%	12% (6%)
RCP6.0			32%	1%		10%	14% (16%)
RCP8.5	19%	16%	37%	18%	22%	25%	23% (8%)
Avg	16%	11%	32%	8%	17%	11%	
(SD)	(9%)	(8%)	(4%)	(13%)	(4%)	(12%)	

The statistics of temperature are shown in Table 3-9. The historical temperature shows an average yearly minimum of 7.6 °C and an average yearly maximum of 18.4 °C. The difference between maximum and minimum is around 11 °C. Except the model6 at RCP2.6, all other climate models in all RCPs shows a significantly higher temperature, for both minimum and maximum values.

Table 3-9. Statistics of Future Temperature (°C) from 2080 to 2099

Model	Min	Max	Average	DailyDifference
NCDC Historical Baseline	7.6	18.4	13.0	10.8
Model1_RCP2.6	10.1	21.4	15.7	11.3
Model1_RCP4.5	11.5	22.8	17.1	11.3
Model1_RCP8.5	14.5	25.6	20.0	11.1
Model2_RCP4.5	10.7	22.0	16.4	11.3
Model2_RCP8.5	12.9	24.3	18.6	11.3

Model3_RCP2.6	10.6	22.4	16.5	11.8
Model3_RCP6.0	12.2	24.3	18.3	12.1
Model3_RCP8.5	14.2	26.4	20.3	12.2
Model4_RCP2.6	9.1	20.6	14.9	11.6
Model4_RCP4.5	10.8	22.2	16.5	11.5
Model4_RCP6.0	11.3	23.0	17.2	11.7
Model4_RCP8.5	13.7	25.4	19.5	11.7
Model5_RCP2.6	10.3	22.0	16.2	11.7
Model5_RCP4.5	11.5	23.4	17.5	11.9
Model5_RCP8.5	14.4	26.2	20.3	11.8
Model6_RCP2.6	7.5	18.1	12.8	10.6
Model6_RCP4.5	9.4	20.6	15.0	11.2
Model6_RCP6.0	9.9	21.0	15.4	11.2
Model6_RCP8.5	11.4	22.7	17.1	11.3

Table 3-10 shows the relative increase of the average temperature between climate models and historical data. Unlike the precipitation data, the differences among scenarios are significant. The RCP8.5 shows the greatest temperature increase, which is similar to that of precipitation data. The temperature difference among models are large as well, the model 6 shows a significantly lower temperature increase than other models, which also corresponds to the performance in the precipitation data. The model1 model 3 and model 5 at scenario RCP8.5 show an average increase larger than 7 degree at the end of century, which are extremely high.

Table 3-10. The Change of Temperature (°C) in End-century Relative to Historical Baseline

	Model1	Model2	Model3	Model4	Model5	Model6	Avg (SD)
RCP2.6	2.8		3.4	2.1	3.3	-0.2	2.3 (1.5)
RCP4.5	4.2	3.4		3.8	4.6	2.0	3.6 (1.0)
RCP6.0			5.2	4.5		2.5	4.0 (1.4)
RCP8.5	7.1	5.6	7.2	6.8	7.4	4.1	6.4 (1.3)
Avg (SD)	4.7 (2.2)	4.5 (1.6)	5.3 (1.9)	4.3 (1.9)	5.1 (2.1)	2.1 (1.7)	

Overall, the precipitation and temperature data indicate a warmer and wetter future in almost all cases. Higher precipitation would normally cause increases in surface runoff as well as in those water quality variables correlated with runoff. The higher air temperature contributes to higher soil temperature and water temperature, and may influence snow cover, humidity, and nutrient cycling processes such as mineralization and decomposition. For example, other factors including the rates of denitrification and volatilization both increase when the temperature increases, so the TN may slightly decrease as a result of higher temperatures.

3.2.3 Reach Output Data

The output data from SWAT was extracted and analyzed by RStudio. Whereas Reach11 was used in the calibration, the reach at the outlet, reach20, was used for analyzing the average runoff and total in-stream TSS, TN and TP at the outlet.

Table 3-11 shows the average yearly in-stream variables at the outlet of Wilde Lake in the NCDC historical period with the NCDC historical climate data (1970 to 1989). The historical surface runoff is 0.0054 m^3/s with the NCDC historical climate data, and the TSS yields is 44.4 tons. The TN and TP yields are 592kg and 72 kg respectively. The historical periods of all 6 climate models show similar results, which indicates that the models are all agreed with historical observations, at least in the mean.

Table 3-11. Historical Baseline of NCDC Observation and Model Simulations

	NCDC	Model1	Model2	Model3	Model4	Model5	Model6
SufQ [cms]	0.0054	0.0053	0.0056	0.0051	0.0062	0.0056	0.0053
TSS [ton]	44.4	42.9	46.5	43.2	48.4	46.2	45.1
TN [kg]	592.2	502.3	535.1	567.0	546.6	550.9	531.1
TP [kg]	72.2	71.7	76.7	73.3	82.3	75.2	71.0

Figure 3-10 shows the time series plot of surface runoff among different climate models and RCPs for both historical periods from 1965 to 2015 and future periods from 2016 to 2099. In the figure, the black lines are the yearly time series lines, and the blue line is the trend line. The first column shows the modeled historical surface runoff with NCDC data and six models. The historical value should be similar principally, but some of models still show different patterns. As is shown at the last row, the NCDC-domain model outputs a slightly increase surface runoff at the outlet. The model 1, 3 and 5 show a faster increase than the NCDC data at historical period. The model 2 shows a slightly slower increase, while the model 4 and 6 show a decrease at the historical period.

The results indicate although climate model inputs are bias corrected by the historical period, there would still be a large difference between models at the historical period. Therefore, in this study, for each model, the future simulations are compared to their own historical periods, which can represent their increment of changes.

A summary of the increase rate by comparing the mean surface runoff in the future period to the historical period is shown in the Table 3-12. Comparing the models, model3 has the largest increase in surface runoff for all RCPs, while model1 has the smallest increase in all RCPs. This result corresponds to the precipitation data analyzed in the section 3.2.2. Comparing the scenarios, the RCPs from 2.6 to 8.5 should show a continuous growth, but RCP4.5 and 6.0 do not follow the expected trend. In some cases, the RCP4.5 has a lower value than the RCP2.6, and the RCP6.0 may have a lower value than RCP4.5. This also corresponds to the precipitation and temperature data, which indicates some models at some scenarios may not produce reasonable predictions in

specific years. For most of cases, the RCP2.6 shows the lowest values, and the RCP8.5 shows the highest values.

From the Figure 3-10, we can see in RCP2.6 or RCP4.5, Model2, 4 and 5 show a negative slope in the trend line, which means a possible decrease of surface runoff in the far future may happen. This is also possible because the RCP2.6 and RCP4.5 assume a peak of radiative forcing at 2020s and 2050s respectively, and then it may decrease. In RCP 6.0 and RCP8.5, all models show increasing trends, and this corresponds with the continued growth in radiative forcing.

From Table 3-12, when comparing the last 20 years in the 21st century to the historical baseline, the RCP2.6 shows the mean increase rate of surface runoff ranging from -10.6% to 40.0%, with an average value of 15.8%. The RCP8.5 shows the mean increase rate of surface runoff ranging from the 25.9% to 56.6%, with an average value of 34.7%.

Table 3-12. Increase in SurfQ by Comparing the Mean Value of End-century to Their Own Historical Baseline

	Model1	Model2	Model3	Model4	Model5	Model6	Avg (SD)
RCP2.6	32.4%		40.0%	-10.6%	20.3%	-3.2%	15.8% (22.0%)
RCP4.5	11.6%	8.5%		31.2%	13.3%	25.4%	18.0% (9.8%)
RCP6.0			44.7%	1.4%		15.5%	20.6% (22.1%)
RCP8.5	25.9%	28.7%	56.6%	27.4%	30.5%	39.1%	34.7% (11.7%)

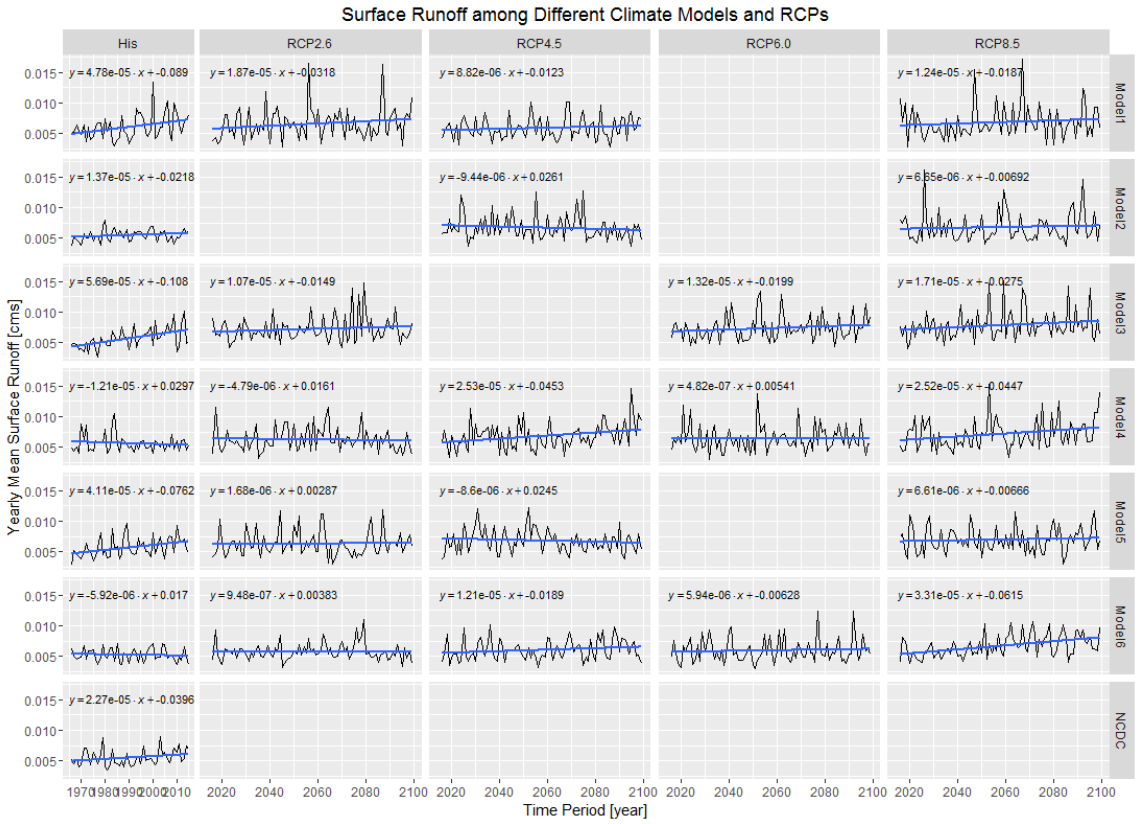

Figure 3-10. Yearly SurfQ from 1965 to 2100 among Different Models and Scenarios

The results of water quality variables, including TSS, TN and TP are shown in Figures 3-11 to 3-13. During the historical period driven by the NCDC weather data, all three water quality constituents show an increasing trend. Different to the hydrology results, almost all models show an increase trend similar to the NCDC output data in historical period. However, the results for the future, the results vary widely. For TSS, at the scenario RCP8.5, Model1, 2, 3 and 5 show a slight increase, while Model 4 and 6 show a significantly increasing trend. For TN, at the scenario RCP8.5, Model 2, 4 and 6 show a significantly increasing trend, while Model 3 and 5 show a significantly decreasing trend. The TP has a special story, which is analyzed late in the section. The wide variance represents great uncertainties among the study period, in particular, the historical period even after the bias correction. This is corresponded to the statement by

Maurer et al., (2014) that the downscaled climate data cannot represent specific days, only the statistics are reasonable.

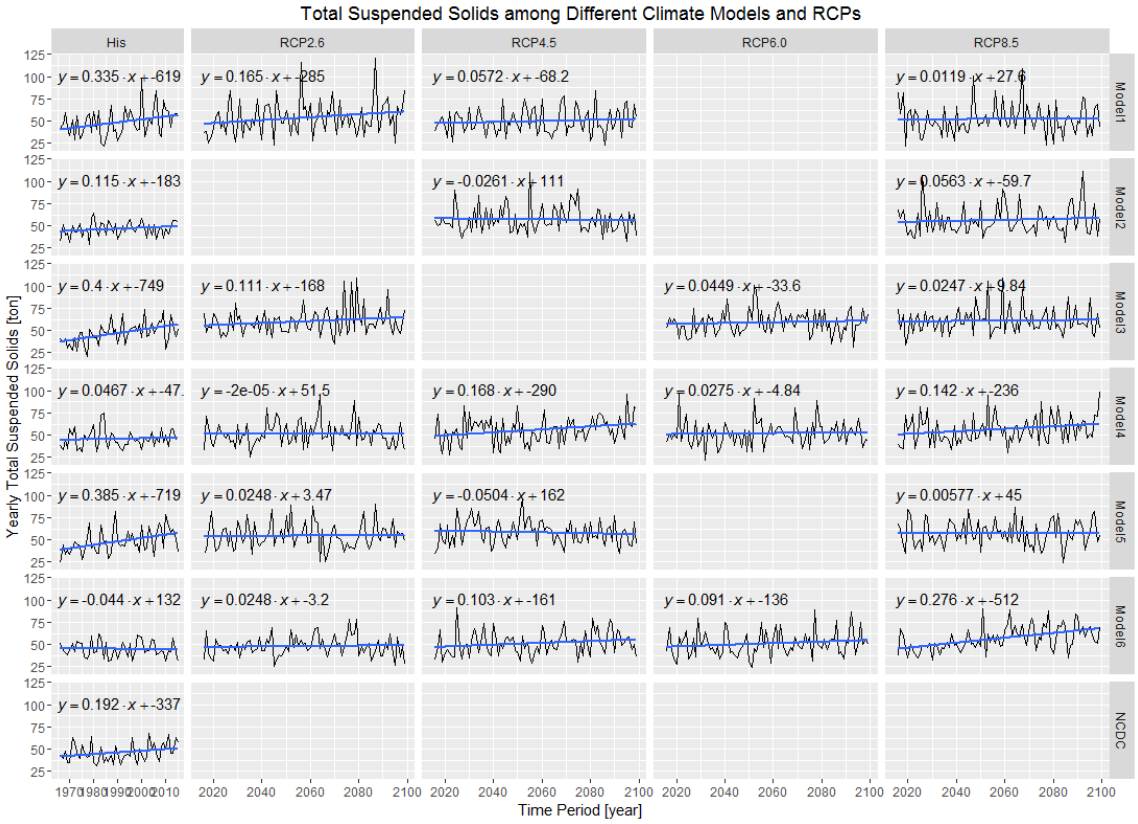

Figure 3-11. The Yearly TSS from 1965 to 2100 among Different Models and Scenarios

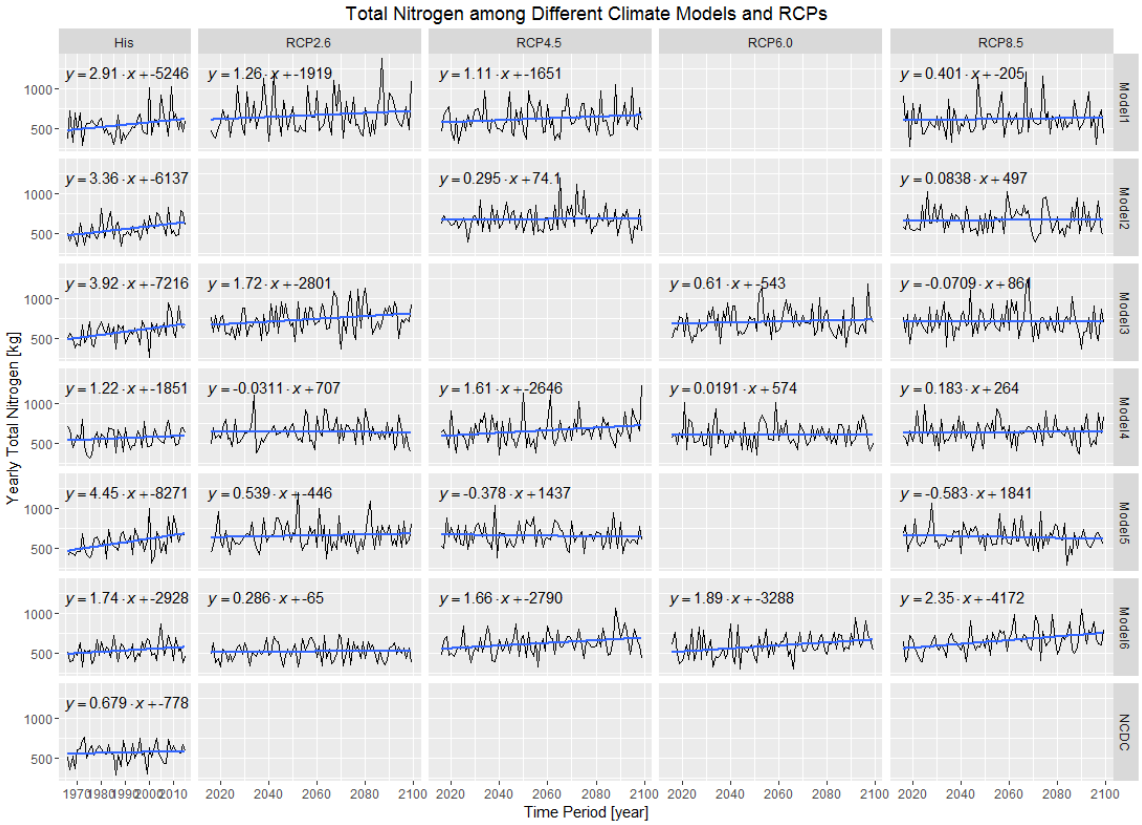

Figure 3-12. The Yearly TN from 1965 to 2100 among Different Models and Scenarios

The data of relative increase for each model are shown in Table 3-13. For the scenario RCP2.6, the TSS would increase -4.5% to 44.3%, with an average of 20.1% among six models. For the RCP8.5, the TSS would increase 15.7% to 37.9%, with an average of 28.6%. When comparing the TSS to the surface runoff, it is easily to find the increase rates are very close to each other. Among 19 outputs from different models and scenarios, 13 of them show a difference within ±5%. Erosion caused by rainfall and runoff is calculated by the Modified Universal Soil Loss Equation (MUSLE), which is the main soil loss equation used in the SWAT (Neitsch et al., 2011). And within the equation, most parameters, such as USLE_K, are calibrated, and the main variables changing with the different climate data are the surface runoff amount and peak flow.

Therefore, with the increase of surface runoff in the future, the increase of TSS is logical. Moreover, the high intensity precipitation does not increase significantly like the total precipitation do. Therefore, all six models at RCP8.5 show a smaller increasing rate on TSS than surface runoff.

Table 3-13. The Increasing Rate of TSS by Comparing the Mean Value of End-century relative to Their Own Historical Baseline.

	Model1	Model2	Model3	Model4	Model5	Model6	Avg (SD)
RCP2.6	37.2%		44.3%	-1.2%	24.7%	-4.5%	20.1% (22.2%)
RCP4.5	16.5%	13.8%		33.4%	20.2%	23.5%	21.5% (7.6%)
RCP6.0			30.1%	6.1%		19.7%	18.6% (12.0%)
RCP8.5	15.7%	26.0%	37.9%	27.0%	26.4%	38.4%	28.6% (8.5%)

The TN has a different pattern to SurfQ and TSS. The average increase rate at RCP4.5 is the highest, but the RCP 8.5 is the lowest. This indicates that RCP4.5 and RCP6.0 are very close before 2100. Several mechanisms may contribute to the nitrogen increase; the inner cycle of Nitrogen is main reason. In real life, as is mentioned in the section 1.3.3, the denitrification and volatilization are both related to the temperature. The high temperature in the future would increase the denitrification and volatilization and finally decrease the nitrogen yield. Although the high precipitation would increase soil moisture condition in sub-layers and result in a greater amount of leaching, the influence of precipitation is not as significant as the temperature for the transportation of total nitrogen. Therefore, relative low increasing rates of TN are simulated in the future.

As is shown in the Figure 3-13, the in-stream phosphorus show a significantly increase in all models, including the historical periods. The trend line in historical is very steep as well. A test run shows the change of model start year would change the phosphorus time series significantly. There is no similar problems found in journal

articles, but several users reported this issue in the official forum SWAT google groups. The possible reason is the phosphorus environment in SWAT is not in pseudo-steady state conditions. Therefore, the soil chemistry are not in equilibrium with phosphorus application and removal. And in this study, it shows a phosphorus accumulation. On the one hand, this may be caused by the errors in model calibration. Due to the short of observations, it calibrates a result with a slightly increasing trend of phosphorus, although it looks like in an equilibrium during that several years of calibration. This is a big challenge due to the lacking of data. This indicates that phosphorus requires observations on more years, such as decades of data, due to the phosphorus play a complicated role in the soil chemistry. And this also indicates that the SWAT calibration of phosphorus would be good for a short-term prediction, but not for a longer term.

Table 3-14. The Increasing Rate of TN by Comparing the Mean Value of End-century relative to Their Own Historical Baseline.

	Model1	Model2	Model3	Model4	Model5	Model6	Avg (SD)
RCP2.6	37.7%		32.9%	9.6%	20.7%	-7.1%	18.7% (18.1%)
RCP4.5	27.5%	16.6%		25.9%	14.5%	25.6%	22.0% (6.0%)
RCP6.0			19.2%	10.0%		24.5%	17.9% (7.3%)
RCP8.5	14.1%	17.8%	9.7%	11.6%	6.9%	29.4%	14.9% (8.0%)

On the other hand, the modeled phosphorus accumulation may be a real phenomenon. As a sub-urban area, Wilde Lake used large amount of fertilizer, which is also covered in the SWAT model, and this would possibly result in an increasing of phosphorus both in soil and stream. Due to the lack of data, to verify the model correctness, data from several other lakes in Maryland were obtained and compared.

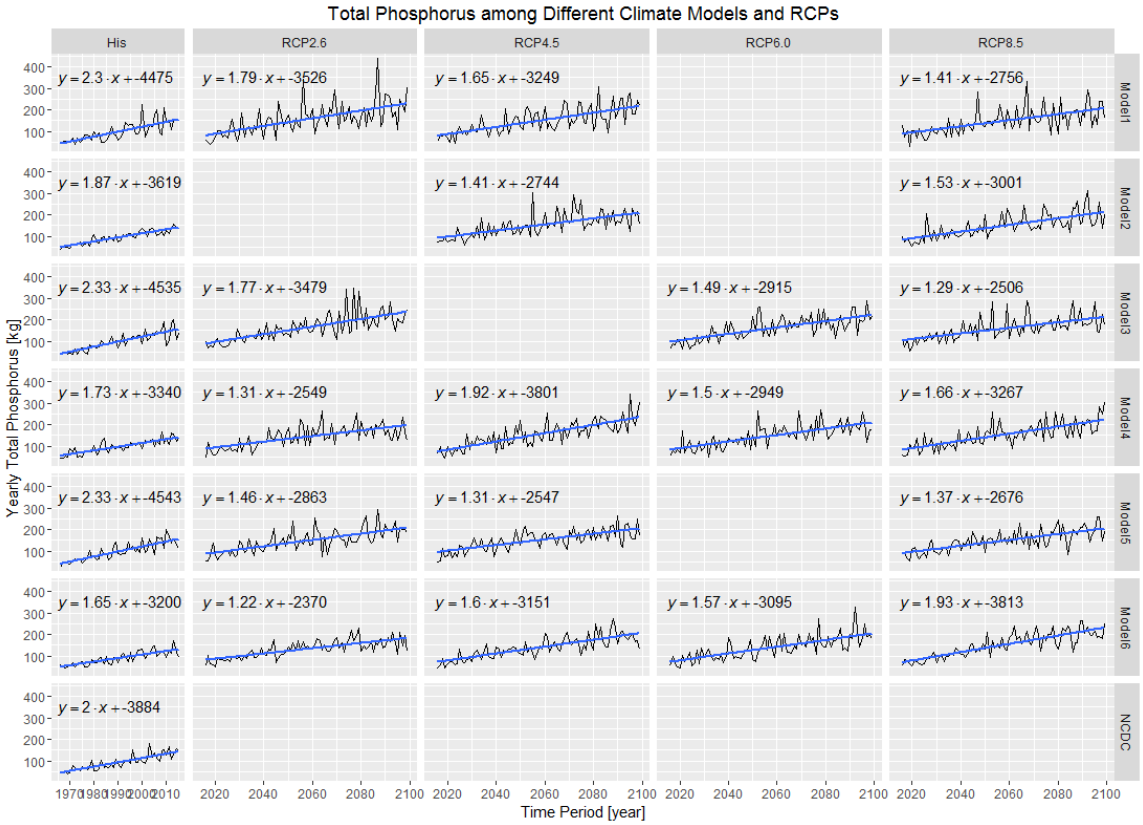

Figure 3-13. The Yearly TP from 1965 to 2100 among Different Models and Scenarios

Totally two sets of phosphorus statistical data were obtained from USGS stations. These two stations are less than 30 miles away from the Wilde Lake observation location. One is the station located at Northeast Branch Anacostia River at Riverdale, MD, another is located at Paint Branch Near College Park, MD. The Figure 3-14 shows the median of the total phosphorus observations at Anacostia River, the unit is kilograms per hour. The data range from 2007 to 2015. The total phosphorus at Paint Branch is not readable, so the median of phosphorus concentrations and the discharge observations at Paint Branch were obtained (Figure 3-15). The unit is kilograms per liter and cubic feet per second, and the time range from 2008 to 2015. The total phosphorus is increasing significantly during among these 9 years. Although the total amount of phosphorus at Paint Branch data is not

available, both phosphorus concentration and the discharge show increases. Therefore, the TP would have increased significantly as well.

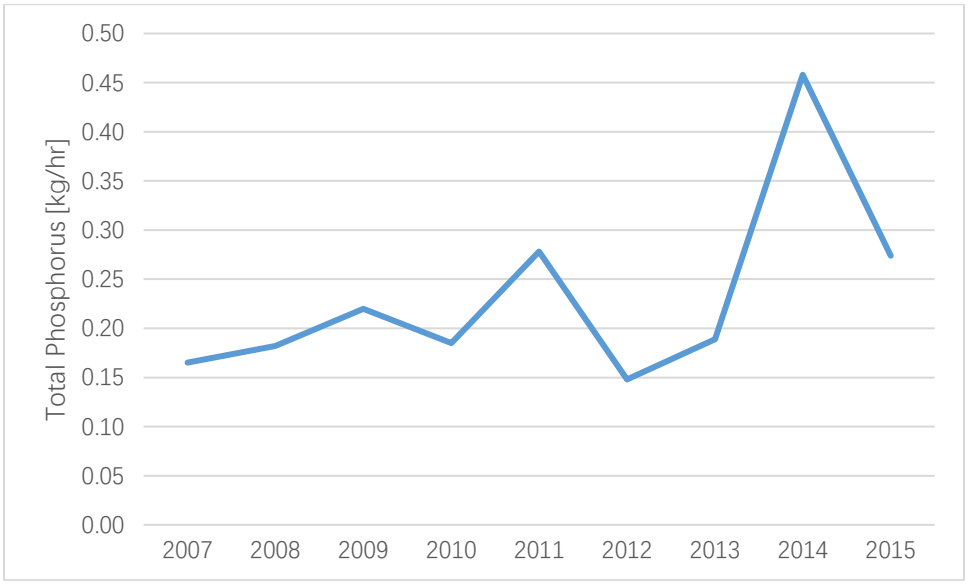

Figure 3-14. Median TP in Northeast Branch Anacostia River at Riverdale from 2007 to 2015

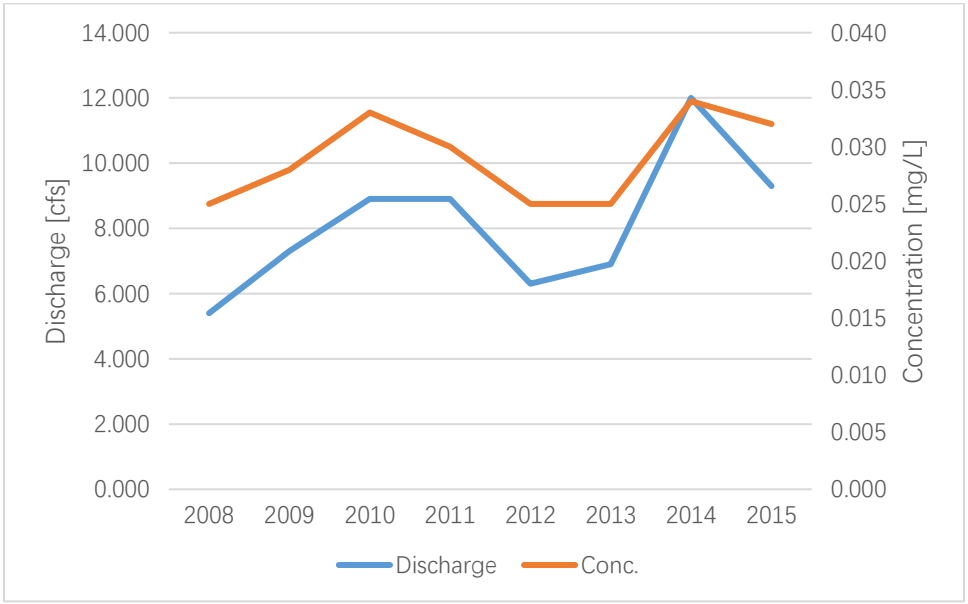

Figure 3-15. Discharge and Concentration of TP in N Paint Branch near College Park from 2008 to 2015

Thus, the continuous increase of TP in SWAT outputs from 1970 to 2010 is not necessarily a mistake by the model. It would possibly be a fact around the study area. For the study of the impact of climate change, additional simulations with the same spin-up years were tested for the phosphorus. Table 3-15 shows the average increasing rate of total phosphorus in all models without the possible bias of phosphorus accumulation. It shows an average increase rate of 20.6%, 23.8%, 19.2% and 22.5% for RCP2.6, 4.5, 6.0 and 8.5 respectively comparing the yields at the end-century to historical baseline. Different models still show significant differences, but the average values among different scenarios are very close to each other. This is because the phosphorus mainly related to the very top soil layer, which is not influenced by the climate models and scenarios as much as other variables.

Table 3-15. The Increasing Rate of TP by Comparing the Mean Value from 2080 to 2099 to Their Historical Periods from 1970 to 1989.

	Model1	Model2	Model3	Model4	Model5	Model6	Avg (SD)
RCP2.6	46.4%		45.5%	-6.4%	21.8%	-4.5%	20.6% (25.7%)
RCP4.5	31.4%	12.9%		33.6%	16.8%	24.0%	23.8% (9.0%)
RCP6.0			27.6%	6.8%		23.1%	19.2% (10.9%)
RCP8.5	18.3%	18.0%	25.7%	17.4%	15.5%	40.0%	22.5% (9.2%)

3.2.4 Summary

With the analyses on input data, the climate models show significant increase in both precipitation and temperature. The mean precipitation would increase on average by approximately 12% to 23% in different RCPs, and the temperature would increase by 2.3 to 6.4 °C. Different models show different rates of increase. The model3, GFDL-CM3, developed by NOAA, shows the most increase among all six models, and the precipitation increase is on average twice that other models. Therefore, a warmer and

wetter climate would be the real future based on 19 Models/RCPs at Wilde Lake area. The increase of precipitation and the intensity would cause a higher surface runoff, and then influence the TSS and nutrients directly. The increasing of temperature would mainly affects the plants and nutrient cycle, and then affects the nutrients indirectly.

The output at the outlet of Wilde Lake in the NCDC historical baseline for the SurfQ, TSS, TN and TP are 0.0054 cms, 44.4 tons, 592.2 kg, and 72.2 kg respectively. In the RCP8.5 at the end-century, the average increasing rate in all six models of SurfQ, TSS, TN and TP is 34.7%, 28.6%, 14.9%, and 22.5% respectively. These are directly caused by the climate change such as the higher precipitation and high temperature. The TP yield from the SWAT model shows an increase with time, and the increasing rate would be high than 100% at the end of 21st century. This may be caused by the limitation of observation data, but is still possible to be a fact in the study area due to the overuse of fertilizer, and the phosphorus control is necessary if this is true.

All in-stream variables at the outlet show a significant increase in the future, which indicates the climate change would cause a negative impact on the water quality issues at the study area. It also indicates the sub-urban watersheds of Chesapeake Bay may face the similar problem, and this would critical issues on the bay environment.

3.3 Results for Objective 3: Climate Change Impacts on On-land Variables and CSA Identification

3.3.1 Watershed Response to Current Climate

The on-land yields are obtained from model output for both historical and future climate scenarios. In this section, the time periods are selected as follows: the historical data from 1970 to 1989, the mid-term future from 2040 to 2059 , and the far-term future from 2080 to 2099.

The on-land per area outputs historical baseline values are shown below (Table 3-16). The Surface runoff by HRU has a maximum yield of 899 mm, and the average yields for all 1334 HRUs are 200 mm. The TSS show a maximum yield of 142 ton/ha, which is much higher than the average yield of 0.55 ton/ha. The standard deviation is 11.8 for TSS, which is also much higher than the weighted average yield. This indicates that the TSS yields are very high in several HRUs, but the most areas with good plant cover have a low TSS yields. The nutrients show an average yield of 9.42 kg/ha for TN and 1.09 kg/ha for TP, and their standard deviations are about twice higher than the average as well. Overall, the variation of surface runoff yields among RHUs are small, while that of the water quality variables are high.

Table 3-16. The Statistics of Pollutant Yields among HRUs in Historical Baseline

	SurfQ [mm]	TSS [ton/ha]	TN [kg/ha]	TP [kg/ha]
Max	899.29	142.18	100.09	44.66
Min	0	0	0	0
Avg (Weighted)	200.47	0.55	9.42	1.09
SD	226.71	11.80	18.42	3.63

The surface water amount and water quality variables in each HRU were mapped using ArcMap and are shown in Figures 3-16 to 3-19. For each variable, the colors are classified in method of quantile. The sediment yield shows a more spatially polarized distribution than that of surface runoff in Wilde Lake watershed. The figure for nutrients are similar to one other, and their distributions are slightly polarized as well.

By comparing to the land use types in Figure 2-4, it is clear that the surface runoff yields are closely related to the land use types. For example, the high density residential areas have a high surface runoff amount as well as TSS yields. The TSS yields are much more concentrated in the top 10% HRUs because the maximum value of 142.18 is much higher than average. The 95^{th} percentile is 13.98, and the 90^{th} percentile is 7.13, which are much below the maximum. One also observes that most areas have small sediment yields, so TSS control may not be very challenging in this area. This result corresponds to Chesapeake Bay program's perspective that nutrient reduction, not TSS reduction is the main issue in the Chesapeake Bay TMDL (MDDoE, 2012). The nitrogen and phosphorus are the principal nutrients of concern in urban water management, and the results show high nutrient concentrations in urban areas were simulated in SWAT as well. The phosphorus distribution map (Fig. 3-19) shares a similar pattern to the surface runoff, which is physically reasonable that the phosphorus mainly detached by the runoff from the soil surface. The Nitrogen map (Fig. 3-18) shows a high concentration at the urban area as well.

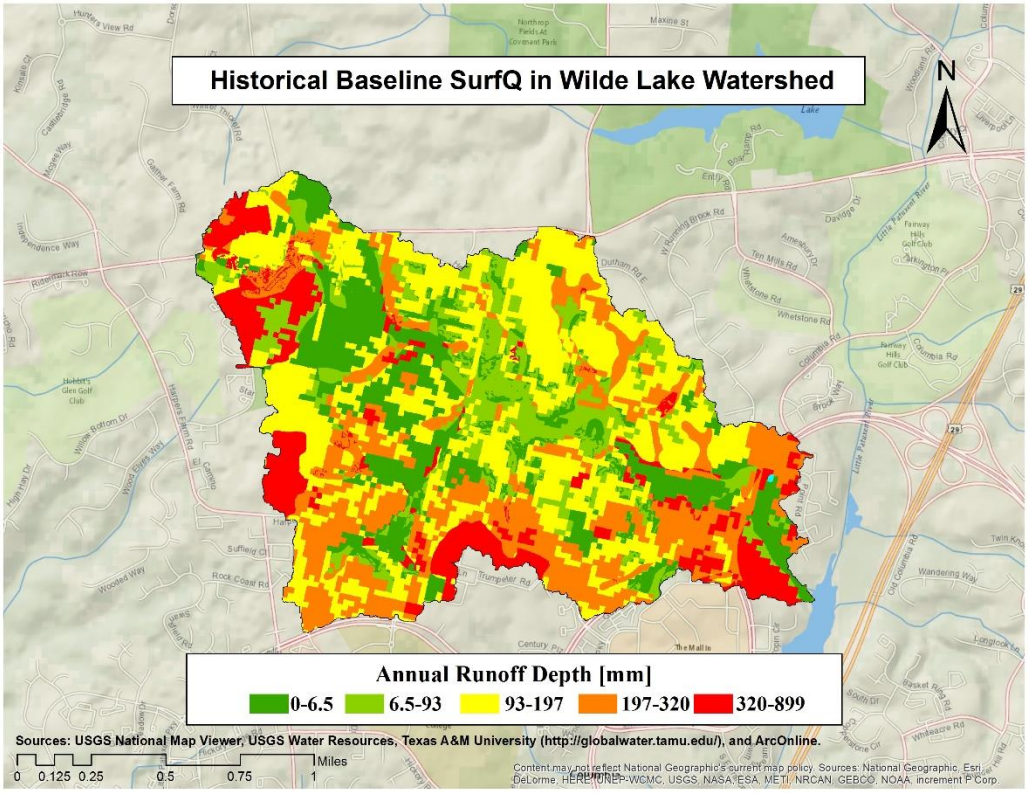

Figure 3-16. SurfQ Distribution of HRUs at Historical Baseline in Wilde Lake Watershed

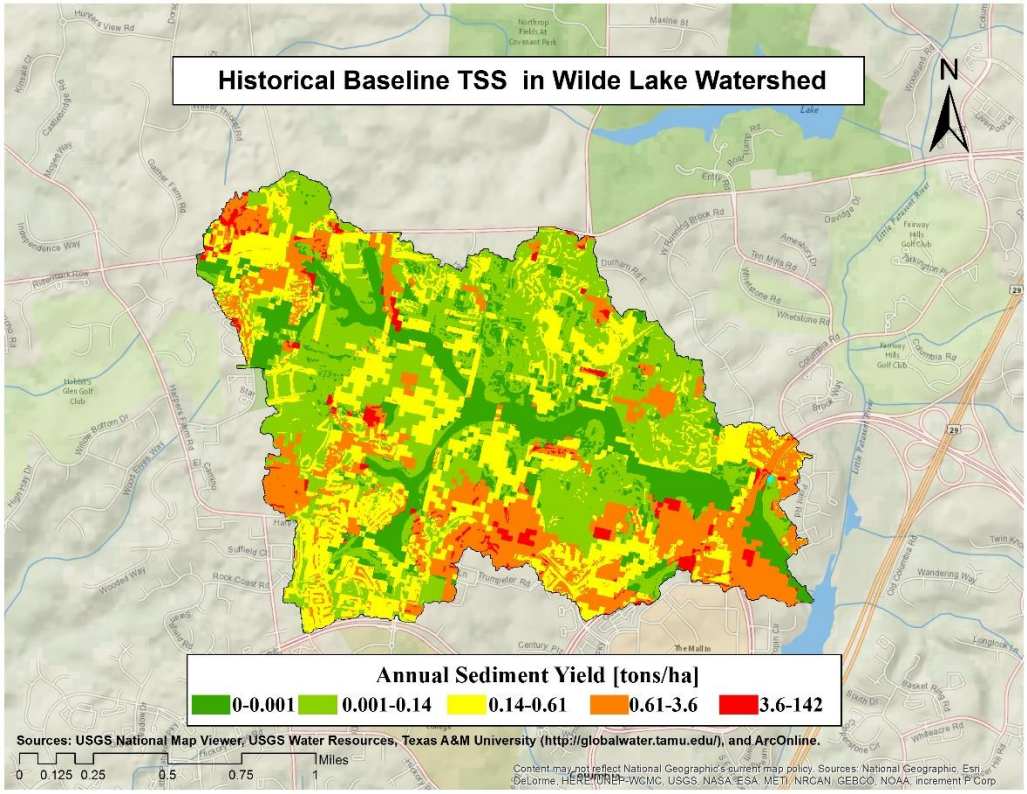

Figure 3-17. TSS Distribution of HRUs at Historical Baseline in Wilde Lake Watershed

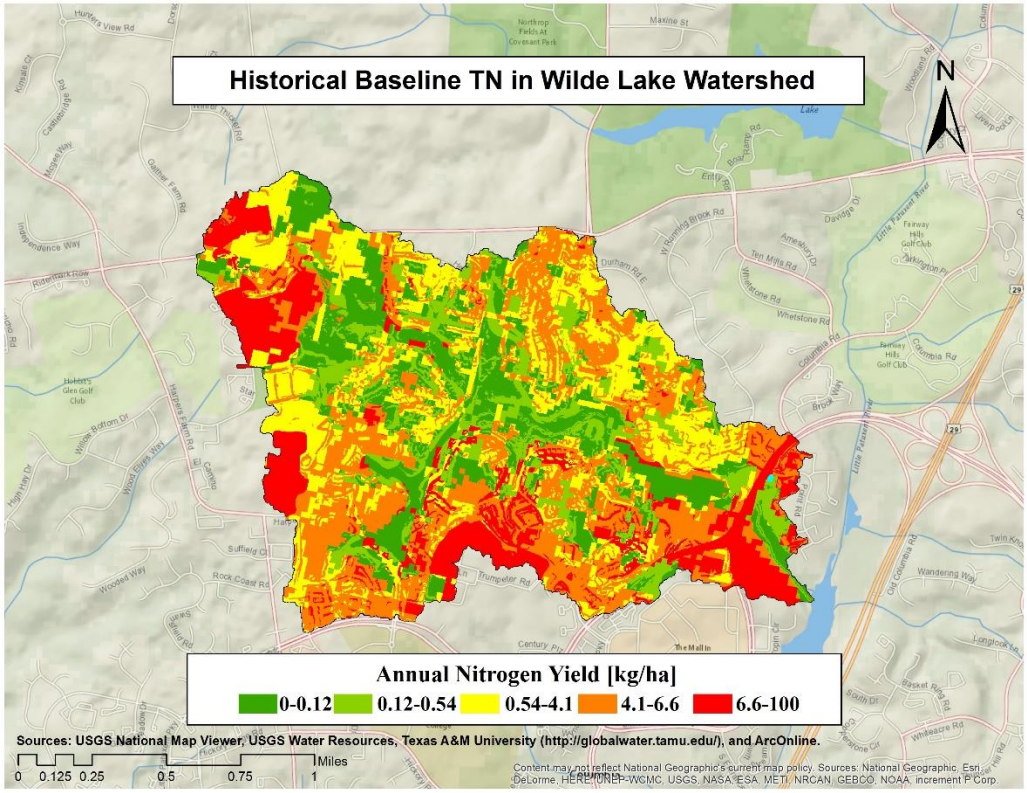

Figure 3-18. TN Distribution of HRUs at Historical Baseline in Wilde Lake Watershed

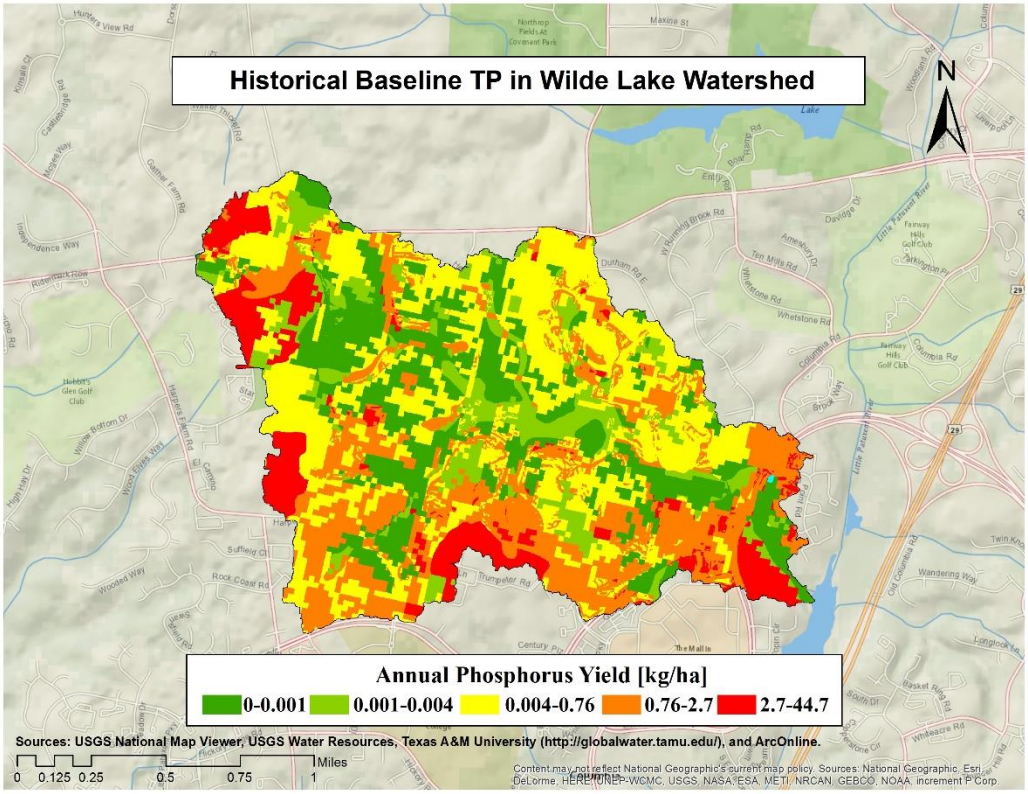

Figure 3-19. TP Distribution of HRUs at Historical Baseline in Wilde Lake Watershed

3.3.2 Watershed Response to Current and Future Synthetic Climate

The variables of historical periods in six climate models are shown in Figure 3-20. The NCDC historical baseline show slightly lower values in SurfQ and TSS, but slightly higher values in TN and TP yields when comparing the yields of NCDC observation to that of the modeled historical periods. There are very slight differences for all variables in all models, except the surface runoff in model 4. The surface runoff in model 4 shows a 21.0% change on the surface runoff in historical periods. Although the climate inputs were bias-corrected based on the years of 1961 to 2000, the model 2 and 4 show still show significant changes of higher than 5% difference on all variables on the 1970-1989. This indicates each model has different historical performance, and the complexity may cause some problems in the in CSA identification.

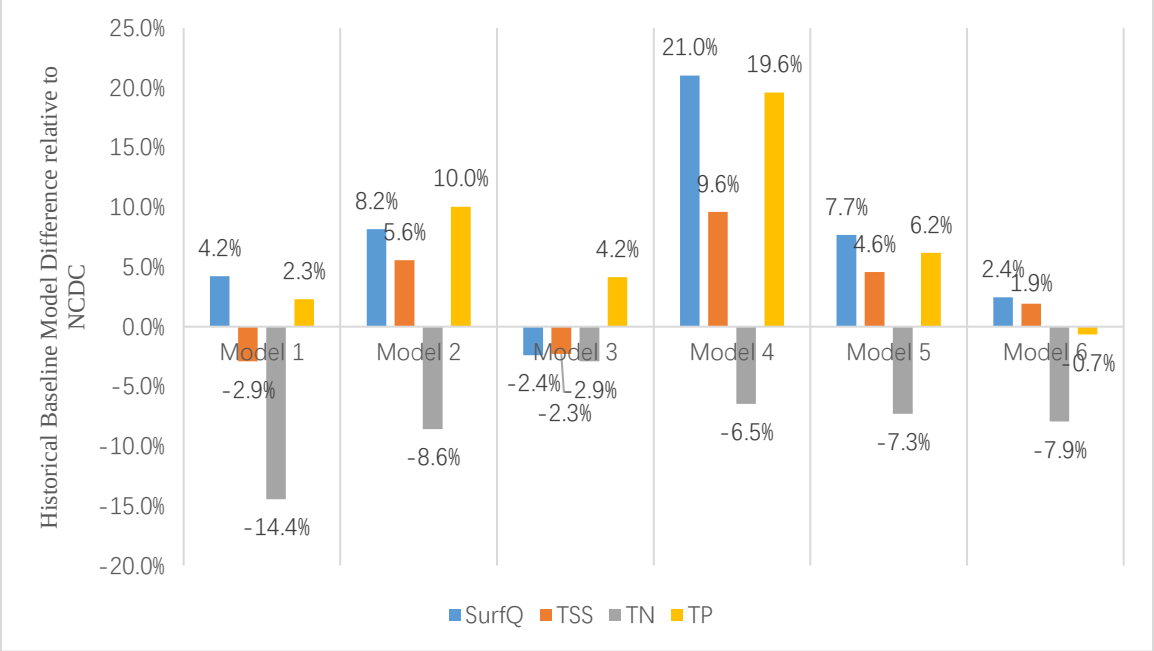

Figure 3-20. Mean Historical Yearly Runoff, TSS, TN and TP Amount Comparing to NCDC Historical Baseline.

A comparison of the mid-term (2040-2059) and far-term (2080-2099) future to their own historical periods was assessed as well. The results show no clear pattern for different models and scenarios in the two periods, which indicates the uncertainties of models among the years are great. Specifically, as is shown in the Figure 3-21, at the scenario RCP8.5, the model 1 and 3 show a relative lower increase of surface runoff from mid-century to end-century than other models, and the model 1, 3, 4 and 5 show a relative lower increase of water quality variables from mid-century to end-century. This corresponds to the results in the section 3.2.3, several peaks in the years around 2050s may lead to a higher mean value than that of the end of century.

Still at the scenario RCP8.5, models show an average increasing rates of 30.5%, 34.5%, 27.2% and 36.8% for the on-land surface runoff, TSS, TN and TP yields respectively at mid-century. And the average increasing rates are 37.3%, 30.7%, 16.4%, 26.6% for the on-land surface runoff, TSS, TN and TP yields respectively at end-century

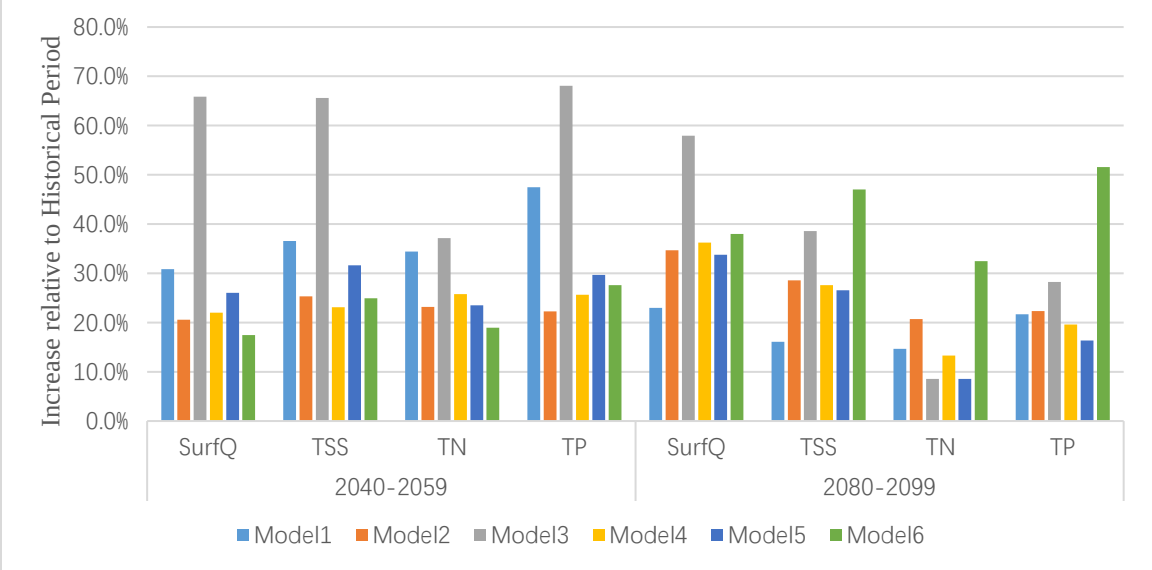

Figure 3-21. Increase Rates at scenario RCP8.5 in different models to their Historical Period

The mean increase of six models at different scenarios are shown in the Figure 3-22. The average increase rate ranges from 16.4% to 37.7% of all variables in the future. The RCP8.5 shows the highest increasing rates than other scenarios for all variables at both periods except the TN at the end-century. This indicates the future water amount and water quality yields would increase significantly in all scenarios with a huge variance, and this may cause great uncertainties and may influence the CSA identification.

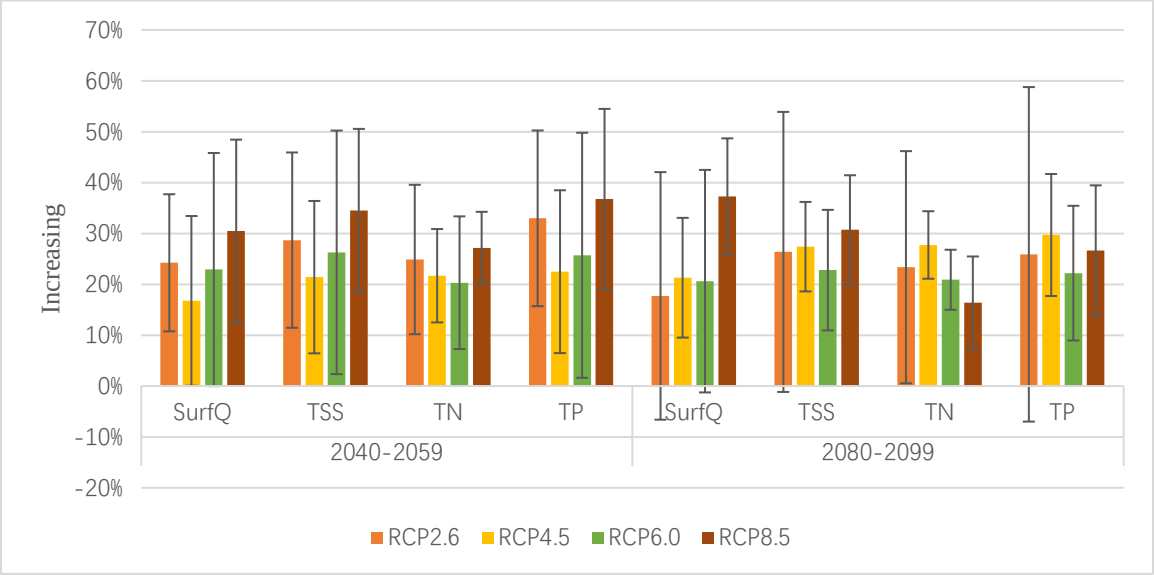

Figure 3-22. The Averaged Increase of Six Models in Different Scenarios Relative to Their Historical Period

3.3.3 CSA Identification Under Current Climate

The CSAs evaluated by the historical data based on the NCDC climate data were shown in Table 3-17. For different percentage, different amount of CSAs are identified. If 10% HRUs based on SurfQ are identified, 133 HRUs includes 8.5% of all area are targeted, where 29.2% of total amount SurfQ are generated from these 133 HRUs. Therefore, treat 29.2% by amount with only 8.5% areas for the surface runoff is considered as efficient. If 10% HRUs based on TSS are identified, 0.6% of area and

13.7% of TSS are targeted. The main reason to have the area difference is the size of HRUs vary widely. The Figure 3-23 shows the Mass/Area efficiency ratio of the NCDC historical baseline. By comparing the Mass/Area ratio, the TSS is more efficiency to be treated than Surface Runoff because a higher Mass/Area ratio. The nutrients show a high Mass/Area ratio as well. Especially, the TN and TSS shows a 92.0% and 89.3% by mass at 40% percentile of HRUs. Table 3-17 and Figure 3-23 shows when the target percentile increases, the total targeting area and mass increase, but the efficiency, or the Mass/Area ratio decreased.

Table 3-17. Targeted Area and Mass at Certain Percentile of HRUs in the Historical Baseline

Percentile of HRUs	By Area				By Mass			
	SurfQ	TSS	TN	TP	SurfQ	TSS	TN	TP
10%	8.5%	0.6%	9.0%	3.3%	29.2%	13.7%	69.2%	19.5%
20%	12.1%	4.4%	16.3%	10.9%	37.7%	40.9%	75.8%	50.2%
30%	24.7%	15.9%	27.3%	23.9%	56.6%	72.9%	82.7%	70.5%
40%	35.8%	31.0%	46.4%	37.6%	70.7%	89.3%	92.0%	82.5%

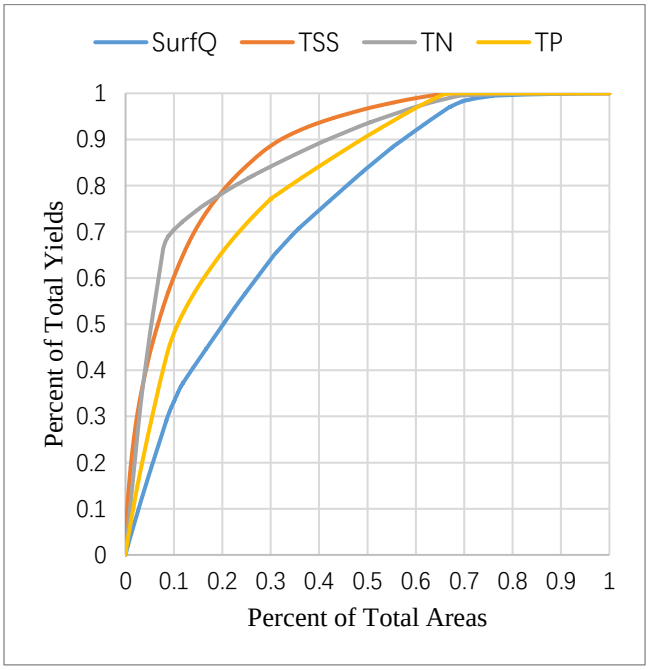

Figure 3-23. Mass/Area ratio of water quantity and quality variables in NCDC historical baseline

Therefore, from the figure we can see the fewer areas or the HRUs targeted the more efficiency. In the usage of the BMP location selection, for example, if we need to target more than 50% by mass, about 30%, 30%, 10%, and 20% of HRUs are targeted for the SurfQ, TSS, TN and TP respectively. And these HRUs contributes to the 20%, 10% of total area is enough for the TSS, TN and TP, but it needs about 20%, 7%, 5%, 11% of total area for the SurfQ, TSS, TN and TP respectively. This graph also shows that there are at least 30% of area contributes negligible surface runoff or pollutants, therefore these areas can be neglected for the control and regulations.

3.3.4 Climate Change Impacts on CSAs Identified with a Relative Threshold

Due to the climate change, the pollutant distribution on land may different to the historical baseline. In addition, different climate models may lead to different distributions of SurfQ, TSS, TN and TP in HRU levels, and this would generate new CSAs in the future. If the BMPs or TMDLs were set based on the current CSAs while they are no longer CSAs based on future climate, these regulations would be inefficient in the future. This section try to answer two questions. The first question is if the CSAs are identified in a certain amount of HRUs will they still be critical in the future. The second question is if CSAs are identified as the HRUs that contributes to the per-area yields high than a threshold, would there be more or fewer CSAs in the future.

The comparisons for each model were made to answer the first question. Among 19 climate model/scenarios at three different periods (historical, mid-century and end-century), totally 44 different sets of CSAs identified based on the HRU percentile were

compared to CSAs identified in the NCDC historical baseline. The results are shown in the Table 3-18. If 10% of HRUs are identified as TN CSAs, the poorest match rate is 88.0% for the worst case in all models, RCPs and periods, which means 117 out of 133 HRUs are still the TN CSAs in the worst case. At the 20% CSAs targeting method, the median show 98.1% of SurfQ CSAs, 99.6% of TSS CSAs, 91.8% of TN CSAs, and 97.0% of TP CSAs identified based on the NCDC historical climate are still the CSAs in the future climate conditions. And overall results among all 44 possibilities and 4 investigation variables show at least 83% of HRUs would still be the CSAs. This indicates that the relative per-area yields rankings are mainly caused by the physical terrestrial conditions, and the influence of future climate or the simulated historical climate are limited on the critical rankings. Therefore, the CSAs identified by historical baseline would not change significantly, and they would still be hotspot in the future no matter what kind of the future climate would be.

Table 3-18. The Percent of HRUs which are both CSAs in NCDC Historical Baseline and Simulated Models/Scenarios/Periods

	10% CSAs, 133 HRUs		20% CSAs, 267 HRUs		30% CSAs, 400 HRUs		40% CSAs, 534 HRUs	
	Minimum	Median	Minimum	Median	Minimum	Median	Minimum	Median
SurfQ	97.0%	100.0%	95.1%	98.1%	95.0%	96.3%	97.2%	99.8%
TSS	99.2%	99.2%	99.3%	99.6%	98.3%	99.0%	93.3%	97.9%
TN	88.0%	90.2%	83.9%	91.8%	85.3%	88.1%	83.3%	91.1%
TP	92.5%	97.0%	94.0%	97.0%	92.8%	99.5%	86.1%	89.3%

Figures 3-24 to 3-27 show the yields of SurfQ, TSS, TN and TP with the model3 at the scenario RCP8.5 and end-century period. The yields in this model/scenario/period is the highest among all situations, but the spatial distributions are almost the same to maps of historical baseline (Fig. 3-16 to 3-19), which shows the robustness as well.

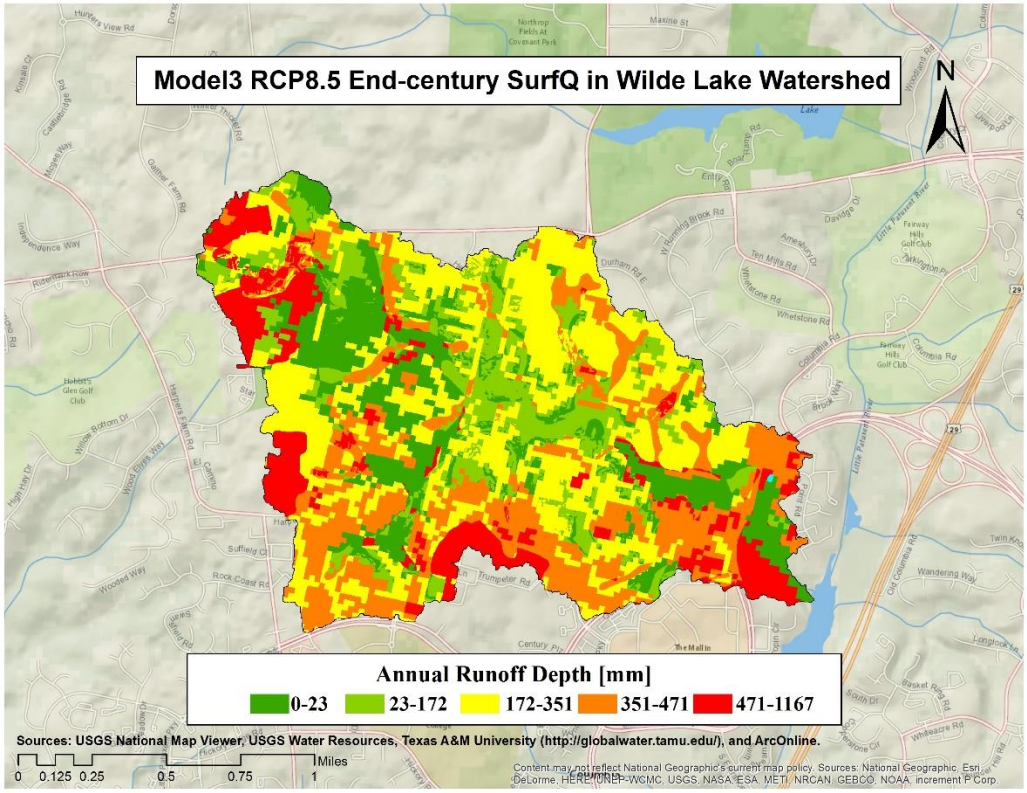

Figure 3-24. SurfQ Distribution at Model3 RCP8.5 at 2090s in Wilde Lake Watershed

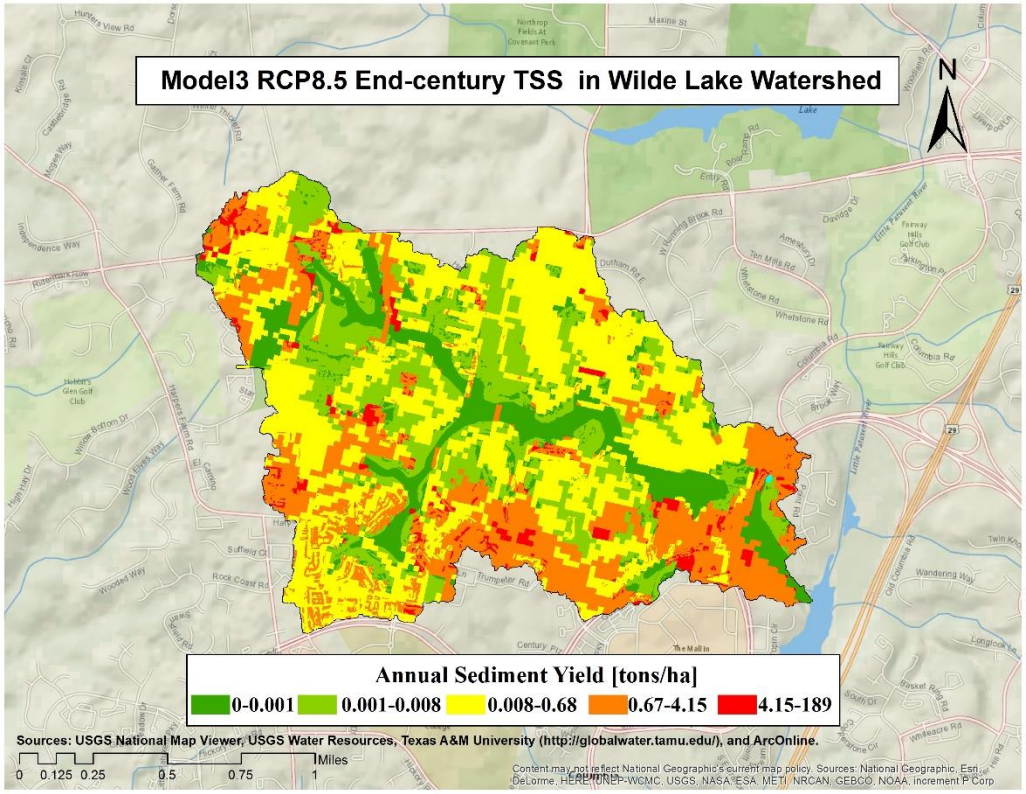

Figure 3-25. TSS Distribution at Model3 RCP8.5 at 2090s in Wilde Lake Watershed

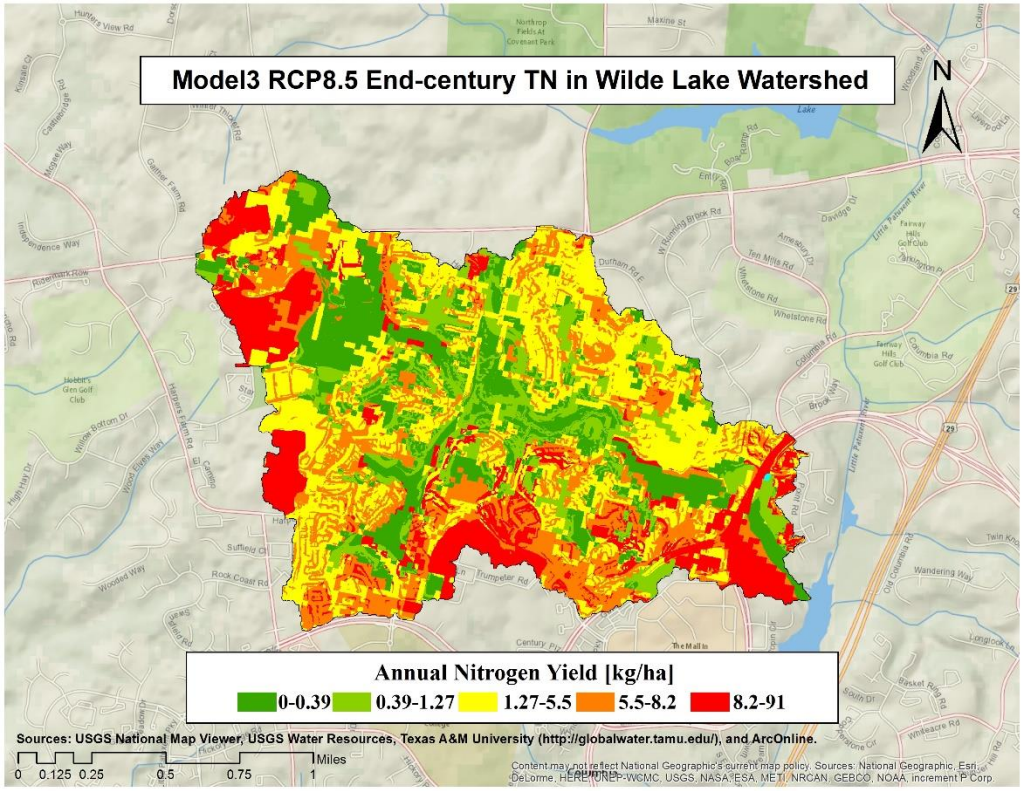

Figure 3-26. TN Distribution at Model3 RCP8.5 at 2090s in Wilde Lake Watershed

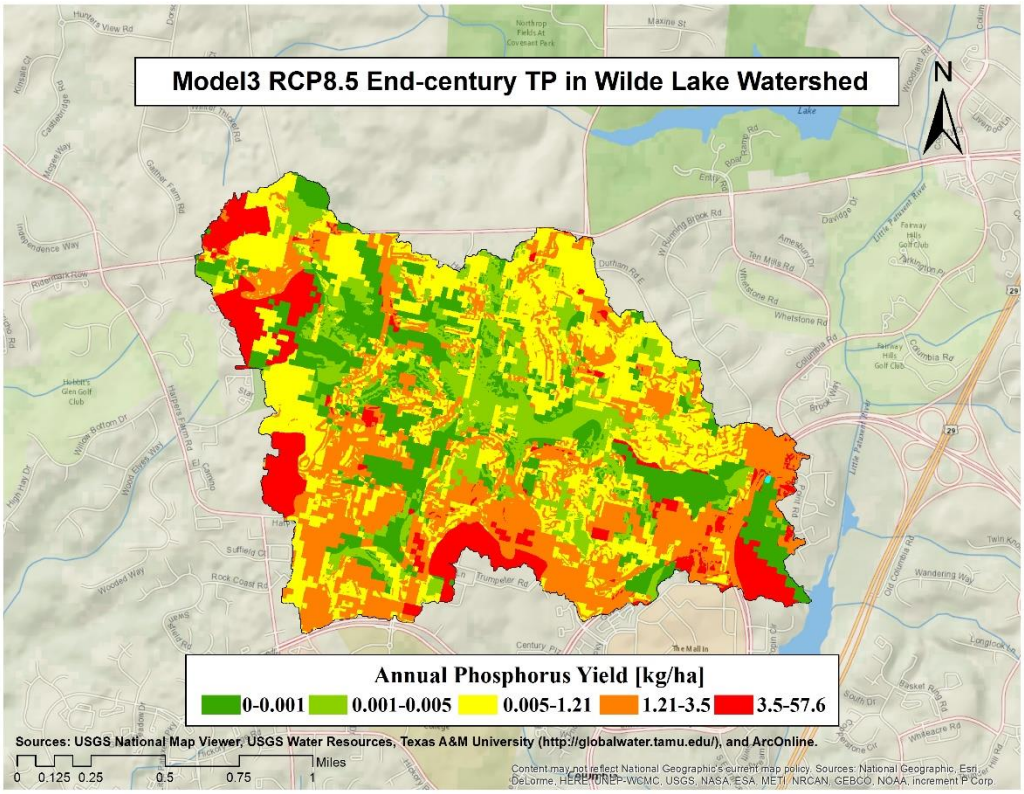

Figure 3-27. TP Distribution at Model3 RCP8.5 at 2090s in Wilde Lake Watershed

3.3.5 Climate Change Impacts on CSAs Identified Using a Fixed Threshold

When the thresholds of CSAs were set under the historical baseline, there would be some new CSAs with the per-area yields of water quantity or quality variables higher than the threshold, and eventually results in more CSAs in the future.

Figure 3-28 shows the average increasing of CSAs among six models at the scenario RCP8.5 at end of century. The results show almost all models show an increase of the CSAs in the future when using the threshold defined from the NCDC historical baseline. The Model 4 computed the most CSAs in almost all situations, and the Model 1 computed the fewest CSAs in all cases. If the value of the baseline 10% HRUs were selected as the threshold, 104, 46, 29, 56 more HRUs would be identified as the surface runoff, TSS, TN and TP CSAs respectively. It is model 3 rather than model 4 contributes the most yields in previous analyses, but the model 4 has the most CSAs increasing amount. This is because different models contribute different on-land yield patterns. The increase of surface runoff and nutrients are not the same among different area due to their precipitation and temperature patterns are not the same. And they would work differently on the HRUs with different features including slope, land use and soil type. It represents the greater on total yields does not means the more CSAs under a certain thresholds among different models.

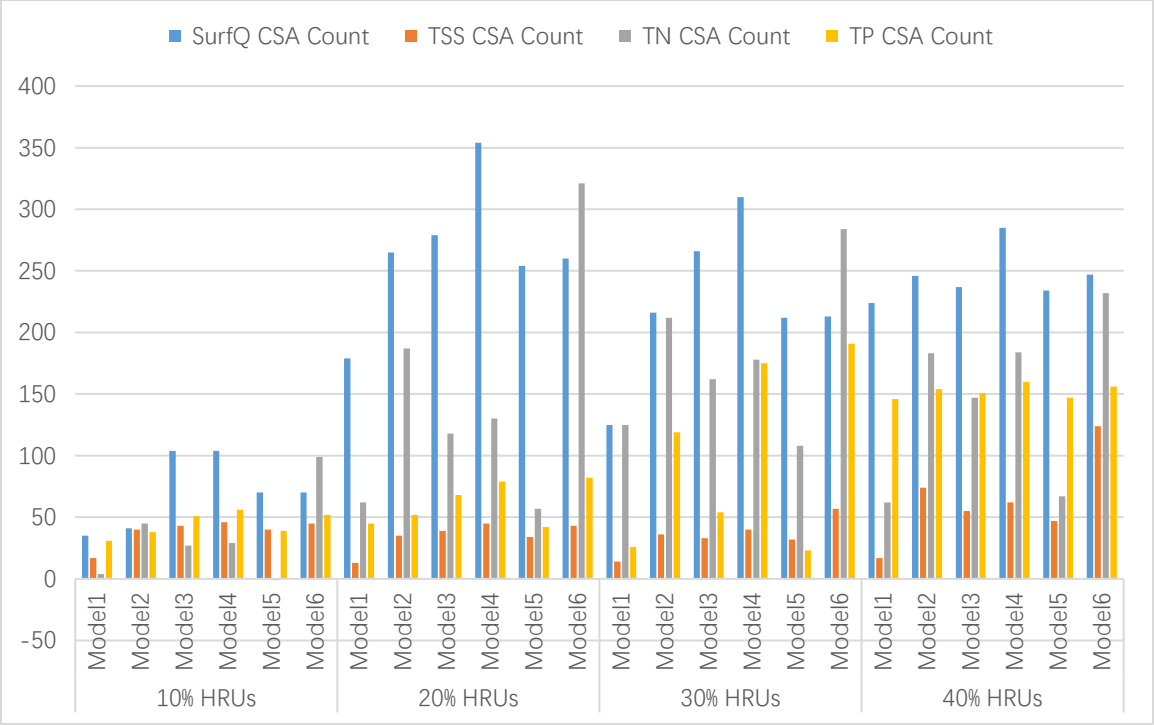

Figure 3-28. The Increasing Amount of HRUs Identified as CSAs in RCP8.5 at end-century when comparing to the CSAs Identified by Historical Baseline

Figure 3-29 to 3-32 shows the same distribution of SurfQ, TSS, TN and TP at Model3 RCP8.5 at 2090s in Wilde Lake watershed, but with the same threshold as the historical baseline. These figures show significant expanding of red and orange colors when comparing to the Figure 3-24 to 3-27, which represents the CSA areas are increased in the future using a fixed thredhold.

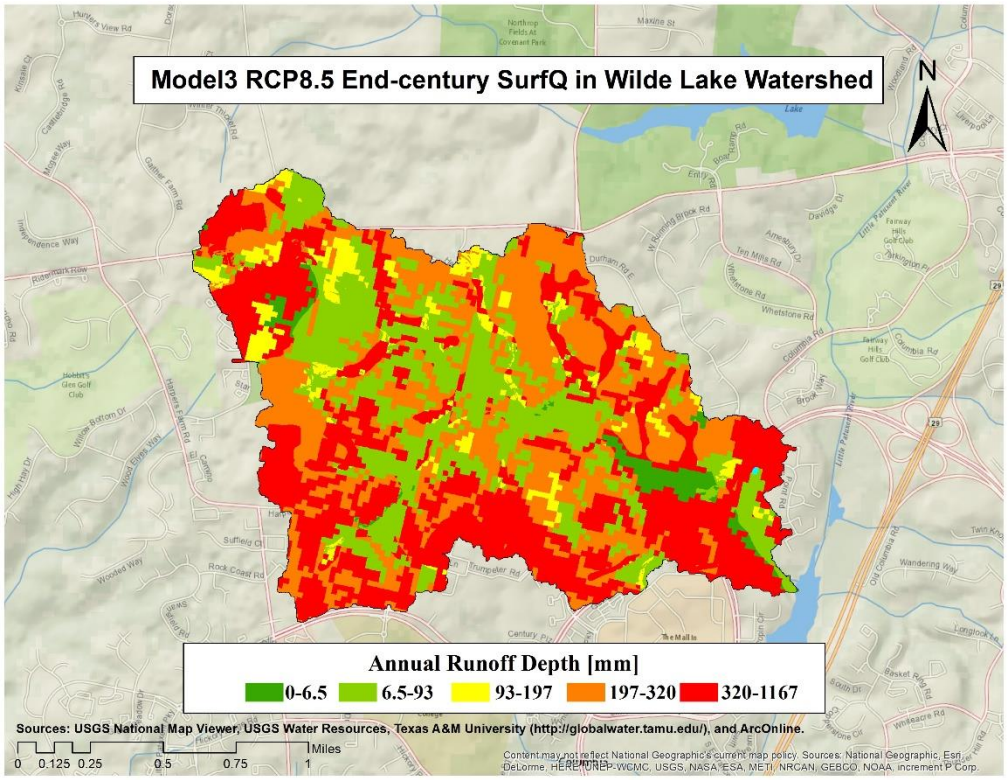

Figure 3-29. SurfQ Distribution at Model3 RCP8.5 at 2090s in Wilde Lake Watershed in Fixed Threshold

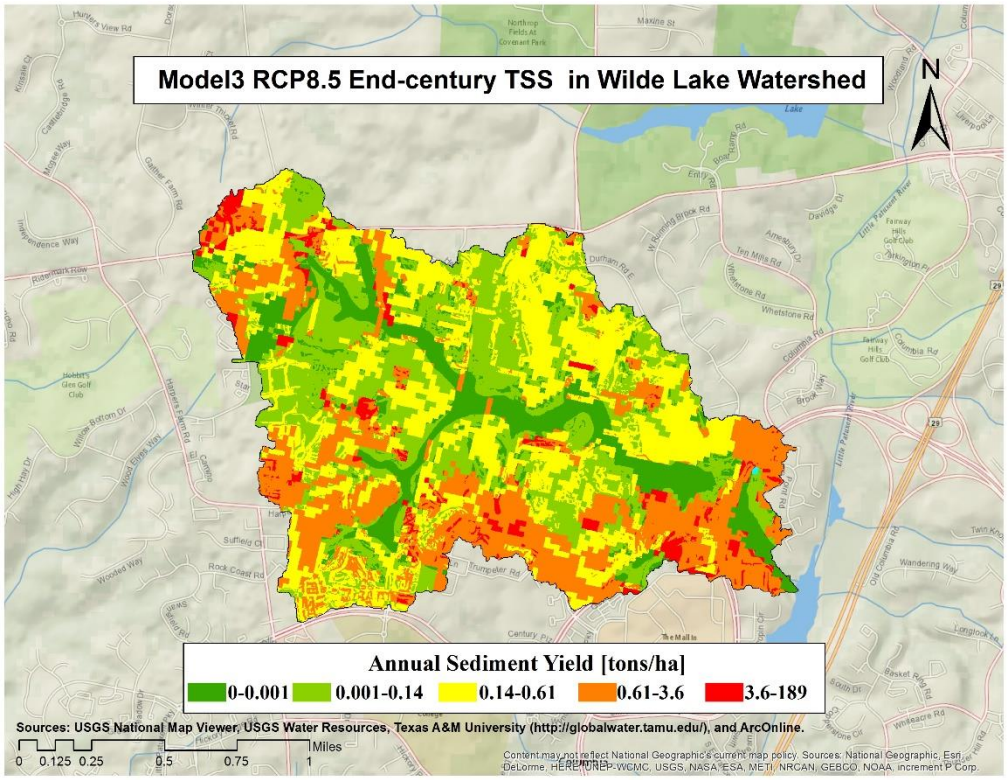

Figure 3-30. TSS Distribution at Model3 RCP8.5 at 2090s in Wilde Lake Watershed in Fixed Threshold

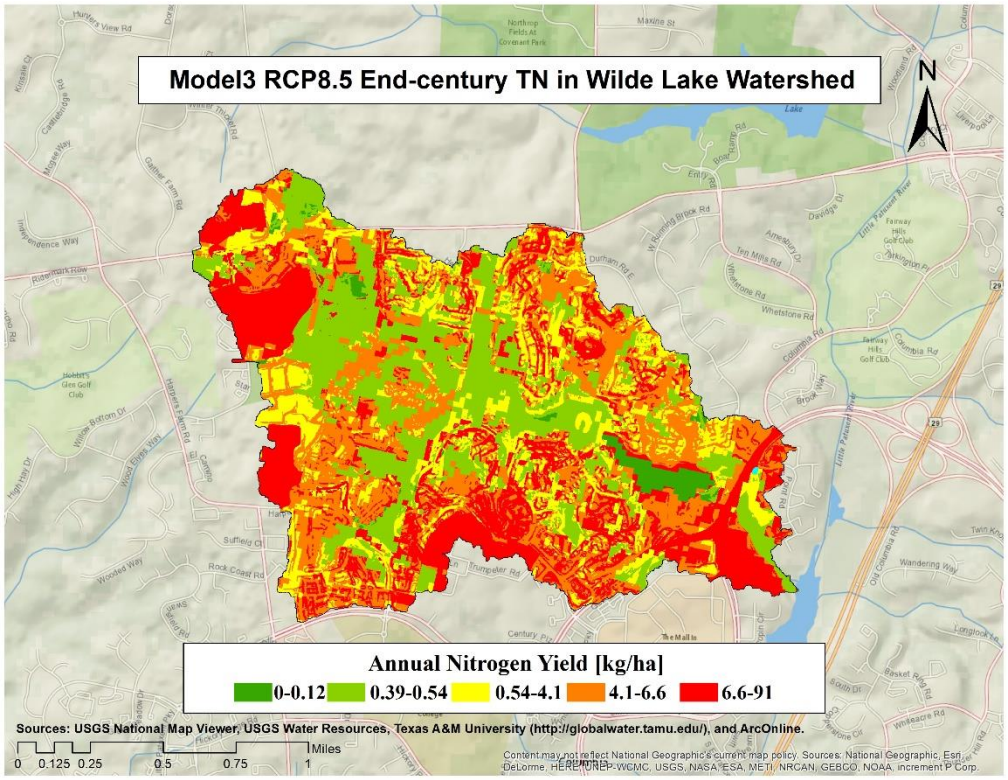

Figure 3-31. TN Distribution at Model3 RCP8.5 at 2090s in Wilde Lake Watershed in Fixed Threshold

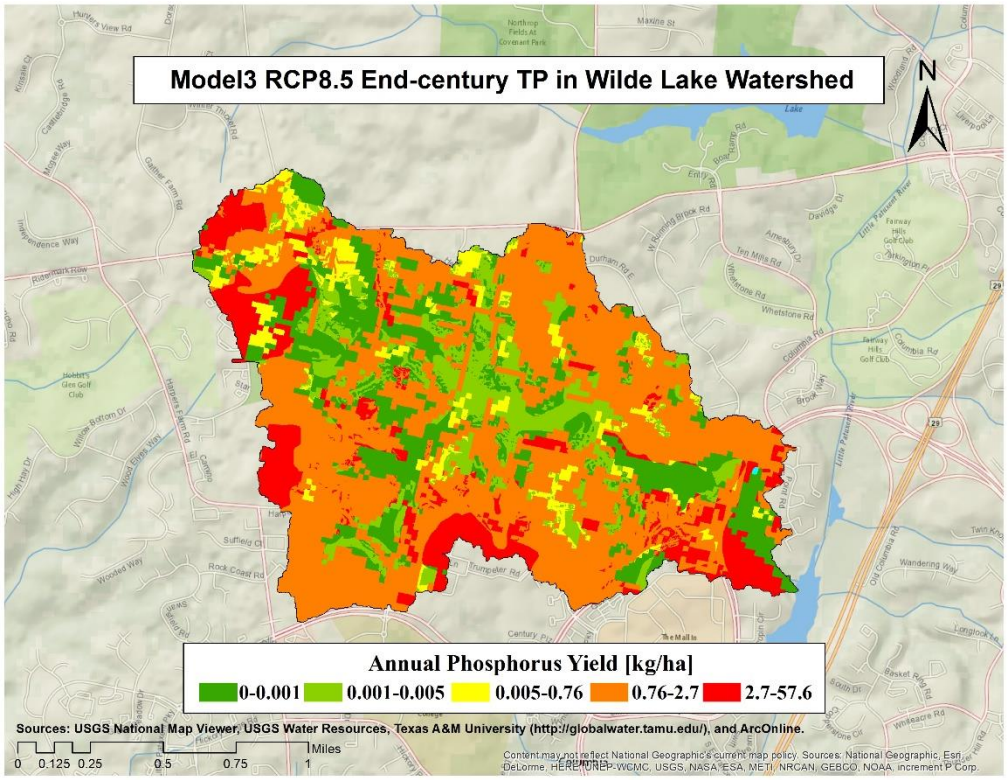

Figure 3-32. TP Distribution at Model3 RCP8.5 at 2090s in Wilde Lake Watershed in Fixed Threshold

Table 3-19. CSA Targeting Percentage Area and Standard Deviation in Different Periods

HRU Threshold	Period	SurfQ CSAs Percent Area (SD)	TSS CSAs Percent Area (SD)	TN CSAs Percent Area (SD)	TP CSAs Percent Area (SD)
10%	Baseline	8.5%	0.6%	9.0%	3.3%
	2050s	9.3% (0.7%)	1.0% (0.2%)	13.9% (4.1%)	7.1% (1.6%)
	2090s	9.5% (1.4%)	1.0% (0.2%)	13.7% (4.6%)	7.2% (1.7%)
20%	Baseline	12.1%	4.4%	16.3%	10.9%
	2050s	32.7% (7.1%)	5.9% (0.9%)	41.4% (9.6%)	15.5% (3.6%)
	2090s	32.5% (9.0%)	6.1% (1.0%)	38.1% (12.3%)	15.2% (4.1%)
30%	Baseline	24.7%	15.9%	27.3%	23.9%
	2050s	40.1% (8.8%)	20.3% (2.3%)	56.8% (8.8%)	45.3% (9.7%)
	2090s	42.3% (10.7%)	20.3% (2.5%)	53.7% (11.3%)	41.4% (11.7%)
40%	Baseline	35.8%	31.0%	46.4%	37.6%
	2050s	63.8% (5.6%)	44.8% (6.4%)	64.9% (4.7%)	64.7% (1.7%)
	2090s	62.1% (8.5%)	42.1% (7.9%)	61.7% (7.8%)	62.8% (7.2%)

Table 3-20. CSA Targeting Percent Area and Standard Deviation in Scenario RCP2.6 and RCP8.5 at both future periods

		SurfQ	TSS	TN	TP
10%	RCP2.6	8.5% (2.0%)	0.9% (0.3%)	14.6% (5.7%)	6.2% (3.0%)
	RCP8.5	10.3% (1.0%)	1.2% (0.2%)	13.7% (5.8%)	7.6% (0.8%)
20%	RCP2.6	27.9% (10.8%)	5.8% (1.2%)	38.4% (16.9%)	15.5% (5.1%)
	RCP8.5	37.2% (6.4%)	6.7% (1.0%)	35.7% (15.1%)	15.8% (5.5%)
30%	RCP2.6	39.0% (11.3%)	19.9% (3.4%)	52.6% (17.0%)	39.5% (14.3%)
	RCP8.5	49.8% (8.6%)	21.1% (2.8%)	50.8% (12.6%)	41.5% (14.1%)
40%	RCP2.6	67.1% (1.4%)	40.8% (9.4%)	60.0% (8.5%)	65.3% (0.3%)
	RCP8.5	57.0% (14.1%)	43.4% (10.7%)	59.1% (11.8%)	56.9% (13.2%)

As is shown in the Table 3-19, when calculating the total areas of CSAs, the percent area in the future at two periods are both higher than the historical baseline, and much more area is targeted. At a fixed threshold of the 20% HRU from the historical baseline, 12.1%, 4.4%, 16.3%, and 10.9% total areas are targeted for SurfQ, TSS, TN and TP respectively, but the new CSAs area would be 32.5%, 6.1%, 38.1% and 15.2% at the

end of 21 century. Approximately 40% more TSS and TP area and 100% more increase of SurfQ and TN area on the mean are simulated. At the fixed threshold of the 20% HRUs, the standard deviation is only 9.0%, 1.0%, 12.3% and 4.1% on the total area for SurfQ, TSS, TN and TP. The CSAs percent areas of SurfQ, TSS, TN and TP at scenario RCP2.6 and RCP8.5 are shown in the Table 3-20. The difference between scenarios are not significant for the water quality targeted area. For the fixed threshold of 20% HRUs, the TSS CSAs are 5.8% and 6.7% of total area at RCP2.6 and RCP8.5 respectively, and the areas are 38.4% and 35.7% for TN, 15.5% and 15.8% for TP. Unlike the pollution yields, the areas in two scenarios are very close. The increases are large compared to the historical baseline, but the standard deviations are very low among the models and scenarios. This implies the CSAs targeting area would definitely increase and the influence is very limited among climate models and scenarios.

The increase of total yields would not only cause the increase of CSAs in HRU level, but also decrease the Mass/Area ratio. Figure 3-33 shows the Mass/Area ratio of the Model6/RCP2.6 and Model4/RCP8.5 in the end-century. Compared to Figure 3-23, it is easy to find from the curve shape that the mass/area ratio of all four variables significantly decreases at Model4/RCP8.5, but it shows no much changes in Model6/RCP2.6 due to unnoticeable increasing rates. This means a low targeting efficiency under the future climate would be caused by the higher yields, with the possible result a low removal efficiency if BMPs are implemented.

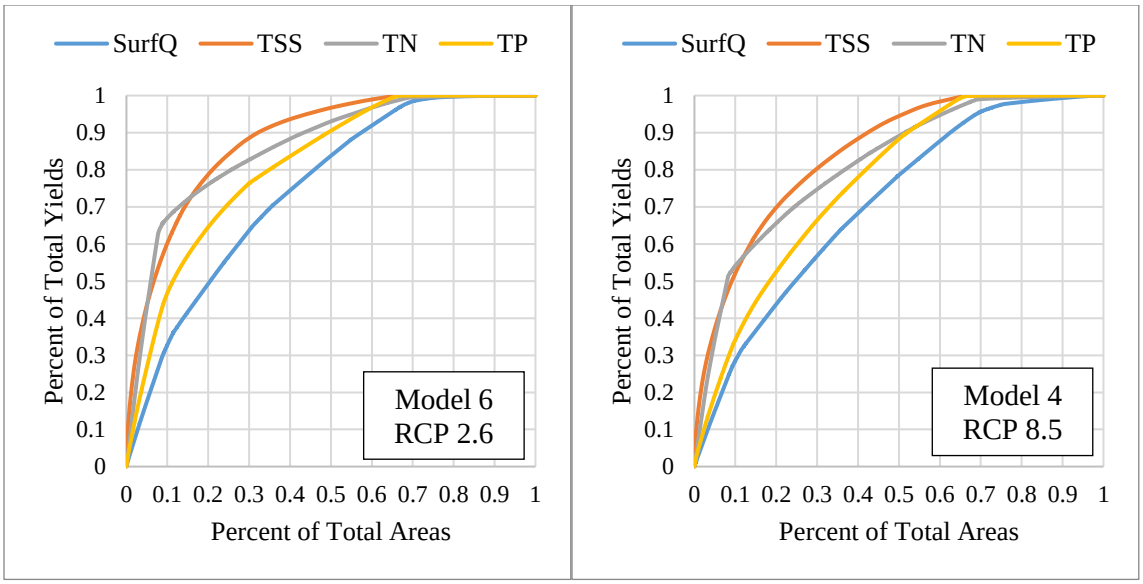

Figure 3-33. The Mass/Area ratio of Model6/RCP2.6 (Left) and Model4/RCP8.5 at End-century

3.3.6 Summary

Under the future climate, the on-land yields of all four variables increase in all HRUs. The historical baseline shows a high Mass/Area ratio on all four variables in Wilde Lake, and the increasing of yields in the future may result in a low Mass/Area ratio, which indicates a low treatment efficiency in the future. The CSAs identification based on the historical baseline by the quantile method shows that at least 83% of top levels of HRUs remain critical in the future. This shows the strong robustness of the CSAs targeting under the consideration of climate change. If CSA targeting was based on the fixed threshold from the historical baseline, the CSAs amounts may increase due to the increase of yields on land. From the Figure 3-28, if the value of the 10% HRUs of baseline were selected as the threshold, there will be 104, 46, 29, 56 more HRUs identified as the surface runoff, TSS, TN and TP CSAs respectively under the Model4 RCP8.5, and the increasing of HRUs represents much more targeting areas of CSAs.

When comparing the percentage area of CSAs, significant increase of CSAs are projected for all four variables. However, the increase area of CSA targeting are not highly related to the models and scenarios due to low standard deviations, which shows a relative strong robustness to the models and scenarios.

Chapter 4. Conclusions and Future Works

4.1 Summary

The objective of this study was to quantify the impact of climate change on runoff and water quality in a suburban watershed in Maryland.

A hydrological and water quality model was developed for the Wilde Lake watershed with the modeling software SWAT. This model was calibrated and validated using a daily time-step based on observed daily discharge from Oct 2012 to 2015 and event-based water quality sample data from 2007 to 2015. The NSE of the surface runoff were 0.66 and 0.52, and the PBIAS were -24.1% and -10.4% for the calibration and validation periods respectively. For the water quality variables (TSS, TN and TP), the NSE were 0.54, 0.41 and 0.71 respectively, and the PBIAS is 85.7%, 15.0% and 21.8% respectively, in the calibration period.

These results indicate that the model explains more than 50% of observed variations in surface runoff, sediment yields, and total phosphorus for this watershed, and 40% of observed variations in total nitrogen. The calibrated model was considered to produce a satisfactory representation of Wilde Lake hydrology based on criteria published in the literature, but could be improved in the future as more monitoring data becomes available.

Six climate models (CanESM2.5, CNRM-CM5.1, GFDL-CM3, IPSL-CM5A-MR, MIROC5, MRI-CGCM3) with up to four radiative concentration pathway scenarios (RCP2.6, RCP4.5, RCP6.0 and RCP8.5) were used to represent future weather over the study watershed. The predictions of these models were downscaled and bias-corrected,

using standard techniques, against historical NCDC data (baseline) from 1960 to 2000. The historical NCDC data showed an average daily precipitation of 2.93 mm, with 95th percentile of 18.46 mm and an average temperature of 13.0°C. The average future precipitation of the six selected models showed an increase of 12%, 12%, 14%, and 23% relative to the baseline for scenarios RCP2.6, RCP4.5, RCP6.0 and RCP8.5, respectively, at the end of century. The average future daily mean temperature was predicted to increase by 2.3, 3.6, 4.0 and 6.4°C for the four scenarios (averaged on the 6 models). This general consensus of different models represents a warmer and wetter future for the study area. The higher precipitations are expected to cause an increase of surface runoff, and this may cause higher sediment and nutrient yields. It may also affect soil water content and distribution, resulting in changes in nutrient cycles. The higher temperature in air, soil and water might also influence plant and bacteria growth processes, which may affect the land biosphere and yields of water quality variables.

The six climate models and for scenarios were used as input to the watershed model, and the runoff, sediments, and nutrients predicted at the outlet (in-stream) at the end of century were compared to those predicted for the historical baseline period. Table 4-1 summaries the obtained results, averaged by scenarios (across the 6 models). Outlet variables were predicted to increase by 14% to 35% as a result of climate change. The increase in runoff and sediments were found to be monotonic as RCP scenarios increased in intensity from 2.6 to 8.5, but nitrogen and phosphorus showed peaks at RCP4.5 possibly due to a combination of hydrologic and biological factors.

Results further indicated that the variance between predictions obtained from the 6 climate models, within a given scenario, can be greater than the variance in predictions

between scenarios. Accordingly, the choice of a specific climate model can have a more significant impact on the outcome of a climate study than the choice of a specific scenario and, therefore, such studies should consider several models, jointly, to address the uncertainty about the further climate. The GFDL-CM3 model was observed to lead to generally higher predictions than other models and could be used for worst-case analyses in the study area.

Table 4-1. Average Increase and Standard Deviation of In-stream Variables for 2080-2099 compared to 1970-1989.

	Precipitation	SurfQ	TSS	TN	TP
RCP2.6	12% (16%)	15.8% (22.0%)	20.1% (22.2%)	18.7% (18.1%)	20.6% (25.7%)
RCP4.5	12% (6%)	18.0% (9.8%)	21.5% (7.6%)	22.0% (6.0%)	23.8% (9.0%)
RCP6.0	14% (16%)	20.6% (22.1%)	18.6% (12.0%)	17.9% (7.3%)	19.2% (10.9%
RCP8.5	23% (8%)	34.7% (11.7%)	28.6% (8.5%)	14.9% (8.0%)	22.5% (9.2%)

Results of hydrologic simulations performed using the climate change models as input were analyzed in terms of on-land variables and compared to the baseline. The percentage change in yield of each surface constituent, relative to predictions for the baseline, were calculated for each combination of climate model and scenario. Averages and standard deviations of these percentages were then computed across models, for each scenario. Results of this analysis were presented in Section 3.3 and are summarized in Table 4-2 (including all HRUs) for mid-century and end-century predictions. All scenarios lead to increases in surface runoff, sediments, nitrogen and phosphorus, with the largest increases generally produced by the most severe RCP8.5 scenario (up to 37% increase). One exception was nitrogen yield at end-century where RCP8.5 produced the smallest increase, possibly due to rainfall patterns that favor surface runoff generation

over infiltration and leaching in this scenario. The standard deviations of predicted increases ranged from 6% to 33%, indicating notable variability between individual climate models.

Table 4-2. Average Increase and Standard Deviation of On-land Yields Compared to the Historical Baseline

	2040-2059				2080-2099			
	SurfQ	TSS	TN	TP	SurfQ	TSS	TN	TP
RCP2.6	24.2% (13.5%)	28.7% (17.2%)	24.9% (14.7%)	33.% (17.3%)	17.7% (24.3%)	26.4% (27.5%)	23.4% (22.8%)	25.9% (32.9%)
RCP4.5	16.7% (16.7%)	21.4% (15.%)	21.7% (9.2%)	22.5% (16.%)	21.3% (11.8%)	27.4% (8.8%)	27.7% (6.6%)	29.7% (12.%)
RCP6.0	22.9% (22.9%)	26.3% (23.9%)	20.3% (13.%)	25.7% (24.1%)	20.6% (21.9%)	22.8% (11.8%)	20.9% (5.9%)	22.2% (13.2%)
RCP8.5	30.5% (18.%)	34.5% (16.%)	27.2% (7.1%)	36.8% (17.7%)	37.3% (11.4%)	30.7% (10.7%)	16.4% (9.1%)	26.6% (12.8%)

Critical Source Areas (CSAs) were identified from simulation results using both a relative threshold and a fixed threshold approach. In both approaches, the 1334 HRUs of the Wilde Lake watershed model were ranked by their yield of the four constituents (on a per-area basis). Curves of cumulative yield per contributing area were produced from the ranked HRUs and indicated high Mass/Area ratio, which indicates that a great efficiency in targeting the high-yield HRUs (a small number of HRUs contribute the bulk of the watershed's yield). In the relative threshold approach, the top 10%, 20%, 30% and 40% of HRUs were selected as CSAs in the baseline and in each of the 44 future climate simulations. The future CSAs were compared to the baseline CSAs and it was found that, considering all cases, at least 83% of them were identical. This indicates robustness of CSA targeting by this method, whereby the top yielding HRUs from the historical baseline would still be the critical ones under future climate.

In the fixed threshold approach, the top 10%, 20%, 30% and 40% of HRUs were selected as CSAs from the baseline simulations and the per-area yields at NCDC historical baseline from each group were used as thresholds to select CSAs in simulations with future climate. This approach mimics a situation where CSAs are identified based on a TMDL criterion that remains fixed into the future. The percentages of watershed area occupied by CSAs were computed (for each constituent) from the results of each simulation and their averages and standard deviations were calculated for each threshold level, for the baseline and for the end-century. Results, summarized in Table 4-3, indicated that the area of fixed-threshold CSAs increased (on average) in all cases and could more than double due to climate change (eg. SurfQ and TN at the 20% baseline threshold). Additionally, the standard deviation of CSA area, between models and scenarios, was generally small (0.2% to 12%), which indicated that differences among climate models have a relatively low influence on CSA targeting with this method.

Table 4-3. Average and Standard Deviation of Watershed Area Occupied by CSAs at the Historical Baseline and End-century

	Period	SurfQ CSAs Percent Area (SD)	TSS CSAs Percent Area (SD)	TN CSAs Percent Area (SD)	TP CSAs Percent Area (SD)
10%	Baseline	8.5%	0.6%	9.0%	3.3%
	End-century	9.5% (1.4%)	1.0% (0.2%)	13.7% (4.6%)	7.2% (1.7%)
20%	Baseline	12.1%	4.4%	16.3%	10.9%
	End-century	32.5% (9.0%)	6.1% (1.0%)	38.1% (12.3%)	15.2% (4.1%)
30%	Baseline	24.7%	15.9%	27.3%	23.9%
	End-century	42.3% (10.7%)	20.3% (2.5%)	53.7% (11.3%)	41.4% (11.7%)
40%	Baseline	35.8%	31.0%	46.4%	37.6%
	End-century	62.1% (8.5%)	42.1% (7.9%)	61.7% (7.8%)	62.8% (7.2%)

4.2 Conclusions

Climate change models are in general agreement that rainfall will increase (up to 37%) in the future in the study area. The hydrologic modeling performed in this study demonstrated that this will result in up to 35% increases in runoff, sediment and nutrient yields from a suburban watershed in Maryland. The increase in runoff could generate flooding in downstream areas and the increases in sediments and nutrients could further degrade water quality, in a direction opposite to the goals of the Chesapeake Bay Program (CBP). In the study watershed, CSAs are quite localized and therefore Best Management Practices (BMPs) can be advantageously used to control runoff and other constituents. These CSAs may be determined using a relative or a fixed threshold. A relative threshold may be most appropriate where the focus of BMPs is on water quality and sediment and nutrient yield increases, due to climate change, are nearly proportional to increases in runoff. In this situation, CSAs are stable against climate change and targeting BMPs to baseline CSAs is expected to be adequate. These BMPs would, however, need to be designed to handle the increased loading resulting from future climate. A fixed CSA threshold may be most appropriate where BMPs are focused on preventing downstream flooding or where the goal is to meet TMDLs that remain fixed into the future. In this case, CSAs may more than double in area due to climate change, and it is therefore important to consider this expansion when deciding on the locations at which BMPs should be implemented, if they are to remain effective into the future. Either way, climate change is expected to have a significant impact on the design of BMPs for flood prevention or water quality protection in the study watershed.

4.3 Future Study

This study was focused on climate change impacts on a single suburban site: the Wilde Lake watershed in central Maryland. Results may be representative of suburban watersheds in this region of the Chesapeake Bay area but may not represent other regions or watersheds due to spatial variability of landscapes and of future climate. Future studies may wish to extend the analysis to additional watersheds in the Chesapeake Bay region. In particular, it would be interesting to determine the degree to which relative- and fixed-threshold CSAs may vary as a result of climate change in watersheds with different locations, topography, soil types and land use. The degree of uncertainty of the related predictions should also be quantified.

The developed watershed model was based on SWAT in this study. It would be interesting to use other hydrologic modeling frameworks, such as MIKE SHE, to develop a comprehensive model of both surface water and groundwater, at the 3D level, and assess how that affects the conclusions of the study.

In this study, CSAs were determined individually for each constituent, but each identified hotspot may have been critical for more than one constituent. For example, a phosphorus CSA could also be a surface runoff CSA, and controlling surface runoff on this hotspot may be the key to controlling phosphorus exports there. A deeper analysis of CSAs and BMP allocation to control them, using a Diagnostic Decision Support System (DDSS) for example, would be an important follow-up to this study. With the DDSS, the CSAs could be identified as a hotspot for a single or multiple constituents, and BMP design methods could be adjusted accordingly to provide maximum benefit at the lowest

cost. Applying this approach within the context of climate change would then help ensure that the investment in BMPs would maintain its value into the future.

Appendix A

The appendix A lists 169 parameters used for the SWAT calibration.

SWAT Parameter	Fitted Value
r__CN2.mgt_____URLD	0.309346
r__CN2.mgt_____URMD	0.102088
r__CN2.mgt_____URHD	0.342002
r__CN2.mgt_____FRSD	-0.34403
r__CN2.mgt_____FRST	0.136054
r__CN2.mgt_____HAY	-0.0828
r__CN2.mgt_____AGRR	0.242674
r__CN2.mgt_____RNGB	-0.3748
r__CN2.mgt_____WETF	0.373823
r__CN2.mgt_____WATR	-0.08819
r__CN2.mgt_____FRSE	-0.41539
r__CN2.mgt_____UIDU	-0.46317
r__OV_N.hru_____URLD	0.375821
r__OV_N.hru_____URMD	0.342757
r__OV_N.hru_____URHD	-0.48904
r__OV_N.hru_____FRSD	-0.50061
r__OV_N.hru_____FRST	0.321291
r__OV_N.hru_____HAY	0.43164
r__OV_N.hru_____AGRR	0.374423
r__OV_N.hru_____RNGB	0.046666
r__OV_N.hru_____WETF	0.172267
r__OV_N.hru_____WATR	0.310839
r__OV_N.hru_____FRSE	-0.3568
r__OV_N.hru_____UIDU	0.338772
r__CANMX.hru_____URLD	0.24723
r__CANMX.hru_____URMD	-0.06288
r__CANMX.hru_____URHD	-0.22681
r__CANMX.hru_____FRSD	-0.47159
r__CANMX.hru_____FRST	-1.00000
r__CANMX.hru_____HAY	-0.36288
r__CANMX.hru_____AGRR	0.093875
r__CANMX.hru_____RNGB	-0.72465
r__CANMX.hru_____WETF	0.421728
r__CANMX.hru_____WATR	-0.24563

r__CANMX.hru_____FRSE	0.171568
r__CANMX.hru_____UIDU	-0.21257
v__ESCO.hru_____URLD	0.905565
v__ESCO.hru_____URMD	0.844256
v__ESCO.hru_____URHD	0.932294
v__ESCO.hru_____FRSD	0.82428
v__ESCO.hru_____FRST	0.718049
v__ESCO.hru_____HAY	1.047615
v__ESCO.hru_____AGRR	1.045946
v__ESCO.hru_____RNGB	0.924101
v__ESCO.hru_____WETF	0.857869
v__ESCO.hru_____WATR	1.016254
v__ESCO.hru_____FRSE	0.472758
v__ESCO.hru_____UIDU	0.537165
v__ALPHA_BF.gw_____URLD	0.056875
v__ALPHA_BF.gw_____URMD	0.170625
v__ALPHA_BF.gw_____URHD	0.045625
v__ALPHA_BF.gw_____FRSD	0.198125
v__ALPHA_BF.gw_____FRST	0.004375
v__ALPHA_BF.gw_____HAY	0.080625
v__ALPHA_BF.gw_____AGRR	0.064375
v__ALPHA_BF.gw_____RNGB	0.089375
v__ALPHA_BF.gw_____WETF	0.154375
v__ALPHA_BF.gw_____WATR	0.124375
v__ALPHA_BF.gw_____FRSE	0.013125
v__ALPHA_BF.gw_____UIDU	0.020625
v__GW_REVAP.gw_____URLD	0.024315
v__GW_REVAP.gw_____URMD	0.01256
v__GW_REVAP.gw_____URHD	0.00627
v__GW_REVAP.gw_____FRSD	0.007273
v__GW_REVAP.gw_____FRST	0.007964
v__GW_REVAP.gw_____HAY	0.018298
v__GW_REVAP.gw_____AGRR	0.003366
v__GW_REVAP.gw_____RNGB	0.008341
v__GW_REVAP.gw_____WETF	0.012666
v__GW_REVAP.gw_____WATR	0.012936
v__GW_REVAP.gw_____FRSE	0.019746
v__GW_REVAP.gw_____UIDU	0.004597
v__EPCO.hru_____URLD	0.992261
v__EPCO.hru_____URMD	0.906803
v__EPCO.hru_____URHD	1.00863

v__EPCO.hru_____FRSD	0.847595
v__EPCO.hru_____FRST	0.872283
v__EPCO.hru_____HAY	0.871851
v__EPCO.hru_____AGRR	0.893218
v__EPCO.hru_____RNGB	0.709603
v__EPCO.hru_____WETF	0.912597
v__EPCO.hru_____WATR	0.944178
v__EPCO.hru_____FRSE	0.940672
v__EPCO.hru_____UIDU	0.901926
v__CH_N1.sub_____1	0.012108
v__CH_N1.sub_____2	0.013761
v__CH_N1.sub_____3	0.011269
v__CH_N1.sub_____4	0.010522
v__CH_N1.sub_____5	0.010648
v__CH_N1.sub_____6	0.015995
v__CH_N1.sub_____7	0.012234
v__CH_N1.sub_____8	0.012081
v__CH_N1.sub_____9	0.011356
v__CH_N1.sub_____10	0.011187
v__CH_N1.sub_____11	0.018222
v__CH_N1.sub_____12	0.014579
v__CH_N1.sub_____13	0.012504
v__CH_N1.sub_____14	0.014781
v__CH_N1.sub_____15	0.011251
v__CH_N1.sub_____16	0.014701
v__CH_N1.sub_____17	0.011615
v__CH_N1.sub_____18	0.012005
v__CH_N1.sub_____19	0.009641
v__CH_N1.sub_____20	0.012704
v__CH_N2.rte_____1	0.060531
v__CH_N2.rte_____2	0.032524
v__CH_N2.rte_____3	0.078561
v__CH_N2.rte_____4	0.083105
v__CH_N2.rte_____5	0.104756
v__CH_N2.rte_____6	0.03715
v__CH_N2.rte_____7	0.078627
v__CH_N2.rte_____8	0.120419
v__CH_N2.rte_____9	0.055607
v__CH_N2.rte_____10	0.031237
v__CH_N2.rte_____11	0.070641
v__CH_N2.rte_____12	0.118304

v__CH_N2.rte_____13	0.097888
v__CH_N2.rte_____14	0.056287
v__CH_N2.rte_____15	0.038497
v__CH_N2.rte_____16	0.016429
v__CH_N2.rte_____17	0.070331
v__CH_N2.rte_____18	0.033934
v__CH_N2.rte_____19	0.037035
v__CH_N2.rte_____20	0.008938
v__CMN.bsn	0.000598
v__ERORGN.hru_____URHD	11.625
v__ERORGN.hru_____WETF	13.575
v__ERORGN.hru_____URLD	10.555
v__ERORGN.hru_____URMD	9.595
v__ERORGN.hru_____FRSD	14.955
v__ERORGN.hru_____FRST	7.685
v__ERORGN.hru_____HAY	10.99
v__ERORGN.hru_____AGRR	9.033055
v__ERORGN.hru_____RNGB	8.494648
v__ERORGN.hru_____WATR	10.195
v__ERORGN.hru_____FRSE	6.649682
v__ERORGN.hru_____UIDU	7.595
v__HLIFE_NGW_BSN.bsn	133.468
v__BC1_BSN.bsn	0.67975
v__BC2_BSN.bsn	0.8525
v__BC3_BSN.bsn	0.136375
v__CDN.bsn	1.999
v__CH_ONCO_BSN.bsn	7.385
v__N_UPDIS.bsn	50.225
v__P_UPDIS.bsn	109.821
v__NPERCO.bsn	0.24725
v__PHOSKD.bsn	39.67183
v__PSP.bsn	0.522762
v__ADJ_PKR.bsn	0.54125
v__BIOMIX.mgt_____URMD,URHD,UIDU,URLD	0.031223
v__BIOMIX.mgt_____FRSD,FRST,HAY,RNGB,WETF,WATR,FRSE	0.350879
v__BIOMIX.mgt_____AGRR	0.718104
v__PRF_bsn.bsn	0.76625
a__USLE_K(1).sol__B	-0.15225
a__USLE_K(1).sol__C	-0.36675

a__USLE_K(1).sol__D	-0.43661
v__HLIFE_NGW.gw	1.071
v__USLE_P.mgt_____URLD	0.61975
v__USLE_P.mgt_____URMD	0.600103
v__USLE_P.mgt_____URHD	0.79425
v__USLE_P.mgt_____FRSD	0.295906
v__USLE_P.mgt_____FRST	0.411866
v__USLE_P.mgt_____HAY	0.3045
v__USLE_P.mgt_____AGRR	0.153125
v__USLE_P.mgt_____RNGB	0.76427
v__USLE_P.mgt_____WETF	0.56947
v__USLE_P.mgt_____WATR	0.87132
v__USLE_P.mgt_____UIDU	0.112346
v__USLE_P.mgt_____FRSE	0.362733

The land use codes used in SWAT-CUP are shown in the table below.

Abbreviation	Land Use
URLD	Urban Low Density
URMD	Urban Medium Density
URHD	Urban High Density
FRSD	Deciduous Forest
FRST	Mixed Forest
HAY	Hay
AGRR	Row Crops
RNGB	Range Shrubland
WETF	Woody Wetlands
WATR	Water
UIDU	Urban Industrial
FRSE	Evergreen Forest

Appendix B

This section list two R scripts used in this study.

The first piece of code is the statistical analysis on precipitation and temperature data in the future. All 19 models/RCPs were analyzed, and Table 3-7 and 3-9 were directly generated.

```
setwd("G:/Summer/Climate Change/CMIP5/Analyses_on_Input")    ## set directory
library(data.table)
Sys.setlocale("LC_ALL", "English")

filenames <- list.files("G:/Summer/Climate Change/CMIP5/Analyses_on_Input", pattern
= ".pcp")       ## load the filenames of all precipitation files in the future
total_pcp<-data.table(NULL)
total_tmp<-data.table(NULL)
for (i in filenames){
      label_1<-substr(i,1,nchar(i)-4)
      i2<-paste(label_1,".tmp",sep="")
      if (label_1!="His_His"){
            #Data Cleaning
            data_temp <- data.table(NULL)
            data_temp2 <- data.table(NULL)
            data_summary <- data.table(NULL)
            data_temp <- data.table(readLines(i))
            data_temp<-data_temp[-(1:47486),]
            for (j in 1:length(data_temp$V1)){
                  data_temp$V2[j]<-as.numeric(substr(data_temp$V1[j], 8, 12))
            }
            data_temp$V3<-"pcp"
            Avg_pcp<-aggregate(V2~V3,data_temp,mean)
            SD_pcp<-aggregate(V2~V3,data_temp,sd)

            summary_pcp<-
cbind(Avg_pcp,SD_pcp$V2,quantile(data_temp$V2,probs=0.25),quantile(data_temp$V2
,probs=0.5),quantile(data_temp$V2,probs=0.75),quantile(data_temp$V2,probs=0.9),quan
tile(data_temp$V2,probs=0.95))
            colnames(summary_pcp) <-
c("Input_type","Average","SD","Percentile25","Percentile50","Percentile75","Percentile9
0","Percentile95")
            summary_pcp$area <- label_1
            total_pcp<-rbind(total_pcp,summary_pcp)
```

```
        data_temp <- data.table(readLines(i2))
        data_temp<-data_temp[-(1:47486),]
        for (j in 1:length(data_temp$V1)){
            data_temp$V2[j]<-as.numeric(substr(data_temp$V1[j], 8, 12))
            data_temp$V3[j]<-as.numeric(substr(data_temp$V1[j], 13, 17))
        }
        data_temp$V4<-"tmp"
        Avg_tmpmin<-aggregate(V3~V4,data_temp,mean)
        Avg_tmpmax<-aggregate(V2~V4,data_temp,mean)
        summary_tmp<-cbind(Avg_tmpmin,Avg_tmpmax$V2)
        colnames(summary_tmp) <- c("Input_type","Min","Max")
        summary_tmp$Average <- (summary_tmp$Min+summary_tmp$Max)/2
        summary_tmp$DailyDifference <- (summary_tmp$Max-summary_tmp$Min)
        summary_pcp$area <- label_1
        total_tmp<-rbind(total_tmp,summary_tmp)
        }
}

write.csv(total_pcp, file="pcp_summary.csv")
write.csv(total_tmp, file="tmp_summary.csv")
```

The second piece of code below includes the pre-treat of the SWAT output .hru files in different models, scenarios and periods. And the CSA targeting areas by a fixed threshold were calculated for each model/scenario/period. With these codes, the results were integrated into the csv files, and then they were further summarized into Table 3-19 and 3-20 in excel.

```
setwd("G:/Summer/Climate Change/CMIP5/Analyses_on_HRU45")
library(data.table)
Sys.setlocale("LC_ALL", "English")

totalsummary <-data.table(NULL)
totaltemp <- data.table(a=c('1','1','1','1'))
colnames(totaltemp) <- c("No")

No<-1

filenames <- list.files("G:/Summer/Climate Change/CMIP5/Analyses_on_HRU45",
pattern = ".hru")
for ( i in filenames){
    label_1<-substr(i,1,nchar(i)-4)
    label_2<-do.call(rbind, strsplit(label_1, "_"))

    #Set Years for different periods
    if (label_2[3]=="His") {
        year1 <- 1969
        year2 <- 1990
    } else if (label_2[3]=="Mid"){
        year1 <- 2039
        year2 <- 2060
    } else if (label_2[3]=="End"){
        year1 <- 2079
        year2 <- 2100
    }

    #Data Cleaning
    data_temp <- data.table(NULL)
    data_summary <- data.table(NULL)
    data_summary2 <- data.table(NULL)
    data_temp <- data.table(read.table(i, skip = 9))
    data_temp$Year <- as.numeric(substr(data_temp$V6, 1, 4))
```

```
    data_temp$Area <- as.numeric(substr(data_temp$V6, 5, 14))
    data_temp <- subset(data_temp, Year>year1 & Year<year2)

    #Data Combination
    data_temp$TOTAL_N <- data_temp$V8 + data_temp$V11 + data_temp$V12 +
data_temp$V13
    data_temp$TOTAL_P <- data_temp$V9 + data_temp$V10 + data_temp$V14 +
data_temp$V15

    #Calculate Average Value
    Avg_Q <- aggregate(V16~V3, data_temp, mean)
    Avg_S <- aggregate(V7~V3, data_temp, mean)
    Avg_N <- aggregate(TOTAL_N~V3, data_temp, mean)
    Avg_P <- aggregate(TOTAL_P~V3, data_temp, mean)
    Area<-data.table(data_temp[1:1334,Area])

    data_summary <-
data.table(cbind(Avg_Q[1],Area,Avg_Q[2],Avg_S[2],Avg_N[2],Avg_P[2]))
    colnames(data_summary) <- c("HRU","Area", "Avg_Q", "Avg_S", "Avg_N",
"Avg_P")

    #Write file for each model/scenario/period
    name1 <- paste(substr(i,1,nchar(i)-4),"_sum1.csv",sep="")
    write.csv(data_summary, file=name1)
}

# read each model/scenario/period pre-treated data
filenames <- list.files("G:/Summer/Climate Change/CMIP5/Analyses_on_HRU45",
pattern = "_sum1.csv")
CSAs<-data.table(NULL)

for (j in c("10","20","30","40")) {
    # Set Threshold No.
    TH<-round(as.numeric(j)*1334/100)

    for (i in filenames){
        label_1<-substr(i,1,nchar(i)-9)
        label_2<-do.call(rbind, strsplit(label_1, "_"))

        #Find the historical baseline file, Set Threshold Value at the TH No.
        if (label_2[1]=="NCDC"){
            data_temp <- read.csv(i)
            Q_TH<-
data_temp$Avg_Q[order(data_temp$Avg_Q,decreasing=TRUE)[TH]]
            S_TH<-
data_temp$Avg_S[order(data_temp$Avg_S,decreasing=TRUE)[TH]]
```

```
            N_TH<-
data_temp$Avg_N[order(data_temp$Avg_N,decreasing=TRUE)[TH]]
            P_TH<-
data_temp$Avg_P[order(data_temp$Avg_P,decreasing=TRUE)[TH]]
        }
    }

    #For each model/scenario/period, calculate CSA area
    for (i in filenames){
        label_1<-substr(i,1,nchar(i)-9)
        label_2<-do.call(rbind, strsplit(label_1, "_"))
        data_temp <- data.table(read.csv(i))
        Q_CSA<-subset(data_temp,Avg_Q >= Q_TH)
        Q_CSA_Area<-sum(Q_CSA$Area)
        S_CSA<-subset(data_temp,Avg_S >= S_TH)
        S_CSA_Area<-sum(S_CSA$Area)
        N_CSA<-subset(data_temp,Avg_N >= N_TH)
        N_CSA_Area<-sum(N_CSA$Area)
        P_CSA<-subset(data_temp,Avg_P >= P_TH)
        P_CSA_Area<-sum(P_CSA$Area)
        Temp_CSA<-
data.table(cbind(Q_CSA_Area,S_CSA_Area,N_CSA_Area,P_CSA_Area,label_2[1],labe
l_2[2],label_2[3],label_1,j))
        CSAs<-rbind(Temp_CSA,CSAs)
    }
}

#write result file
write.csv(CSAs, file="A_CSAs_Area.csv")
```

References

Abbaspour, K. (2015). SWAT-CUP. SWAT-CUP: SWAT Calibration and Uncertainty Programs - A User Manual. Retrieved March 12, 2017, from http://swat.tamu.edu/media/114860/usermanual_swatcup.pdf

Adams, L. W., Dove, L. E., & Franklin, T. M. (1985). Mallard pair and brood use of urban stormwater-control impoundments. *Wildlife Society Bulletin (1973-2006)*, *13*(1), 46-51.

Ahmad, S., & Simonovic, S. P. (1999). Comparison of one-dimensional and two-dimensional hydrodynamic modeling approaches for Red river basin. *Report to the International Joint Commission-Red River Basin Task Force, Ottawa, Washington*, 1-51.

Ambrose Jr, R. B., Wool, T. A., & Barnwell Jr, T. O. (2009). Development of Water Quality Modelingin the United States. *Environmental Engineering Research*, *14*(4), 200-210.

Arnold, J. G., Moriasi, D. N., Gassman, P. W., Abbaspour, K. C., White, M. J., Srinivasan, R., ... & Kannan, N. (2012). SWAT: Model use, calibration, and validation. *Transactions of the ASABE*, *55*(4), 1491-1508.

Arnold, J.G., Kiniry, J.R., Srinivasan, R., Williams, J.R., ... Neitsch, S.L. (2011). Soil and Water Assessment Tool Input/Output File Documentation Version 2009. Retrieved March 12, 2017, from http://swat.tamu.edu/media/19754/swat-io-2009.pdf

Bao, X., & Zhang, F. (2013). Evaluation of NCEP–CFSR, NCEP–NCAR, ERA-Interim, and ERA-40 reanalysis datasets against independent sounding observations over the Tibetan Plateau. *Journal of Climate*, *26*(1), 206-214.

Boesch, D. F., Johnson, Z. P., & Li, M. (2016). Rehabilitating the Chesapeake Bay (USA) ecosystem under changing climate. *Multiple drivers for Earth system changes in the Baltic Sea region*, 1.

Bonan, G. (2015). *Ecological climatology: concepts and applications*. Cambridge University Press.

Bosznay, M. (1989). Generalization of SCS curve number method. *Journal of irrigation and drainage engineering*, *115*(1), 139-144.

Brebbia, C. A., Rico, D. P., & Esteve, Y. V. (2008). *Water Pollution IX* (Vol. 111). WIT Press. 252.

Brekke, L., Thrasher, B. L., Maurer, E. P., & Pruitt, T. (2013). Downscaled CMIP3 and CMIP5 climate projections. *US Dep. Inter. Bur. Reclamation, Tech. Serv. Cent*.

Chesapeake Bay Program (CBP). (1992). Chesapeake Bay Agreement: 1992 Amendments. Retrieved March 12, 2017, from http://www.chesapeakebay.net/content/publications/cbp_12507.pdf

Chesapeake Bay Program (CBP). (2012). The Chesapeake Bay Watershed. Retrieved March 12, 2017, from http://www.chesapeakebay.net/discover/baywatershed

Climate Impacts Research Consortium (CIRC). (n.d.). Comparing CMIP5 and CMIP3 for the Pacific Northwest. Retrieved from https://doi_dev.opengov.ibmcloud.com/sites/doi.gov/files/migrated/csc/northwest/upload/CMIP5-v-CMIP3-two-pager.pdf

Collins, M., Knutti, R., Arblaster, J., Dufresne, J. L., Fichefet, T., Friedlingstein, P., ... & Shongwe, M. (2013). Long-term climate change: projections, commitments and irreversibility.

Columbia Association Watershed Management (CAWM). (2009). Final Columbia Watershed Management Plan. Retrieved March 12, 2017, from https://www.columbiaassociation.org/wp-content/uploads/2016/03/2870.pdf

Daniel, T. C., Sharpley, A. N., & Lemunyon, J. L. (1998). Agricultural phosphorus and eutrophication: A symposium overview. *Journal of Environmental Quality*, *27*(2), 251-257.

Dile, Y. T., & Srinivasan, R. (2014). Evaluation of CFSR climate data for hydrologic prediction in data-scarce watersheds: an application in the Blue Nile River Basin. *JAWRA Journal of the American Water Resources Association*, *50*(5), 1226-1241.

Dile, Y. T., Karlberg, L., Srinivasan, R., & Rockström, J. (2016). Investigation of the Curve Number Method For Surface Runoff Estimation In Tropical Regions. *JAWRA Journal of the American Water Resources Association*, *52*(5), 1155-1169.

Ehret, U., Zehe, E., Wulfmeyer, V., Warrach-Sagi, K., & Liebert, J. (2012). HESS Opinions" Should we apply bias correction to global and regional climate model data?". *Hydrology and Earth System Sciences*, *16*(9), 3391.

El-Khoury, A., Seidou, O., Lapen, D. R., Que, Z., Mohammadian, M., Sunohara, M., & Bahram, D. (2015). Combined impacts of future climate and land use changes on discharge, nitrogen and phosphorus loads for a Canadian river basin. *Journal of environmental management*, *151*, 76-86.

Fuka, D. R., Walter, M. T., MacAllister, C. A., Degaetano, A. T., Steenhuis, T. S., & Easton, Z. M. (2013). Using the Climate Forecast System Reanalysis dataset to improve weather input data for watershed models. Hydrol. *Proc. DOI*, *10*.

Gan, T. Y., E. M. Dlamini, and G. F. Biftu. 1997. Effects of model complexity and structure, data quality, and objective functions on hydrologic modeling. J. Hydrol. 192(1): 81-103.

Great Lakes Commission (GLC). (2006). Assessment of Modeling Tools and Data Needs for TMDL Plan. Retrieved March 12, 2017, from http://swat.tamu.edu/media/90098/glc.pdf

Hagedorn, C., Robinson, S. L., Filtz, J. R., Grubbs, S. M., Angier, T. A., & Reneau, R. B. (1999). Determining sources of fecal pollution in a rural Virginia watershed with antibiotic resistance patterns in fecal streptococci. *Applied and Environmental Microbiology*, *65*(12), 5522-5531.

Horner, R. R. (1994). Fundamentals of urban runoff management: technical and institutional issues. Retrieved March 12, 2017, from http://westwindsornj.org/watershed_meeting_110211/Hydrologic%20Cycle.jpg

Houghton, J. T., Ding, Y. D. J. G., Griggs, D. J., Noguer, M., van der Linden, P. J., Dai, X., ... & Johnson, C. A. (2001). *Climate change 2001: the scientific basis*. The Press Syndicate of the University of Cambridge.

Huber, W., & Roesner, L. (2012). The History and Evolution of the EPA SWMM. Retrieved March 12, 2017, from http://dc.engconfintl.org/cgi/viewcontent.cgi?article=1001&context=watershed

Institut Pierre Simon Laplace (ISPL). (n.d.). IPSL-CM5. Retrieved from http://icmc.ipsl.fr/index.php/icmc-models-2/icmc-ipsl-cm5

Intergovernmental Panel on Climate Change (IPCC). (2014). Carbon Dioxide: Projected emissions and concentrations. Retrieved March 12, 2017, from http://www.ipcc-data.org/observ/ddc_co2.html

Jaeger, K. L., Olden, J. D., & Pelland, N. A. (2014). Climate change poised to threaten hydrologic connectivity and endemic fishes in dryland streams. *Proceedings of the National Academy of Sciences*, *111*(38), 13894-13899.

Jha, M., Arnold, J. G., Gassman, P. W., Giorgi, F., & Gu, R. R. (2006). Climate chhange sensitivity assessment on upper mississippi river basin streamflows using SWAT. *JAWRA Journal of the American Water Resources Association*, *42*(4), 997-1015.

Kalnay, E., Kanamitsu, M., Kistler, R., Collins, W., Deaven, D., Gandin, L., ... & Zhu, Y. (1996). The NCEP/NCAR 40-year reanalysis project. *Bulletin of the American meteorological Society*, *77*(3), 437-471.

Klein, C. A. M. de Pinares-Patino, C. Waghorn, G. C. (2008). Greenhouse gas emissions. Environmental impacts of pasture-based farming'.(Ed. R McDowell) 1-33.

Knutson, T. R., Sirutis, J. J., Vecchi, G. A., Garner, S., Zhao, M., Kim, H. S., ... & Villarini, G. (2013). Dynamical downscaling projections of twenty-first-century Atlantic hurricane activity: CMIP3 and CMIP5 model-based scenarios. *Journal of Climate*, *26*(17), 6591-6617.

Knutti, R., & Sedláček, J. (2013). Robustness and uncertainties in the new CMIP5 climate model projections. *Nature Climate Change*, *3*(4), 369-373.

Knutti, R., Masson, D., & Gettelman, A. (2013). Climate model genealogy: Generation CMIP5 and how we got there. *Geophysical Research Letters*, *40*(6), 1194-1199.

Lammertsma, E. I., de Boer, H. J., Dekker, S. C., Dilcher, D. L., Lotter, A. F., & Wagner-Cremer, F. (2011). Global CO2 rise leads to reduced maximum stomatal conductance in Florida vegetation. *Proceedings of the National Academy of Sciences*, *108*(10), 4035-4040.

Lawrence Livermore National Laboratory (LLNL). (n.d.). CMIP - Overview. Retrieved from http://cmip-pcmdi.llnl.gov/

Liungman, O., & Moreno-Arancibia, P. (2010). Developing a 3D coupled hydrodynamic and ecological model to be used in coastal management. Retrieved March 12, 2017, from https://www.dhigroup.com/upload/publications/mike21/Liungman1_2010.pdf

Ma, X., Li, Y., Zhang, M., Zheng, F., & Du, S. (2011). Assessment and analysis of non-point source nitrogen and phosphorus loads in the Three Gorges Reservoir Area of Hubei Province, China. *Science of the Total Environment*, *412*, 154-161.

Malagò, A., Pagliero, L., Bouraoui, F., & Franchini, M. (2015). Comparing calibrated parameter sets of the SWAT model for the Scandinavian and Iberian peninsulas. *Hydrological Sciences Journal*, *60*(5), 949-967.

Maryland Department of the Environment (MDDoE). (2012). Maryland's Phase II Watershed Implementation Plan for the Chesapeake Bay TMDL. Retrieved March 12, 2017, from http://www.mde.state.md.us/programs/Water/TMDL/TMDLImplementation/Docu

ments/FINAL_PhaseII_Report_Docs/Final_Documents_PhaseII/Final_Phase_II_WIP_MAIN_REPORT_102612.pdf

Maurer, E. P., Brekke, L., Pruitt, T., Thrasher, B., Long, J., Duffy, P., ... & Arnold, J. (2014). An enhanced archive facilitating climate impacts and adaptation analysis. *Bulletin of the American Meteorological Society*, *95*(7), 1011-1019.

Maurer, E. P., Wood, A. W., Adam, J. C., Lettenmaier, D. P., & Nijssen, B. (2002). A long-term hydrologically based dataset of land surface fluxes and states for the conterminous United States. *Journal of Climate*, *15*(22), 3237-3251.

Meinshausen, M., Smith, S. J., Calvin, K., Daniel, J. S., Kainuma, M. L. T., Lamarque, J. F., ... & Thomson, A. G. J. M. V. (2011). The RCP greenhouse gas concentrations and their extensions from 1765 to 2300. *Climatic Change*, *109*(1-2), 213.

Molina-Navarro, E., Trolle, D., Martínez-Pérez, S., Sastre-Merlín, A., & Jeppesen, E. (2014). Hydrological and water quality impact assessment of a Mediterranean limno-reservoir under climate change and land use management scenarios. *Journal of Hydrology*, *509*, 354-366.

Moriasi, D. N., Arnold, J. G., Van Liew, M. W., Bingner, R. L., Harmel, R. D., & Veith, T. L. (2007). Model evaluation guidelines for systematic quantification of accuracy in watershed simulations. *Trans. ASABE*, *50*(3), 885-900.

Moss, R. H., Edmonds, J. A., Hibbard, K. A., Manning, M. R., Rose, S. K., Van Vuuren, D. P., ... & Meehl, G. A. (2010). The next generation of scenarios for climate change research and assessment. *Nature*, *463*(7282), 747-756.

Mostaghimi, S. (2003). A comparison of SWAT and HSPF models for simulating hydrologic and water quality responses from an urbanizing watershed. In *ASAE Annual Int. Meeting*.

Mostaghimi, S. (2003, July). A comparison of SWAT and HSPF models for simulating hydrologic and water quality responses from an urbanizing watershed. In *ASAE Annual Int. Meeting*.

Nasr, A. E., Bruen, M., Moles, R., Byrne, P., & O'Regan, B. (2003). The significance of the differences in soil phosphorus representation and transport procedures in the SWAT and HSPF models and a comparison of their performance in estimating phosphorus loss from an agriculture catchment in Ireland. In *Paper presented at the 2nd International SWAT Conference, Bari, Italy, July 1-4, 2003*. TWRI.

National Aeronautics and Space Administration (NASA). (n.d.). The Fast Carbon Cycle. Retrieved March 12, 2017, from http://earthobservatory.nasa.gov/Features/CarbonCycle/page3.php

National Oceanic and Atmospheric Administration (NOAA). (2015). Technical Report NESDIS 144 - Regional Surface Climate Conditions in CMIP3 and CMIP5 for the United States: Differences, imilarties, and Implications for the U.S. National Climate Assessment. Retrieved from https://docs.lib.noaa.gov/noaa_documents/NESDIS/TR_NESDIS/TR_NESDIS_144.pdf

National Oceanic and Atmospheric Administration (NOAA). (n.d.). Reanalysis. Retrieved March 12, 2017, from https://www.ncdc.noaa.gov/data-access/model-data/model-datasets/reanalysis

Neitsch, S.L., Arnold, J.G., Kiniry, J.R., Williams, J.R. (2011). Soil and Water Assessment Tool Theoretical Documentation Version 2009. Retrieved March 12, 2017, from http://swat.tamu.edu/media/99192/swat2009-theory.pdf

Niraula, R., Kalin, L., Srivastava, P., & Anderson, C. J. (2013). Identifying critical source areas of nonpoint source pollution with SWAT and GWLF. *Ecological Modelling*, *268*, 123-133.

Piniewski, M. (2014). *Scenario-based impact assessment of global and regional change on the semi-natural flow regime.* Munich: GRIN Publishing GmbH.

Pionke, H. B., Gburek, W. J., & Sharpley, A. N. (2000). Critical source area controls on water quality in an agricultural watershed located in the Chesapeake Basin. *Ecological Engineering*, *14*(4), 325-335.

Poleto, C., Merten, G. H., & Minella, J. P. (2009). The identification of sediment sources in a small urban watershed in southern Brazil: an application of sediment fingerprinting. *Environmental Technology*, *30*(11), 1145-1153.

Potsdam Institute for Climate Impact Research (PIK). (n.d.). RCP Concentration Calculations and Data - Final Version, background data, acknowledgements and further info. Retrieved March 12, 2017, from http://www.pik-potsdam.de/~mmalte/rcps/

Radcliffe, D. E., & Mukundan, R. (2016). PRISM vs. CFSR Precipitation Data Effects on Calibration and Validation of SWAT Models. *JAWRA Journal of the American Water Resources Association, 53*(1), 89–100.

Rathjens, H., Bieger, K., Srinivasan, R., Chaubey, I., & Arnold G. J. (2016). CMhyd User Manual. Retrieved March 12, 2017, from http://swat.tamu.edu/media/115265/bias_cor_man.pdf

Rawls, W. J., Brakensiek, D. L., & Miller, N. (1983). Green-Ampt infiltration parameters from soils data. *Journal of Hydraulic Engineering*, *109*(1), 62-70.

Renkenberger, J., Montas, H., Leisnham, P., Chanse, V., Shirmohammadi, A., Sadeghi, A., ... & Lansing, D. (2015). Climate change impact on critical source area identification in a Maryland watershed. *Transactions of the ASABE, in review. ASABE, St-Joseph, MI*.

Robison, M. (1991). *National Pollutant Discharge Elimination System (NPDES) Permit Application Requirement for Storm Water Discharges*. Army Environmental Hygiene Agency Aberdeen Proving Ground MD.

Rossiter, D. G. (2012). Introduction to the R Project for Statistical Computing for use at ITC. *International Institute for Geo-information Science & Earth Observation (ITC), Enschede (NL)*, *3*, 3-6.

Roth, V., & Lemann, T. (2016). Comparing CFSR and conventional weather data for discharge and soil loss modelling with SWAT in small catchments in the Ethiopian Highlands. *Hydrology and Earth System Sciences*, *20*(2), 921-934.

Schewe, J., Heinke, J., Gerten, D., Haddeland, I., Arnell, N. W., Clark, D. B., ... & Gosling, S. N. (2014). Multimodel assessment of water scarcity under climate change. *Proceedings of the National Academy of Sciences*, *111*(9), 3245-3250.

Singh, J., Knapp, H. V., Arnold, J. G., & Demissie, M. (2005). Hydrological modeling of the iroquois river watershed using HSPF and SWAT1. *Journal of the American Water Resources Association,* Volume 41, Issue 2, 343–360.

Solomon, S. (Ed.). (2007). *Climate change 2007-the physical science basis: Working group I contribution to the fourth assessment report of the IPCC* (Vol. 4). Cambridge University Press.

Stocker, T. F., Qin, D., Plattner, G. K., Tignor, M., Allen, S. K., Boschung, J., ... & Midgley, B. M. (2013). IPCC, 2013: climate change 2013: the physical science basis. Contribution of working group I to the fifth assessment report of the intergovernmental panel on climate change.

Stone Environmental, Inc. (2011). Identification of Critical Source Areas of Phosphorus Within The Vermont Sector of The Missisquoi Bay Basin. Retrieved March 12, 2017, from https://northernlakechamplain.files.wordpress.com/2012/04/csa-final-report-stone-enviro-12-15-12.pdf

Streeter, H. W. (1926). The Rate of Atmospheric Reaeration of Sewagepolluted Streams. *Public Health Reports (1896-1970)*, 247-262.

Sun, N., Hong, B., & Hall, M. (2014). Assessment of the SWMM model uncertainties within the generalized likelihood uncertainty estimation (GLUE) framework for a high-resolution urban sewershed. *Hydrological Processes*, *28*(6), 3018-3034.

Taylor, K. E., Stouffer, R. J., & Meehl, G. A. (2012). An overview of CMIP5 and the experiment design. *Bulletin of the American Meteorological Society*, *93*(4), 485-498.

Teutschbein, C., & Seibert, J. (2012). Bias correction of regional climate model simulations for hydrological climate-change impact studies: Review and evaluation of different methods. *Journal of Hydrology*, *456*, 12-29.

U.S. Environmental Protection Agency (USEPA). (2010). Chesapeake Bay TMDL Executive Summary. Retrieved March 12, 2017, from https://www.epa.gov/sites/production/files/2014-12/documents/bay_tmdl_executive_summary_final_12.29.10_final_1.pdf

Verma, S., Bhattarai, R., Bosch, N. S., Cooke, R. C., Kalita, P. K., & Markus, M. (2015). Climate change impacts on flow, sediment and nutrient export in a Great Lakes watershed using SWAT. *CLEAN–Soil, Air, Water*, *43*(11), 1464-1474.

Voldoire, A., Sanchez-Gomez, E., y Mélia, D. S., Decharme, B., Cassou, C., Sénési, S., ... & Déqué, M. (2013). The CNRM-CM5. 1 global climate model: description and basic evaluation. *Climate Dynamics*, *40*(9-10), 2091-2121.

Wang, Y. (2015). *A diagnostic decision support system for selecting best management practices in urban/suburban watersheds* (Doctoral dissertation). Retrieved March 12, 2017, from http://drum.lib.umd.edu/handle/1903/16548

White, M. J., Storm, D. E., Busteed, P. R., Stoodley, S. H., & Phillips, S. J. (2009). Evaluating nonpoint source critical source area contributions at the watershed scale. *Journal of environmental quality*, *38*(4), 1654-1663.

Wilber, D. H., & Clarke, D. G. (2001). Biological effects of suspended sediments: a review of suspended sediment impacts on fish and shellfish with relation to dredging activities in estuaries. *North American Journal of Fisheries Management*, *21*(4), 855-875.

Williams, J. R., & Hann, R. W. (1972). Hymo, A problem-oriented computer language for building hydrologic models. *Water Resources Research*, *8*(1), 79-86.

Woznicki, S. A., Nejadhashemi, A. P., & Smith, C. M. (2011). Assessing best management practice implementation strategies under climate change scenarios. *Trans. ASABE*, *54*(1), 171-190.

Yang, Y., Wang, G., Wang, L., Yu, J., & Xu, Z. (2014). Evaluation of gridded precipitation data for driving SWAT model in area upstream of three gorges reservoir. *PloS ONE*, *9*(11), e112725.